QUANTIFYING HYPORHEIC EXCHANGE FLUXES AND RESIDENCE TIMES USING ENVIRONMENTAL TRACERS.

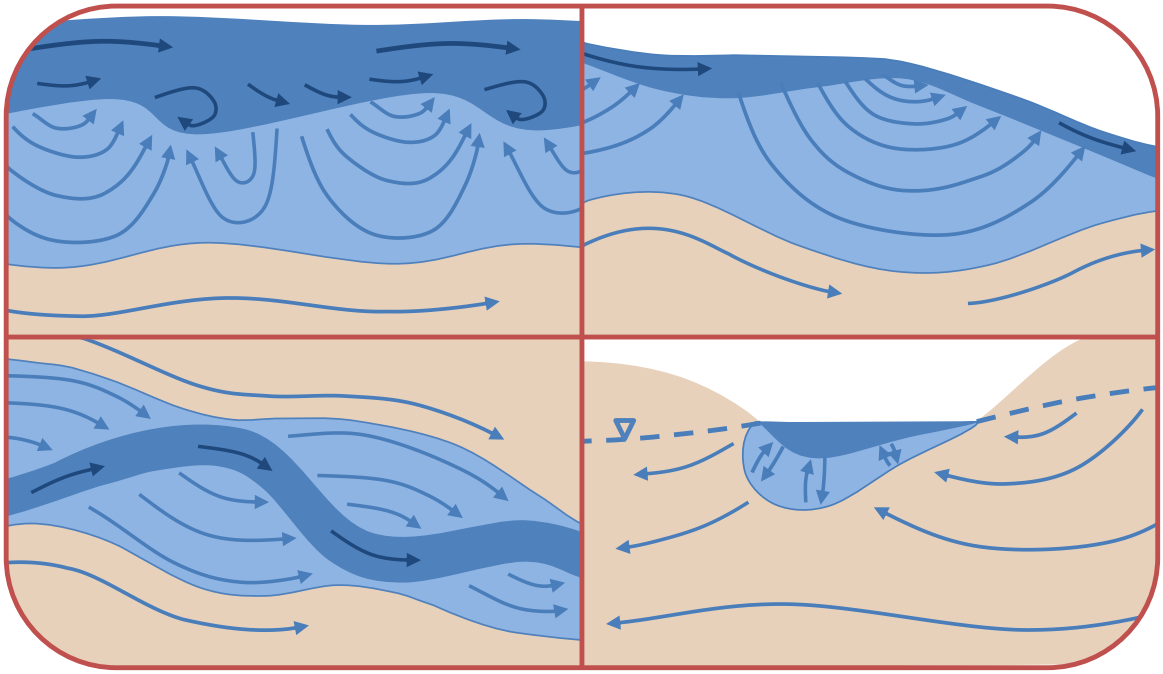

SUBMITTED BY:

ROGER HARVARD CRANSWICK

Bachelor of Science (Honours), Bachelor of Science (Earth Science)

As a requirement in full for the degree of Doctor of Philosophy in the School of the Environment, Flinders University, South Australia

May, 2014

NATIONAL CENTRE FOR GROUNDWATER RESEARCH AND TRAINING

Flinders UNIVERSITY

DECLARATION OF ORIGINALITY

I certify that this thesis does not incorporate without acknowledgment any material previously submitted for a degree or diploma in any university; and that to the best of my knowledge and belief it does not contain any material previously published or written by another person except where due reference is made in the text.

Roger Harvard Cranswick

29th May, 2014

CO-AUTHORSHIP

Roger Harvard Cranswick is the primary author on all manuscripts in this thesis. On all accepted and submitted papers, the co-authors provided intellectual supervision and editorial content.

ACKNOWLEDGMENTS

I would like to acknowledge the funding from the Australian Research Council and the National Water Commission via the National Centre for Groundwater Research and Training (NCGRT). Without this funding and the efforts of Craig Simmons to secure it, I would not have had the opportunity to conduct this research, or to do so with such incredible financial and intellectual support.

My supervisor Peter Cook has been an excellent mentor, providing guidance and direction towards deepening my understanding of all things related to the research presented here. Unfortunately, he has been unable to break up all of my run-on sentences as I know a few have still snuck in here and there. I also would like to thank my co-supervisor Sebastien Lamontagne, who has fostered a particular appreciation for details of the English language through his many rigorous reviews of my writing. There have been a number of other reviewers and colleagues, namely Margaret Shanafield and Dylan Irvine, who have helped significantly in developing the clarity and rigour of some of the research presented here. They and my supervisors have challenged my understanding of the mathematics that underlies many of the concepts I have known intuitively. This has strengthened my ability to more effectively communicate the findings of my own research as well as the work of other colleagues at NCGRT. I would also like to thank everyone who helped me in the field and my fellow PhD candidates. They have provided much enjoyment bouncing ideas around over the last 3.5 years, whether those were about the chemistry of home brewing and tropical aquariums or the languages of Fortran!

Most of all, I would like to thank my wife Becky. Over the time it took to finish this PhD, we met once again, became best friends, fell in love and were married! Your interest, encouragement and the occasional kick in the right direction have been exactly what I needed at the time. You are and will always be the love of my life.

SUMMARY

Hyporheic exchange is a process in which water leaves a river through underlying or adjacent sediments and then returns to the river. This is now widely recognised as a critical process for nutrient cycling and river health but it remains a challenge to adequately characterise the spatial and temporal scales at which hyporheic exchange occurs. The method traditionally used to quantify hyporheic exchange is the applied tracer test. This approach characterises the bulk exchange occurring within the river and riverbed sediments between locations separated by tens to hundreds of metres longitudinally along a river. Although a useful tool for assessing reach scale bulk processes, this approach does not describe the spatial variability of hyporheic exchange within each reach which can be important (e.g. characterising upwelling and downwelling zones). Additionally, the flowpaths that occur over longer temporal scales than the sampling period are not captured within the analysis. More broadly, it is not well understood how the scale and magnitude of hyporheic exchange compares with other groundwater–surface water exchange processes. These include groundwater discharge into rivers and river infiltration into aquifers which are both important processes for water resource managers to be able to accurately quantify.

The key objectives of this thesis are to investigate and directly compare, the use of naturally occurring environmental tracers (temperature and radon) for estimating hyporheic exchange fluxes and residence times. The conceptual assumptions of these approaches are examined with the intention of demonstrating their value for quantifying groundwater–surface water exchange processes. To date, there have not been any studies that directly compare the hyporheic exchange fluxes and residence times derived from detailed vertical profiles of temperature and radon. The research also explores the relative scales and magnitudes of hyporheic and river–aquifer exchange fluxes to demonstrate the importance of conceptualising and quantifying hyporheic exchange within the context of water resource management.

A field investigation on the Haughton River in northeastern Australia, explores the use of naturally occurring environmental tracers to characterise the hyporheic exchange processes occurring along a pool–riffle sequence. To interpret temperature data, a 1D numerical approach is developed and validated by comparison with two synthetic 2D flowfields before applying it to raw temperature data from the field. The validation of the 1D approach shows that the flux calculated between the surface and an observation depth is representative of the mean vertical component of flux along the flowpath the water has travelled to that depth. Thus without describing the horizontal component of flow, this vertical 1D approach inherently contains a "spatial footprint". This is an important improvement on the more commonly applied assumption of pure vertical flow between sequential pairs of subsurface temperature data, which is currently in conflict with our understanding of hyporheic flowfields.

Simple analysis of the temperature, radon and electrical conductivity data collected in a series of vertical profiles, allows us to identify the depth of hyporheic circulation and calculate residence times within the hyporheic zone. Residence times derived from temperature and radon data were compared directly and although they showed general agreement, there were large differences in many cases. When error bounds were taken into account, radon-derived residence times in downwelling profiles were significantly greater than temperature-derived residence times for 57% of samples. These results suggest that small scale heterogeneity may have a different influence on each of these tracers and thus cause the disparity in flux and residence time estimates. The temperature approach appears to be more influenced by zones of high hydraulic conductivity than the radon approach. The use of diel temperature variations can be used to estimate residence times from tens of minutes up to a few days while the radon approach allows residence times from 0.1 to 15 days to be quantified. The uncertainty of residence time values increases outside of these ranges. This research demonstrates the value of using temperature and radon in

combination, as together they allow the quantification of hyporheic residence times from tens of minutes to 15 days using relatively rapid field techniques.

A review of groundwater–surface water exchange flux estimates found in the literature shows that hyporheic exchange fluxes are approximately one order of magnitude larger than river–aquifer exchange fluxes. If methods are applied that cannot specifically distinguish between sources of water (e.g. seepage meters and other point measurements) there is the potential for large hyporheic exchange fluxes to be misinterpreted as river-aquifer exchange fluxes. This would have clear implications for water resource management where accurately quantifying groundwater–surface water interaction is critical for decision making. This thesis also outlines the spatial and temporal scales at which common field methods are applied. Then the importance of considering the scale of measurement and the use of multiple methods to successfully differentiate between exchange flux processes is presented.

CONTENTS

LIST OF FIGURES

LIST OF TABLES

1. INTRODUCTION

1.1. Context for Research Objectives

Hyporheic exchange is the movement of water from a river into the underlying or adjacent sediments and then back into the river. The process was first recognised as important for river ecosystems through ecological studies in the middle of last century (e.g. Orghidan, 1959; Pollard, 1955; Schwoerbel, 1964). The hyporheic zone where this exchange occurs, is now widely recognised as a biogeochemical hotspot in river ecosystems (Boulton *et al.*, 1998). Hyporheic exchange is also important for nutrient cycling (e.g. Triska *et al.*, 1989) and understanding the fate of contaminants within a river (e.g. Harvey and Fuller, 1998). Because of its importance, the characterisation of biological, chemical and hydraulic dynamics of hyporheic processes have been the focus of numerous studies since the mid-1950s (Boulton *et al.*, 2010). Hyporheic exchange occurs across a broad range of spatial and temporal scales depending on the riverbed substrate, geomorphology and larger scale river-aquifer exchanges (Harvey and Wagner, 2000). Hyporheic exchange processes include: current driven exchange due to river flow over bedforms (Thibodeaux and Boyle, 1987; Figure 1.1A); downwelling and upwelling induced by pool–riffle sequences (Vaux, 1968; Figure 1.1B); and parafluvial exchange across meander bends (Boano *et al.*, 2006; Figure 1.1C). The vertical extent of this exchange is partially dependent on the larger scale river–aquifer exchange processes that are influenced by regional hydraulic gradients (Figure 1.1D and 1.1E).

The most common method for characterising hyporheic exchange on the reach scale is the applied tracer test (Stream Solute Workshop, 1990). Generally, a conservative tracer is applied to the stream at a known rate and the breakthrough curve of tracer concentration is measured at a series of observation locations downstream. The shape of the breakthrough curve is used to determine the exchange rate and dimensions of a transient storage zone

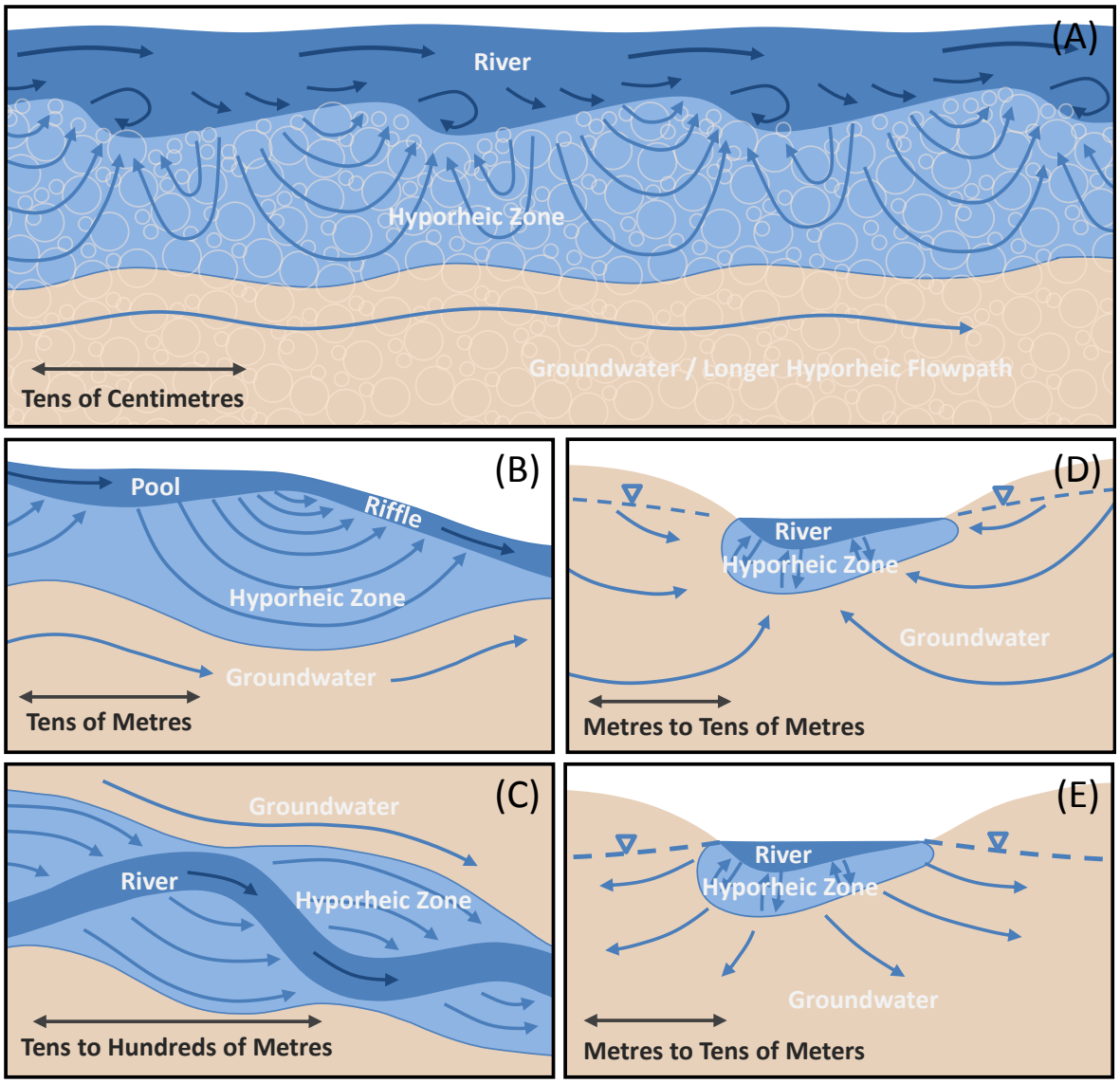

Figure 1.1. Conceptual models for hyporheic exchange processes. (A) Current driven hyporheic exchange induced by dynamic pressure gradients within the river (after Thibodeaux and Boyle, 1987). (B) Downwelling and upwelling hyporheic exchange induced by hydraulic gradients along a pool–riffle sequence (after Vaux, 1968). (C) Parafluvial exchange occurring due to hydraulic gradients across meander bends (after Boano *et al.*, 2006). (D) The vertical extent of hyporheic circulation in a cross section of a gaining reach. (E) The vertical extent of hyporheic circulation in a cross section of a losing reach. Each conceptual model describes hyporheic exchange that occurs across a range of spatial and temporal scales.

(e.g. Bencala e*t al.*, 1983). The ability of this approach to rapidly characterise the transient storage zone and potential for nutrient cycling on the reach scale is one of the reasons why it is so widely applied. However, transient storage includes the exchange occurring in both the river and subsurface, and so represents the bulk exchange between the observation locations rather than only hyporheic exchange. Furthermore, because applied tracer tests can only quantify the exchange that occurs over the temporal scale of the observations

(typically hours to days) it means that flowpaths that have residence times longer than this are not directly described (Harvey *et al.*, 1996). Thus the depth of exchange represented using applied tracer tests is commonly on the order of centimetres to tens of centimetres. To characterise deeper hyporheic exchange on a scale of metres, longer tracer applications and sampling durations are required. However, longer tests are often deemed impractical due to either a lack of resources or prohibitive cost. Additionally, applied tracer tests cannot inform us on the spatial variability of hyporheic exchange within a reach. Our ability to capture this variability can be important if we are interested in the role of larger scale features such as pool–riffle sequences or meander bends. Recently electrical resistivity surveys conducted during applied tracer tests have been used to delineate shallow hyporheic exchange at selected points in time (e.g. Ward *et al.*, 2010). Meanwhile, major ion chemistry sampled in detailed vertical profiles (e.g. Ibrahim *et al.*, 2010) or near hyporheic features (e.g. Fanelli and Lautz, 2010) can be used to investigate the spatial variability of hyporheic biogeochemical processes. To better characterise the spatial variability of hyporheic residence times, alternative methods are also being developed using other environmental tracers.

Two naturally occurring environmental tracers that have potential to be effective in hyporheic studies are temperature and radon (^{222}Rn). Temperature variations originating in the river can be transferred into the subsurface through both conduction and advection, while radon is a naturally occurring noble gas that is produced by the sediments. Both can be measured in vertical profiles from within the hyporheic zone and used to estimate vertical fluxes and residence times of water. Radon has traditionally been used to quantify groundwater discharge into rivers and river loss into an adjacent aquifer (e.g. Ellins *et al.*, 1990 and Hoehn and von Gunten, 1989 respectively). However, fluxes and residence times within the hyporheic zone can also be estimated using radon if samples are collected on small spatial scales beneath or adjacent to the river (e.g. Lamontagne and Cook, 2007 and

Hoehn and Cirpka, 2006 respectively). Likewise temperature has been used to calculate both groundwater discharge and river infiltration (e.g. Conant Jr., 2004 and Constantz *et al.*, 1994 respectively). Recently, temperature has been measured in detailed vertical profiles to estimate vertical fluxes in the hyporheic zone (e.g. Lautz and Fanelli, 2008; Briggs *et al.*, 2012). Temperature based approaches in the hyporheic zone commonly assume that water flux is purely vertical (one dimensional) between vertically spaced pairs of data. However, the validity of this assumption requires further exploration given our conceptual understanding of hyporheic flowpaths. Additionally, there are only a limited number of studies that have used both temperature and radon tracers in conjunction to better describe hyporheic processes (e.g. Hoehn and Cirpka, 2006). There have not been any studies that directly compare the hyporheic exchange fluxes and residence times derived from detailed vertical profiles of temperature and radon.

Numerical models have been used to support field data and explore the theoretical dynamics of hyporheic exchange at a range of scales. Studies have shown that hyporheic exchange is influenced by both large and small scale physical factors. These include: heterogeneity, stream curvature and bedforms (Cardenas *et al.*, 2004); channel sinuosity and valley slope (Cardenas, 2009); regional groundwater gradients and aquifer properties (e.g. Storey *et al.*, 2003 and Cardenas and Wilson, 2006); and both geomorphology and streambed slope (e.g. Gooseff *et al.*, 2006 and Tonina and Buffington, 2007). These and other studies have led to a greater understanding of how hyporheic exchange processes are likely to fit within the context of larger scale processes of river–aquifer interaction (e.g. groundwater discharge from regional aquifers). Woessner (2000) emphasises the need to consider the complexity of the interaction of rivers and alluvial groundwater systems to improve upon traditional and larger scale hydrogeological approaches. Bencala *et al.* (2011) expands on this by suggesting that the established conceptual models of hyporheic exchange could be applied at larger scales by measuring basic hydrological processes and

water chemistry (e.g. groundwater levels, river discharge, river and groundwater salinity). Recent studies have shown the relevance of linking these processes by demonstrating that the residence time distributions of the groundwater–surface water interaction at a range of scales are fractal in nature (Cardenas, 2008; Haggerty *et al.*, 2002; Kirchner *et al.*, 2000; and Stonedahl *et al.*, 2010). In contrast to these theoretical developments, our understanding of the relative flux magnitudes of different groundwater–surface water exchange processes is based on only a small number of field studies. Ruehl *et al.* (2006); Jones *et al.* (2008); and Bourke *et al.* (submitted) for example, show that hyporheic exchange fluxes can be many times greater than river–aquifer exchange fluxes. However it is not clear whether this is a relationship that is true globally, or one specific to the field locations investigated by these authors.

1.2. Knowledge Gaps

Applied tracer tests describe the bulk exchange occurring in the river and riverbed between longitudinal observation locations over the duration of the sampling period. Thus the spatial variability of hyporheic exchange between observation locations is not well characterised and flowpaths that have travel times longer than the sampling duration are not captured using this approach. Hence there is a need to develop methods that can better characterise both the spatial variability of hyporheic exchange and also the longer hyporheic flowpaths without conducting labour intensive and expensive long duration applied tracer tests. If sampled in detailed vertical profiles within the hyporheic zone, environmental tracers (temperature and radon) could be used for this purpose. However these approaches have not been often applied in conjunction, and the resulting fluxes and residence times have not been directly compared. To make this comparison, the conceptual validity of the 1D assumption for temperature transport on a small scale needs to be clearly demonstrated. The relative scale and magnitude of hyporheic exchange fluxes compared with other groundwater–surface water exchange fluxes (river infiltration and groundwater

discharge) are also not well understood. What we know of the relative importance of hyporheic exchange compared to other exchange processes is based on only a small number of field studies.

1.3. Research Objectives

The key objectives of this research are as follows:

1) To investigate the use of naturally occurring environmental tracers (temperature and radon) for estimating hyporheic exchange fluxes and residence times. These methods are applied along a pool–riffle sequence on the Haughton River in tropical northeastern Australia to characterise the spatial variability and temporal scales of hyporheic exchange processes;
2) Examine the conceptual validity of common approaches taken to interpret subsurface radon and temperature data, with the aim to improve upon these approaches by using more robust assumptions;
3) Demonstrate the usefulness of these naturally occurring environmental tracers through the direct comparison of detailed vertical profiles of flux and residence time derived from radon and temperature based approaches;
4) Explore the relative scales and magnitude of hyporheic and river–aquifer exchange fluxes and clarify the importance of distinguishing between hyporheic and other exchange processes.

1.4. Thesis Overview

This thesis is presented in the form of three manuscripts at various stages of publication in peer-reviewed hydrogeological journals. The first manuscript, *"The vertical variability of hyporheic fluxes inferred from riverbed temperature data",* explores the use of temperature as an environmental tracer for understanding the vertical variability of hyporheic exchange fluxes. The second manuscript, *"Hyporheic zone exchange fluxes and*

residence times inferred from riverbed temperature and radon data", uses both temperature and radon to better understand the spatial variability of hyporheic exchange across a pool–riffle sequence in a sandy riverbed and directly compare the two methods. The third manuscript, *"Scales and magnitude of hyporheic, river–aquifer and bank storage exchange fluxes",* is a literature review that compares data from 53 studies of three common groundwater–surface water interaction processes. A summary of the major findings and implications of this research is presented in the Conclusions section and the clear linkages between manuscripts are briefly outlined. The results of a series of radon emanation experiments are presented in Appendix A while other supporting information and data is presented for completeness in Appendix B. Appendix B includes data collected from three field campaigns – two in the Haughton River, Queensland and one to the Cockburn River, New South Wales.

2. MANUSCRIPT I: THE VERTICAL VARIABILITY OF HYPORHEIC FLUXES INFERRED FROM RIVERBED TEMPERATURE DATA

Accepted in Water Resources Research, April 15th 2014:

Cranswick RH. Cook PG, Shanafield M, Lamontagne S. 2014. The vertical variability of hyporheic fluxes inferred from riverbed temperature data. *Water Resources Research*, 50. DOI: 10.1002/2013WR014410.

Authors:

Roger H. Cranswick, Peter G. Cook, Margaret Shanafield and Sebastien Lamontagne

Abstract:

We present detailed profiles of vertical water flux from the surface to 1.2 m beneath the Haughton River in the tropical northeast of Australia. A 1D numerical model is used to estimate vertical flux based on raw temperature time-series observations from within downwelling, upwelling, neutral and convergent sections of the hyporheic zone. A Monte Carlo analysis is used to derive error bounds for the fluxes based on temperature measurement error and uncertainty in effective thermal diffusivity. Vertical fluxes ranged from 5.7 m d^{-1} (downward) to –0.2 m d^{-1} (upward) with the lowest relative errors for values between 0.3 and approximately 6 m d^{-1}.

Our 1D approach provides a useful alternative to 1D analytical and other solutions because it does not incorporate errors associated with simplified boundary conditions or assumptions of purely vertical flow, hydraulic parameter values or hydraulic conditions. To validate the ability of this 1D approach to represent the vertical fluxes of 2D flowfields, we compare our model with two simple 2D flowfields using a commercial numerical model. These comparisons showed that: 1) the 1D vertical flux was equivalent to the mean vertical component of flux irrespective of a changing horizontal flux; and 2) the subsurface temperature data inherently has a "spatial footprint" when the vertical flux profiles vary spatially. Thus, the mean vertical flux within a 2D flowfield can be estimated accurately without requiring the flow to be purely vertical. The temperature-derived 1D vertical flux represents the integrated vertical component of flux along the flowpath intersecting the observation point.

2.1. Introduction

Heat has been used as an environmental tracer for investigating groundwater–surface water interaction for over 50 years and by numerous researchers (see reviews by Anderson, 2005; Constantz, 2008; and Rau *et al.*, 2014). This is made possible because of natural temperature variations at various frequencies in surface water bodies (usually diel or seasonal variations are considered). Meanwhile, temperature variation in the subsurface (shallow groundwater or hyporheic zone) shows less variation, and so there is usually a temperature difference between the surface and subsurface. These differences can be used to estimate the exchange fluxes between the two water sources.

One of the first studies to exploit the temperature difference between surface water and groundwater was Suzuki (1960). He estimated the vertical seepage flux into the shallow groundwater system from rice paddy fields by measuring the downward propagation of the diel surface water signal. Soon after, Stallman (1965) and Bredehoeft and Papadopulos (1965) developed analytical solutions to the 1D heat transport equation that enabled estimation of the vertical water flux from vertical temperature profiles, and these have been widely adopted and applied by many authors (Anderson, 2005; Constantz, 2008). Based on the Stallman (1965) equation, Hatch *et al.* (2006) and Keery *et al.* (2007) used a semi–automated approach to filter field data and calculate seepage rates from the phase lag and amplitude of the diel temperature variation. Other authors have applied these approaches using MATLAB routines (i.e. Ex–Stream by Swanson and Cardenas, 2010; VFLUX by Gordon *et al.*, 2012) to allow large datasets to be more easily analyzed.

The majority of studies looking at groundwater–surface water interaction using heat as a tracer have solved for a single vertical flux (i.e. Conant, 2004; Schmidt *et al.*, 2006; Lautz and Fanelli, 2008). However, in a near–stream environment a constant flux with depth is unlikely. For example, in a gaining stream where a pool–riffle sequence induces hyporheic exchange, the vertical flux through the streambed into the subsurface would be

expected to vary both longitudinally (in the direction of river flow) and with depth. The hyporheic flux immediately below the streambed may be downward, whereas an upward flux might occur beneath the base of the hyporheic zone due to a regional groundwater flow system (Figure 2.1). A gradual transition between these two flow systems would also be expected, so that the magnitude of downward flux would decrease gradually with depth to become an upwelling flux in the deeper flow system. Hence the ability of a model to capture variability in the vertical component of flux within a 2D or 3D flow system is important. If each observation depth in a profile was treated independently, the resultant mean vertical flux profile could provide information on changes in the flow system with depth. A number of recent studies have shown variability of vertical flux with depth by applying an analytical solution to sequential pairs of temperature data down a vertical profile (i.e. Swanson and Cardenas, 2010; Vogt *et al*., 2010a; Gordon *et al*., 2012; Briggs *et al*., 2012). The analysis of paired data with depth implies that the flow direction is purely vertical between the two points, which contradicts the conceptual interpretation of a shallow transition from predominantly vertical to predominantly horizontal flow in downwelling hyporheic flow systems.

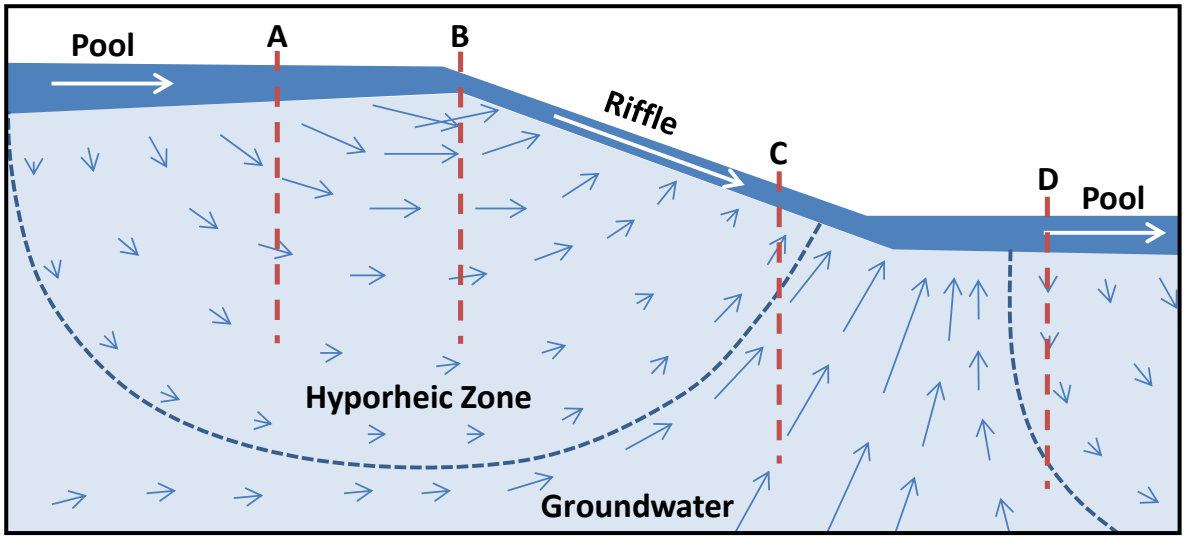

Figure 2.1. A conceptual model of the exchange processes occurring over a pool–riffle sequence longitudinal cross section for a gaining river, including the partitioning between the hyporheic zone and groundwater system. Vertical temperature profiles (red dashed lines) intercept (A) downwelling, (B) neutral, (C) upwelling or convergent and (D) downwelling or divergent flow lines.

Numerical methods for interpreting streambed temperature data are less commonly applied than analytical solutions (Anderson, 2005). Examples of numerical approaches are found in 1D by Lapham (1987) and in 2D using VS2DH or other numerical codes (e.g. Anibas, *et al.*, 2009, Roshan, *et al.*, 2012 or Cuthbert and Mackay, 2013). Heat transport is also included in other commercial groundwater models (e.g. FEFLOW, SUTRA and HYDRUS). Although use of 2D and 3D numerical models would allow vertical variations in flux to be considered, temperature data are usually collected as vertical profiles, and there is often insufficient longitudinal and cross–sectional data to properly constrain a 2D or 3D model of the flow system. Furthermore, most numerical groundwater models also require hydraulic head information and hydraulic conductivity parameters, which are rarely collected in sufficient detail. Although recently these difficulties in data collection have been partially addressed by advancements in measurement techniques using heat pulse probes (Lewandowski *et al.*, 2011) and fibre optic cables (Selker *et al.*, 2006), 1D analytical solutions are still preferred over more complex numerical models due to their simplicity and ease of use.

This study uses vertical temperature profiles to evaluate the vertical distribution of water fluxes beneath a shallow river in northeastern Australia, as a means for understanding pool–riffle scale hyporheic exchange. The 1D heat transport equation is solved numerically, thus avoiding some of the simplifying boundary condition assumptions of analytical solutions. The model is used to examine variations in the vertical component of water flux for each profile, where the mean vertical flux between the river and each observation depth is considered independently. The sensitivity of temperature simulations to mean vertical flux is evaluated using a Monte Carlo analysis, while the error bounds of flux are determined based on temperature measurement error and a range of effective thermal diffusivity values. Our approach is validated by comparison with two 2D flowfields, one with a constant flux upper boundary and the second with a variable flux

upper boundary. We show that the use of a 1D solution allows us to accurately constrain the vertical water flux, but does not provide any information on the horizontal flux. We discuss how vertical fluxes derived using the 1D approach can be conceptualised in terms of hyporheic flowpaths.

2.2. Numerical Modelling Approach

If we are predominantly interested in the vertical component of water flux, a 1D model can sometimes be used. This simplification is possible when the input signal (diel temperature variation in the river) is widely distributed in the horizontal plane. Thus the temperature signal measured below the surface is representative of the travel time from the surface to the observation point, even though we do not know the origin (at the surface) of the flowpath. This approach is used widely for interpreting environmental tracer data to determine groundwater age in unconfined aquifers (e.g., Vogel, 1967; Walker and Cook, 1991). Thus, the vertical distribution of age can be used to calculate the vertical component of the groundwater flux, without the requirement that flow be purely vertical. The vertical component of the groundwater flux will decrease with depth from a maximum value at the watertable, to zero at the base of the aquifer if the aquifer is underlain by an aquiclude or, to a small value if the aquifer is underlain by a leaky aquitard. Alternative flow systems for aquifers with different geometry would be represented by different vertical flux distributions (see Cook and Bohlke, 2000). On the scale of a pool–riffle sequence, information on the vertical temperature variation can be used to provide estimates of vertical flux and therefore provide information about the flow system.

2.2.1. Model Description and Setup

One–dimensional heat transport in a homogenous porous media can be described by the conduction–advection equation:

$$\frac{\partial T}{\partial t} = k_e \frac{\partial^2 T}{\partial z^2} - \frac{q_z}{\gamma}\frac{\partial T}{\partial z} \qquad (2.1)$$

where T is temperature (°C), k_e is effective thermal diffusivity (m^2 day^{-1}), q_z is the vertical water flux ($m\ d^{-1}$), γ is the ratio of the volumetric heat capacity of the saturated sediment to that of water, z is depth (m) and t is time (days). The positive direction for q_z and z is downward into the subsurface. Eq. 2.1 assumes that heat is transported through a representative volume where thermal equilibrium exists instantaneously between the fluid and solid phases and that all terms except temperature are constant both spatially and temporally.

The bulk parameters used in Eq. 2.1 include expressions for gamma (γ) and effective thermal diffusivity (k_e). The effective thermal diffusivity is related to the volumetric heat capacity of the saturated sediments ($\rho_b c_b$), the bulk thermal conductivity (Nield and Bejan, 2006) and thermal dispersivity coefficient (α). Thus the expanded equations:

$$k_e = \frac{K_b}{\rho_b c_b} + \alpha \left| \frac{\rho_w c_w}{\rho_b c_b} q_z \right| \quad (2.2)$$

$$\gamma = \frac{\rho_b c_b}{\rho_w c_w} \quad (2.3)$$

$$K_b = K_w^{\theta} \cdot K_s^{1-\theta} \quad (2.4)$$

$$\rho_b c_b = \theta \rho_w c_w + (1-\theta)\rho_s c_s \quad (2.5)$$

where θ is porosity, ρ is density ($kg\ m^3$), c is specific heat ($J\ kg^{-1}\ °C^{-1}$) and subscripts b, w and s are for the bulk saturated sediment, water and solids respectively, K_b is the bulk thermal conductivity ($W\ m^{-1}\ °C^{-1}$) and α is the thermal dispersivity coefficient (m). Thus Eq. 2.1 includes terms to represent conduction in the solid phase, conduction in the liquid phase and both advection and dispersion in the liquid phase.

There has been discussion in the literature about the influence of thermal dispersion (second term on the right hand side of Eq. 2.2) on heat transport processes as summarised most recently by Rau *et al.* (2014). This term is often neglected or assumed to be small and

incorporated within the bulk value of k_e (as per Eq. 2.2) which includes both conductive and dispersive components (Anderson, 2005). Rau *et al.* (2012) has shown that for a wide range of water fluxes, thermal dispersion can be neglected when heat transport is dominated by conduction (i.e. thermal Peclet number < 0.5). In the field component of this study, the mean grainsize of the river sands is conservatively 0.003 m which means that the thermal Peclet number is < 0.5 for all q_z values (with one exception). Hence, we have not directly applied or further discussed the thermal dispersion term in this study. The heat parameters used in Eq. 2.1 (k_e and γ) are typically estimated or derived from the literature (e.g. in Lunardini, 1981 or Carslaw and Jaeger, 1959) but can also be measured in sediment samples. We have approximated k_e and γ using experimentally derived relationships developed by Lunardini (1981) as presented in Figure 2 of Lapham (1987) for coarse grained sediments, similar to those found at our study site.

The numerical approach used in this study is a finite differencing approximation of Eq. 2.1 and takes the form:

$$T_i^{n+1} = \frac{k_e \Delta t}{(\Delta z)^2} (T_{i+1}^n - 2T_i^n + T_{i-1}^n) - \frac{q_z \Delta t}{\gamma \Delta z} (T_i^n - T_{i-1}^n) + T_i^n \quad (2.6)$$

where Δz is the distance between nodes (m), Δt is the elapsed time between time steps (days), T is temperature (°C) with subscripts *i–1*, *i* and *i+1* referring to spatial nodes and the superscripts *n–1*, *n* and *n+1* referring to time steps. This finite differencing scheme keeps all parameters except temperature constant with depth. The advection term varies with the flow direction so that for upward q_z the $(T_i^n - T_{i-1}^n)$ term is replaced by $(T_{i+1}^n - T_i^n)$ while for downward q_z the advection term is as written in Eq. 2.6. The spatial and temporal discretisation was chosen so that the numerical scheme was stable and numerical dispersion minimised. This was achieved by decreasing spatial and temporal discretisation until the simulated temperatures did not appreciably change and additionally, by applying

stability criteria of $\frac{a^2-a}{2} \leq k_e \frac{\Delta t}{(\Delta z)^2} \leq \left(\frac{1-a}{2}\right)$ where $a = \frac{q_z}{\gamma}\frac{\Delta t}{\Delta z}$ (after Dehghan, 2004). The numerical dispersion for this numerical scheme was calculated using $\frac{q_z \Delta z}{2\gamma}(1-a)$ and discretization adjusted so that this value was far smaller than the effective thermal diffusivity term (after Dehghan, 2004). For most simulations the model spatial discretisation was 0.01 m and the temporal discretisation was 0.0001 days but both were made smaller for q_z > 1 m d^{-1}. The upper temperature boundary (i = 0) is a specified temperature signal that represents the river. The lower temperature boundary was modelled as a constant temperature at a depth of 5 m. For upwelling profiles, this was the mean temperature at the deepest observation point. For downwelling profiles, the mean temperature of surface water observations was used and did not influence temperatures in the areas of interest (from the surface to 2 m).

The time variable temperature signal for each observation depth was modelled in an independent simulation with all other parameters held constant with depth. Because each observation depth was modelled with an independent simulation, the resultant flux profile represents the mean vertical flux of the water travelling from the surface to each observation depth. To determine this value the parameter estimation software PEST was used (Doherty, 2010). PEST iteratively varied q_z to best fit the temperature observation data at selected observation times by minimising the sum of the squared differences between observed and simulated temperature data.

2.2.2. Comparison with Two 2D Flowfields

To validate the 1D representation of a 2D flowfield for heat transport, two 2D models were constructed in HYDRUS 2D (Simunek *et al.*, 1999), a finite–element software package that simultaneously solves the heat and water transport equations. Both models were 20 m wide and 4 m deep with no flow boundaries on the left hand side and bottom. A hydraulic conductivity of 28.8 m d^{-1} was used to allow a diel temperature signal boundary

at the surface to be transported vertically and horizontally into the model (all simulations use a sinusoidal diel temperature signal with amplitude of 3 °C). The heat transport parameters were made to be equivalent between the HYDRUS 2D models and the 1D model (porosity = 0.35, k_e = 0.046 m^2 day^{-1}, γ = 0.82) so that mean vertical fluxes could be compared directly. HYDRUS 2D mesh discretization was refined to ≤ 0.02 m for the top 1 m and ≤ 0.05 m for the remainder of the model domains to ensure numerical dispersion was small. Synthetic temperature observation data from the HYDRUS 2D models were exported from appropriate depths to be used as observations in the 1D model to calculate the vertical flux to that point. Profiles of the vertical component of flux were also extracted from HYDRUS 2D for comparison with the 1D model vertical fluxes.

The first model was designed to determine whether the temperature signal output at depth from a simple 2D flowfield could be matched using our 1D model with the same vertical flux values. The model had a constant flux of 1 m d^{-1} applied to the surface and a constant head boundary on the right hand side (Figure 2.2A). A diel sinusoidal temperature signal was applied at the upper boundary with a third type temperature boundary on the right hand side of the model. In this model the vertical component of flux decreases linearly with depth and the vertical flux profile does not vary spatially, except for very close to the boundaries. The horizontal component of flux increases linearly from left to right in this model (Figure 2.2B). We constructed vertical profiles of temperature observations at x = 2, 6, 10 and 14m from the left hand boundary with observation nodes at 0.1, 0.3, 0.5, 1.0 and 1.5 m below the surface. The temperature time series observations for the same depth from each of the respective profile locations were identical (to within rounding error 0.001 °C), as were the vertical flux profiles taken at the same x locations, despite the water having travelled different horizontal distances. The vertical flux profile calculated from the synthetic temperature observations using the 1D model accurately matched the profiles of mean vertical flux in the HYDRUS 2D simulation (Figure 2.2C).

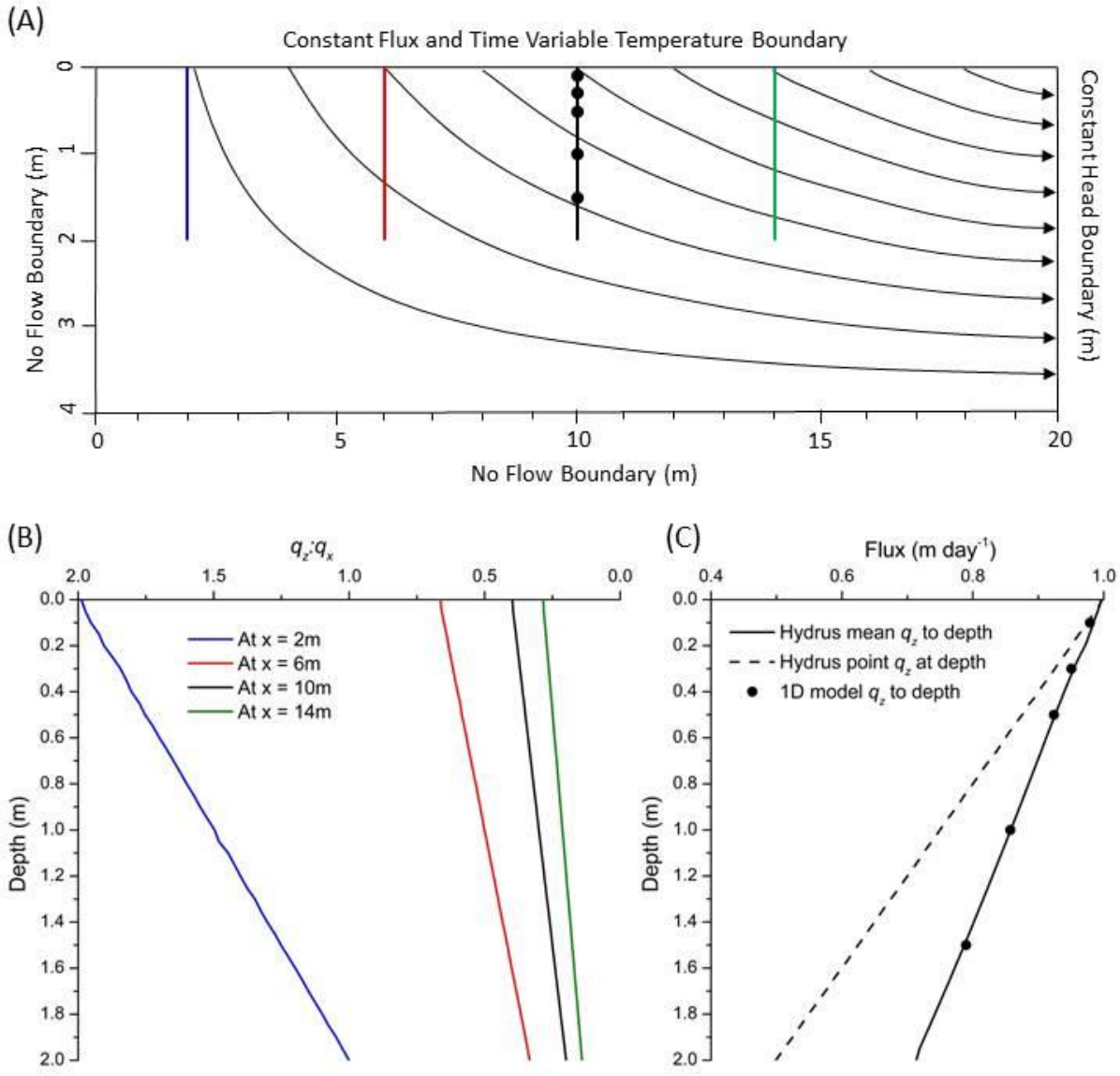

Figure 2.2. Comparison of vertical fluxes based on 1D and 2D models. (A) Calculated flowpaths from the HYDRUS 2D simulation with constant upper boundary flux of 1 m d^{-1}. (B) The flux ratio between vertical and horizontal components for flux profiles taken from x = 2, 6, 10 and 14 m, showing that the horizontal component increases towards the right hand boundary. (C) The vertical fluxes calculated by applying the 1D model to the temperature data extracted from HYDRUS 2D at x = 10 m are compared to the vertical flux profile derived from HYDRUS 2D. The 1D model matches the HYDRUS 2D mean flux profile and thus is representative of the integrated vertical component of flux along a flow path.

The second model represented an idealised pool–riffle sequence where the flux was variable across the upper boundary (Figure 2.3A). The right hand boundary was no flow and a specified head (h) was applied at the surface, decreasing linearly from h = 4 m at the left hand boundary to h = 2 m at the right hand boundary. Three vertical profiles of temperature observations over time were exported from the downwelling (left) side of the

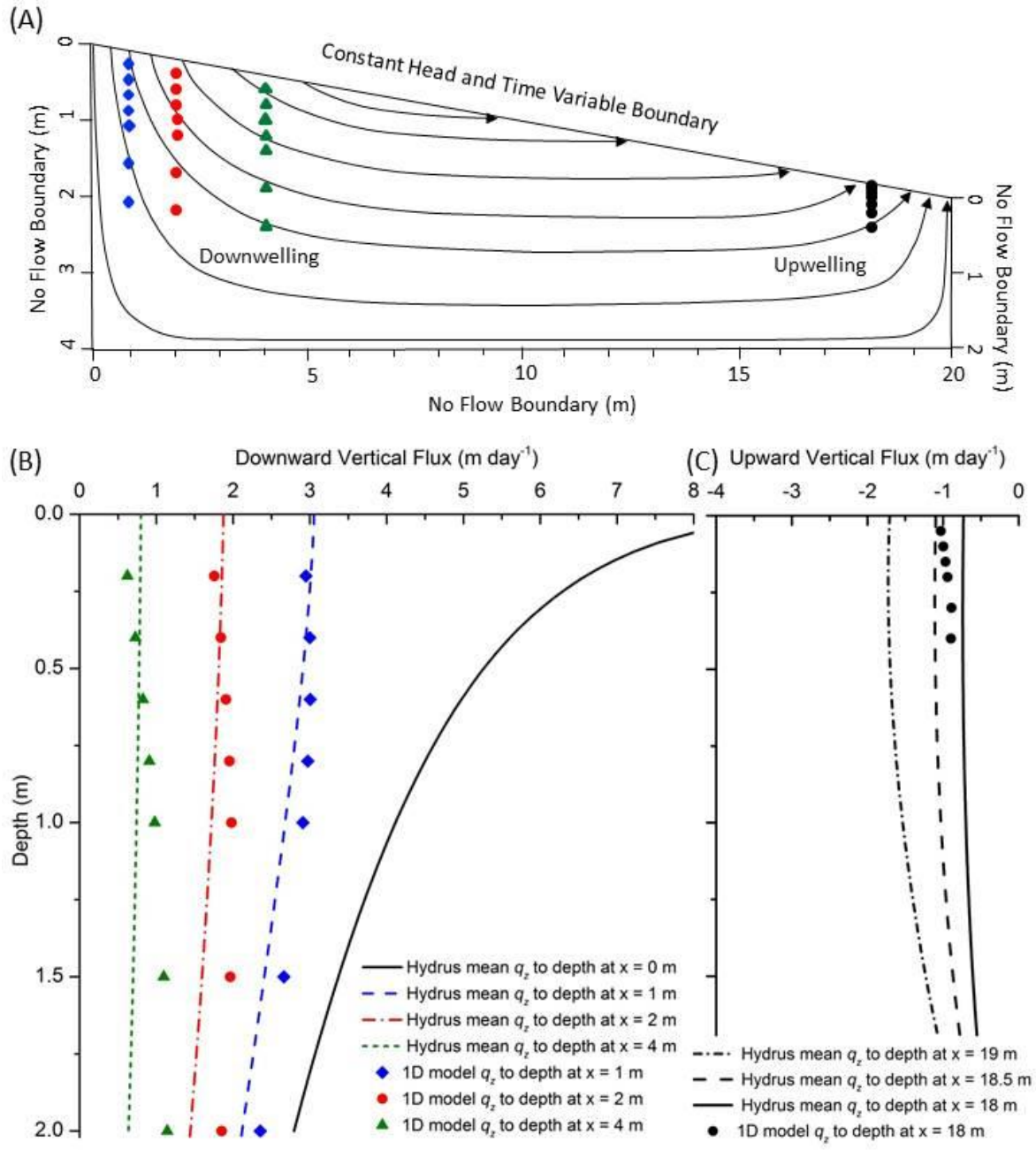

Figure 2.3. Comparison of vertical fluxes based on 1D and 2D models. (A) Calculated flowpaths from the HYDRUS 2D simulation with variable upper boundary flux. For this simulation a specified constant head was applied to the top surface from 4 m elevation on the left, sloping linearly to 2 m elevation on the right, representing a river boundary with variable downwelling and upwelling fluxes. (B) The vertical fluxes calculated by applying the 1D model to the temperature data extracted from HYDRUS 2D are compared to the vertical flux profile derived from HYDRUS. (C) The upwelling vertical flux profiles calculated by applying the 1D model to the temperature data extracted from HYDRUS 2D at 18 m are compared to the vertical flux profile derived from HYDRUS. Fluxes could not be determined between depths where synthetic temperature data had no diel signature or difference in temperature. Constant temperatures were observed below 0.4 m and so only six 1D numerical model-derived fluxes are shown in (C).

model at x = 1, 2, and 4 m from the left hand boundary at vertical depths of 0.2, 0.4, 0.6, 0.8, 1.0, 1.5 and 2.0 m below the surface. One vertical profile was exported from the

upwelling (right) side of the model at x = 18 m, at vertical depths of 0.05, 0.1, 0.15, 0.2, 0.3 and 0.4 m below the surface (Figure 2.3). The synthetic temperature data extracted from HYDRUS 2D were then simulated for each profile using the 1D model to estimate the mean vertical water flux from the surface to each depth.

At shallow depths, the vertical fluxes obtained from the 1D model at the downwelling location were similar to the HYDRUS 2D mean vertical fluxes at the same location (Figure 3B). However, at greater depths the fluxes from the 1D model plotted to the right of the HYDRUS 2D mean flux profiles for the same x location and were similar to upgradient fluxes (Figure 2.3B). This makes sense conceptually, since the temperature observations at a point in a profile should be representative of the integrated temperature signal of a parcel of water after it has travelled from the surface to the observation point within the aquifer (i.e. along a flowpath). Flowpaths that originate upgradient carry the surface water temperature signal downward more rapidly in this flowfield because they experience higher vertical fluxes. Thus, vertical profile measurements made at a particular downwelling location are unlikely to represent the fluxes only at that location, but rather represent the flow conditions along a flowpath originating some distance upgradient. This distance depends on the horizontal component of flux.

At the upwelling location, diel variations in temperature propagated downward to only 0.4 m depth. Although the profile location is at 18 m, the vertical fluxes obtained from the 1D model were more representative of those at 18.5 m at shallow depths (Figure 2.3C). In this case it appears that the downgradient temperatures have influenced the temperatures at 18 m through horizontal conduction rather than advection. Similar to the downwelling profile, a flux determined using subsurface temperature measurements is unlikely to be purely representative of the flux at that location but rather is influenced by surrounding heat transport processes.

2.3. Field Application

2.3.1. Location

The Haughton River is located approximately 100 km south of Townsville in the tropical northeast of Australia (Figure 2.4) and receives approximately 1200 mm of precipitation per year (BoM, 2012). The river is highly seasonal, with mean dry season (May to October) flows of 2 $m^3 s^{-1}$ and mean wet season (November to April) flows of 25 $m^3 s^{-1}$. The median wet season peak flow rate is 725 $m^3 s^{-1}$ with the highest recorded flow of 2200 $m^3 s^{-1}$ (DERM, 2012). In the dry season however, the upper Haughton River flows as a narrow and shallow meandering or braided river (< 30 m width and < 0.5 m depth) with some pool–riffle sequences that are contained within a wide sandy alluvial channel. Adjacent to the alluvial channel are other Late Tertiary to Quaternary alluvial sediments containing interbedded sands, clays, silty sands and silty clays. Underlying these sediments is igneous bedrock, which also outcrops in the hills to the north and upper catchment to the northwest. The river is thought to be primarily gaining due to its largely perennial nature and the high precipitation within the catchment. Losing reaches are expected to occur locally during the sugar cane irrigation season, when groundwater is heavily pumped from the alluvial aquifer. In addition to natural dry season flows, it is common for flow to be augmented by diversions from the nearby Burdekin River to supply downstream irrigators.

2.3.2. Data Collection

A four day field campaign was conducted along a 300 m reach of the upper Haughton River in late September 2011. At gauging station 119003a (located approximately 300 m downstream from the study site) the river level had been relatively constant (Figure 2.5) with flows <2 $m^3 s^{-1}$ for the previous 4 months (DERM, 2012). During the study period there was a gradual increase in river stage before a relatively rapid decrease (stage level from 0.64 to 0.67 m then down to 0.60 m above the reference elevation). This rapid fall in river stage was most likely due to a decrease or shutting off of upstream river

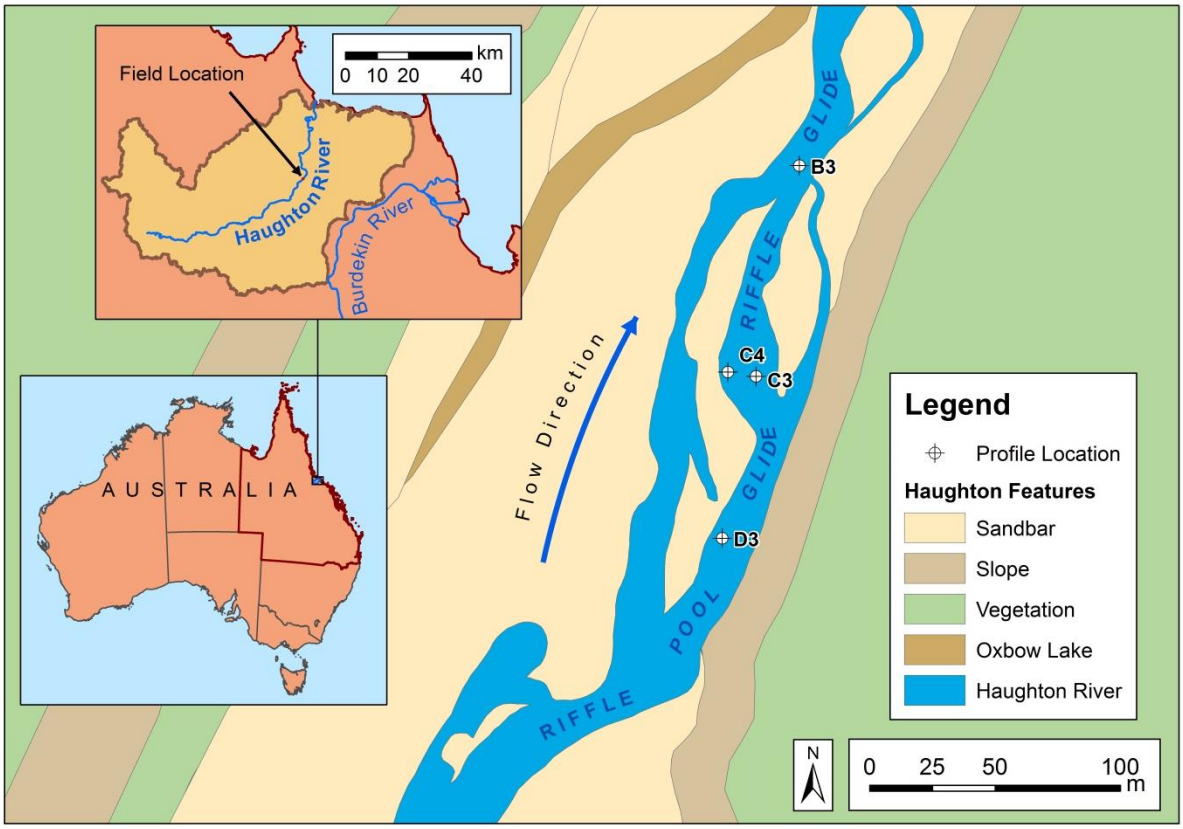

Figure 2.4. Overview of the study reach showing profile locations and generalised descriptions of the nature of flow in the river. Other land features are also shown including the extent of the sandy channel and adjacent slopes and tropical scrub vegetation. Additional profile locations that complete the three cross sections are not displayed as their data is not presented here (see Cranswick *et al.*, Submitted (2014) for further analysis).

augmentation from the Burdekin River. The mean river discharge was 1.09 m^3 s^{-1} for the time period before the decrease in stage occurred. The selected site contained an upper pool followed by a split riffle that converged as the river gradient flattened. Across the study site, the depth of water varied from 0.5 m in the slower pools to <0.1 m across riffle sections, and riverbed sediments consisted of relatively homogenous medium to coarse grained sands with some small cobble armouring present on the riverbed surface across the faster flowing sections.

Three cross sections were established perpendicular to the flow direction: across the upper pool, at the head of the riffle below the pool, and at the tail of the same riffle (Figure 2.4). Thermochron iButton© thermistors (Maxim Integrated, San Jose CA) were installed at depths of 0.0, 0.05, 0.1, 0.15, 0.2, 0.3, 0.4 (or 0.45), 0.6, 0.8 (or 0.75), 1.0 (or 0.9) and 1.2 m below the streambed at each of 12 locations, and recorded streambed temperatures

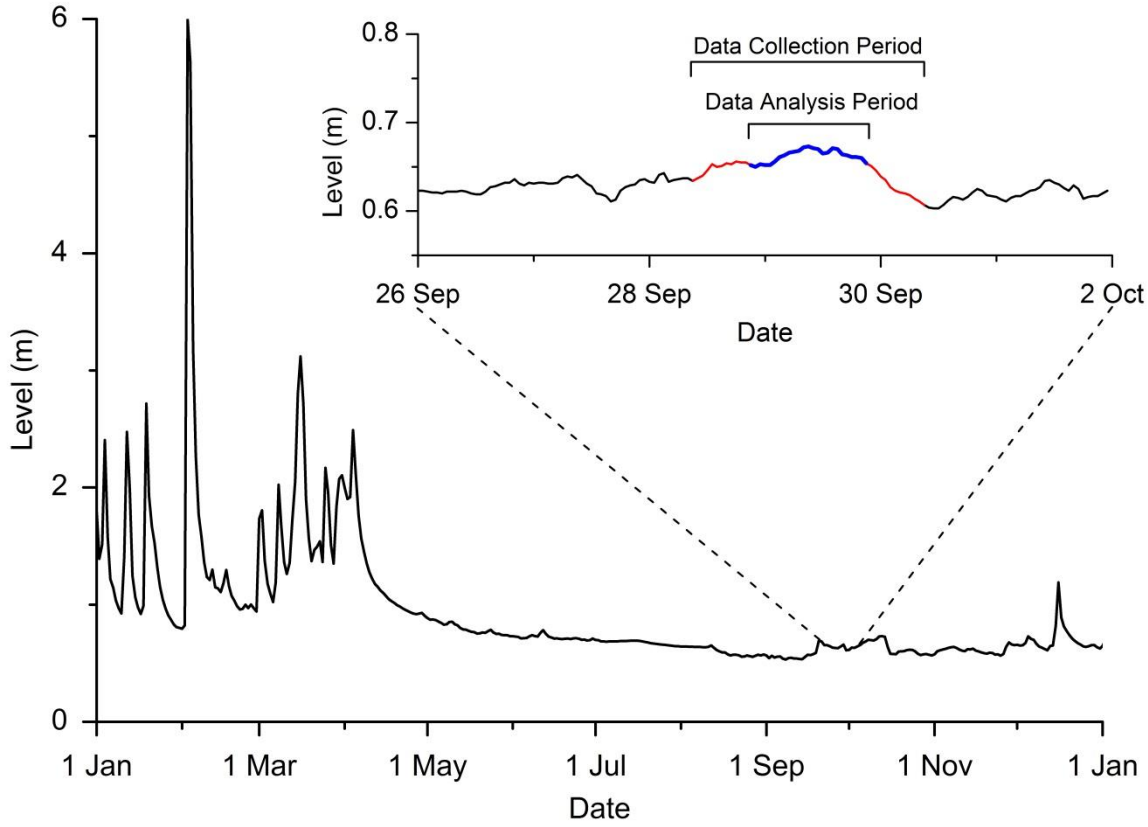

Figure 2.5. Hydrograph from river gauge (119003A) approximately 300 m downstream of the study reach, showing historical river stage with typical seasonal variation between the wet season (November to April) and the dry season (May to October). Inset hydrograph shows the river stage variation at the time of the field campaign and specifically the 48 hours of data collected (red line) and the 24 hour interval over which the temperature data was analysed (blue line).

for 2 days at 5 minute intervals. Four of these temperature profiles are presented in this paper to demonstrate a range in temperature profile behaviour along a pool–riffle sequence: profiles C3 (strongly downwelling), B3 (strongly upwelling) and C4 and D3 (neither strongly upwelling nor downwelling). The thermistors were installed by driving a 0.025 m steel pipe with disposable tip into the sediments to the desired depth, placing a 0.015 m diameter plastic rod (with thermistors inset) into the pipe and then gently removing the steel pipe while keeping downward pressure on the plastic rod. The thermistors have a reported accuracy of ± 0.2 °C and a resolution of 0.0625 °C. All thermistors used in the field were post calibrated in a water bath over a similar temperature range as those observed over the study period. The temperature data from the 132 thermistors used in the field were then compared with three NIST-certified thermistors in a

calibration bath. The mean residual between the 132 thermistors and the mean of the three NIST-certified thermistors was 0.039 °C with a standard deviation of 0.091 °C (n = 23100).

At each site, drivepoint piezometers (with 0.05 m slotted screens) were temporarily installed at 1.2 m depth. Vertical hydraulic head gradients (*dh*) were measured between the surface water and the piezometer screen depth using an air–water manometer (after Winter *et al.*, 1998). The site was surveyed to evaluate the gradient of the riverbed. Sediment cores from the riverbed were collected using a 44 mm Undisturbed Wet Soil Sampler (Dormer Engineering, Murwillumbah South NSW), to later measure porosity and bulk density. Hydraulic tests were conducted to estimate the hydraulic conductivity of the alluvial sediments.

2.3.3. Model Setup and Implementation

The observed river temperature data at each profile location provided the upper temperature boundary condition for that profiles simulations. Because only two days of temperature data were collected (from 9 AM 28 September 2011 to 9 AM 30 September 2011), these short river data sets were repeated six times to allow for spin-up in the numerical model, minimizing the influence of initial conditions. The first 0.5 days of temperature observations showed some unexpected behaviour (i.e. sharp changes in temperature), thought to be due to the disruption of the temperature profile when installing the thermistors. Also, a drop in stage over the last 0.5 days of the dataset was seen to influence the nature of temperature signal propagation. These two time periods were therefore not used for model calibration. The central 1 day period (9 PM 28 September 2011 to 9 PM 29 September 2011) was considered to be at steady state hydraulically (i.e. little change in river stage) and the temperature observations at depth for this period were used in the PEST optimization. We assume that heat parameters k_e and γ are constant with

depth, and these values are fixed for all simulations, with the exception of those run for the Monte Carlo analysis where the values are varied between simulations.

To quantify the sensitivity of the modelled temperature signal to model parameters, a Monte Carlo analysis was applied for each temperature simulation using a range of q_z and k_e values. Two thousand combinations of random numbers between set ranges were used to determine the relationships between the root mean square error (RMSE) and the values of q_z and k_e. A uniformly distributed set of random values of k_e were generated between ±50% of the k_e value estimated from field measurements of sediment bulk density and porosity. Uniformly distributed random values for q_z were generated with an initial range between 15 and –5 m d^{-1}. It was clear from the relationship between RMSE and q_z that the upper and lower error bounds of q_z should be thought of separately since the RMSE versus q_z curve was not symmetrical. Additionally, some scatter was observed in this curve because the q_z values were paired with randomly generated k_e values. The uncertainty of the true k_e value was thus incorporated into the relationship between RMSE and q_z. For consistency, an observation error of 0.091º C (standard deviation of field thermistors compared with NIST certified thermistors during calibration, see Data Collection) was added to the minimum RMSE and all values of q_z that fell within this range were considered plausible values. In order to accurately resolve the error bounds, the range of random q_z was subsequently narrowed to better define the relationship between RMSE and q_z, The Monte Carlo analysis was then run a second time for each observation depth of each profile (i.e. a further 2000 simulations using random q_z and k_e to simulate the temperature signal at each observation depth). Hence the upper and lower bounds of plausible q_z values could be identified as shown in the two example depths of Figure 2.6.

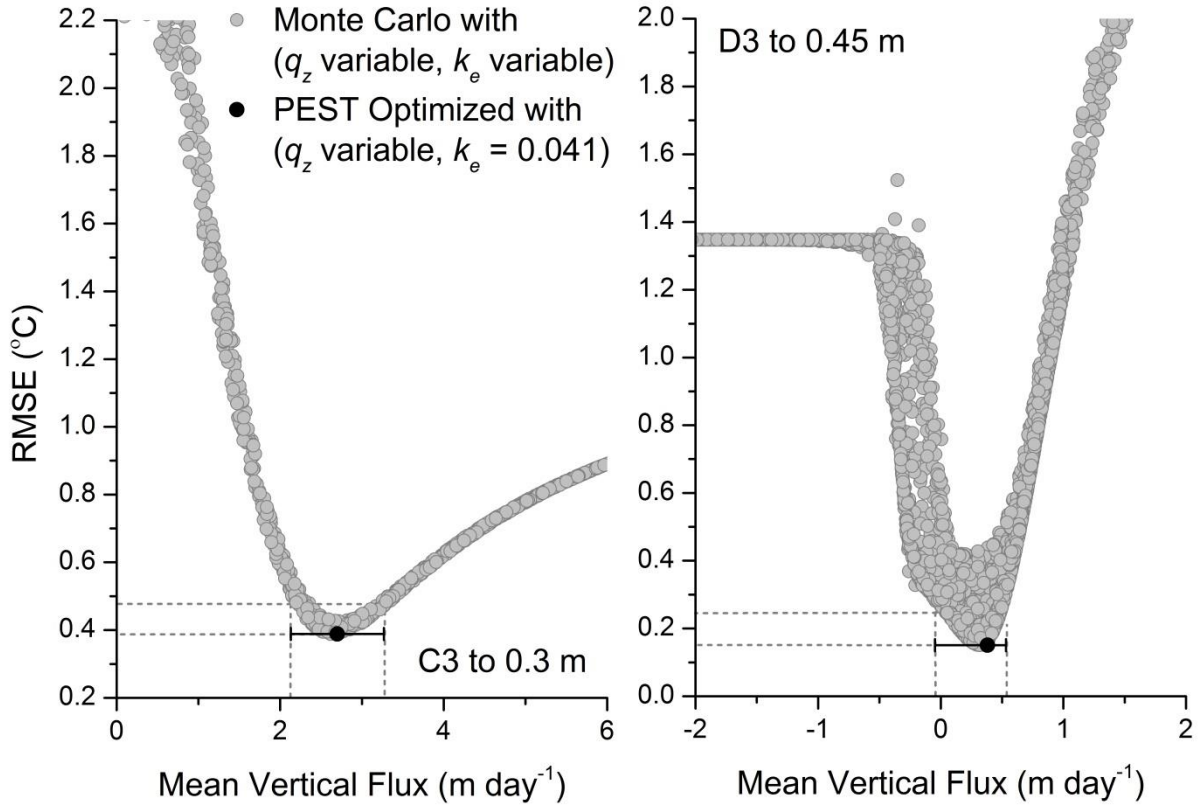

Figure 2.6. The relationship between RMSE and q_z is shown for the temperature observation data at 0.3 m of the downwelling profile C3 and at 0.45 m of the close to neutral profile D3. It is clear that the temperature simulation is more sensitive to variation of k_e for the D3 profile as there is less scatter in the RMSE vs q_z relationship. This is due to smaller vertical flux in the D3 example and hence greater importance of conduction. Upper and lower error bars represent the range of q_z values for which the RMSE is within 0.091 °C of its minimum value. These error bars represent the range of plausible mean vertical fluxes between the river and this depth.

2.4. Results

Profiles C3 (downwelling), B3 (upwelling) and C4 and D3 (close to neutral) had vertical hydraulic gradients of 0.027, –0.015, –0.002 and –0.001 respectively (Table 2.1). Hydraulic tests conducted in the near river sediments resulted in a mean hydraulic conductivity (K) of 91 m d^{-1} and standard deviation of 44 m d^{-1} (n = 25). The mean hydraulic conductivity and the observed vertical hydraulic gradients together imply vertical fluxes ranging between approximately 2.4 and –1.4 m d^{-1} (using Darcy's Law for C3 and B3 hydraulic gradients). Sediments collected from the core samples had a mean porosity of 0.34 and a mean dry bulk density of 1.28 g cm^{-3} (n = 3). The magnitude of the diel temperature variation in the river at these profile locations ranged from 8.48 °C at C3, to

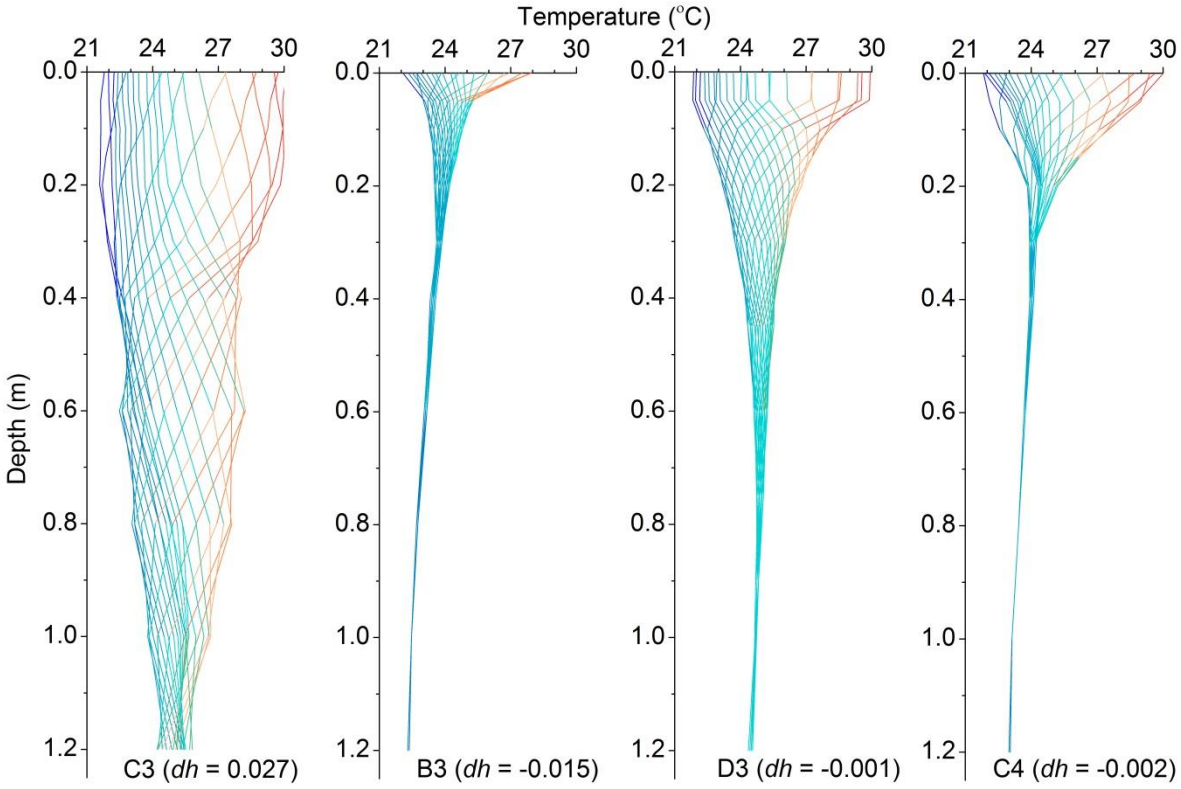

Figure 2.7. Temperature envelopes for profiles C3, B3, D3 and C4 where each of the 24 lines shows the temperature profile each hour over the 24 hours of analysed data. The left skewed profiles are indicative of the duration of colder temperatures being greater than that of warmer temperatures. The hydraulic gradient (*dh*) was measured between the river and 1.2 m below the riverbed; a negative sign indicates an upward gradient and a positive sign indicates a downward gradient.

6.12 °C at B3. At profile C3, the diel temperature signal from the river was seen to propagate rapidly into the subsurface and beyond the deepest measurement depth, suggesting the presence of a large downward flux (Figure 2.7). Conversely, the diel temperature signal at profile B3 was considerably damped with depth as might be expected for an upwelling profile. In profile C4, the river temperature signal was transferred to a depth of 0.10 m with little attenuation but was considerably damped at greater depths. The diel temperature signal at profile D3 decreased in amplitude with depth and became almost constant below 0.8 m.

2.4.1. Single Vertical Flux Approach

Using the mean dry bulk density of our sediments (1.28 g cm^{-3}) we estimated heat parameter values of k_e = 0.041 m^2 day^{-1} and $\gamma = 0.81$ (after Lapham, 1987) and these

values are used in the numerical model. The model was first run to optimise a single q_z value for each profile that best fit the temperature observations from all depths. This is a common approach when limited depth observations are collected or when a single flux is considered representative of the groundwater–surface water exchange. The optimised vertical fluxes for C3, B3, C4 and D3 were 1.35, –0.04, –0.03 and 0.49 m d^{-1} respectively, and resulted in relatively poor fits to the observed temperature data for all profiles (RMSE for all depths of 1.368, 0.314, 0.752 and 0.696 °C for C3, B3, C4 and D3 respectively) (Table 2.1). Although these single flux estimates were similar in magnitude and general trend to the mean of the multiple fluxes (see below), they do not provide information on the nature of the exchange (i.e. small scale differences in vertical flux due to converging or diverging flow systems). In the following, we consider only the model results where each observation depth was treated independently to allow vertical flux profiles to be presented.

Table 2.1. Head gradients, optimised mean vertical fluxes and RMSE for each profile location.

	Multiple Independent Fluxes					Single Flux	
	dh	$q_{z\,max}$ (m d^{-1})	$q_{z\,min}$ (m d^{-1})	$q_{z\,mean}$ (m d^{-1})	RMSE (° C)	q_z (m d^{-1})	RMSE (° C)
C3	0.027	5.69	0.91	2.68	0.297	1.35	1.368
B3	–0.015	–0.17	–0.04	–0.07	0.070	–0.04	0.314
C4	–0.002	0.83	–0.12	0.08	0.241	–0.03	0.752
D3	–0.001	42.3	0.08	0.39*	0.196	0.49	0.696

* Mean vertical flux calculated excluding the high value from 0 to 0.05 m.

Values for all simulations for k_e and γ were approximated to be 0.041 m^2 day^{-1} and 0.81 respectively, based on a porosity of 0.34 and dry bulk density of 1.28 g cm^{-3} (n = 3) for the Haughton River alluvial sediments (after Lunardini, 1981). The hydraulic gradient (*dh*) was measured between the river and 1.2 m below the riverbed; a negative sign indicates an upward gradient and a positive sign indicates a downward gradient.

2.4.2. Vertical Flux Patterns with Depth

When the vertical flux value was optimised for each depth independently, the combined RMSE of each profile was much lower compared to using a single vertical flux and showed good fits for each depth of the four profiles (Figure 2.8).The combined RMSE for

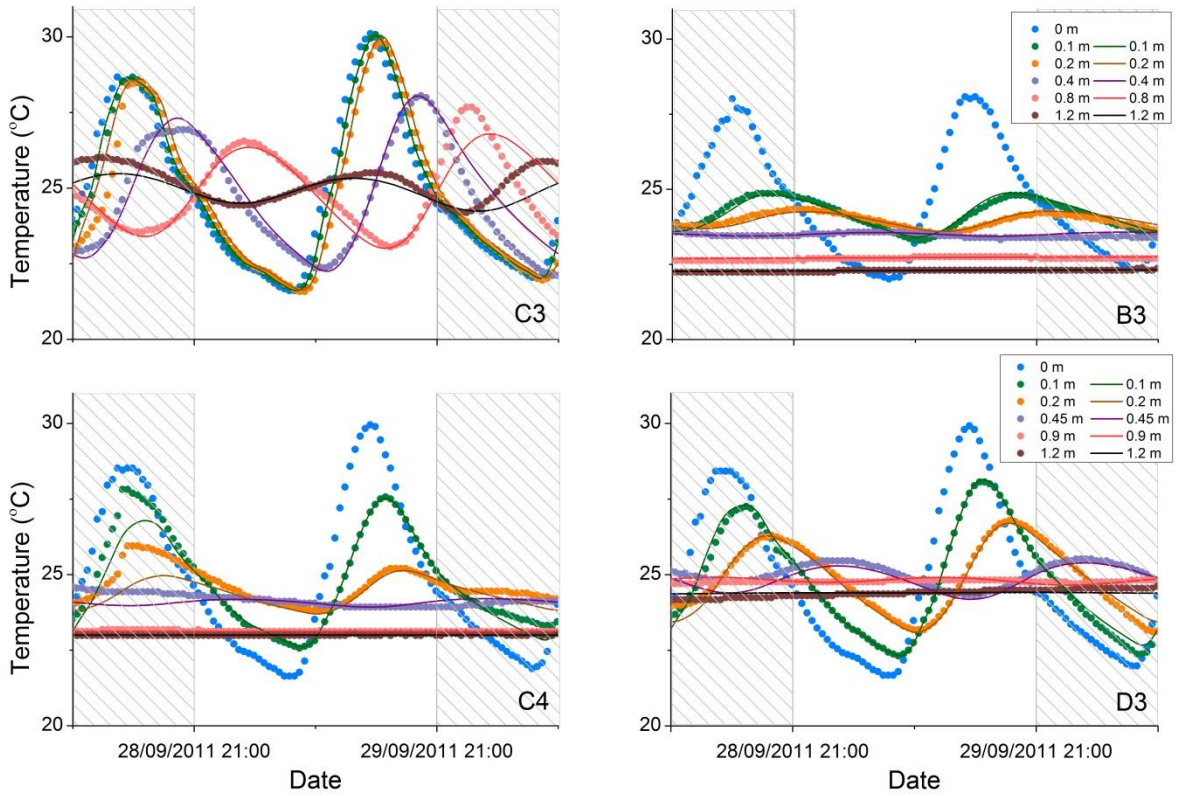

Figure 2.8. Time series data for observed (circles) and modelled (lines) temperature profiles from C3, B3, C4 and D3 locations. The first and last 0.5 days of the dataset (hatched grey) were not used for the optimization of q_z because the profile was disrupted upon installation and hydraulic conditions were changing respectively. Modelled lines for 0 m depth are not displayed as the observation temperatures displayed were used as the model temperature boundary condition at 0 m. The legend for B3 applies also to C3 while the legend from D3 applies to C4 due to different depths of observation.

all depths in each profile was 0.297, 0.070, 0.241 and 0.196 °C for C3, B3, C4 and D3 respectively (Table 2.1). The optimised values of q_z ranged from 5.69 m d^{-1} (downward) to –0.17 m d^{-1} (upward), with the exception of a high downward flux of 42.3 m d^{-1} between the surface and 0.05 m at D3 (Table 2.1).

Profile C3, located at the head of a riffle, was a downwelling flow system (based on the measured head gradient) where the vertical component of flux was seen to dramatically decrease with depth (Figure 2.9). This is consistent with our conceptual model for the downwelling section of a pool–riffle sequence (Figure 2.1). If the deeper vertical fluxes became constant with depth, they might represent the net loss from the river (i.e. losing

river). However, because the fluxes continued to decrease with depth, we suggest that these measurements capture and represent hyporheic exchange only. The hyporheic zone at this location is therefore deeper than 1.2 m.

At the tail of the riffle where upwelling was expected (based on a measured upward head gradient), profile B3 displayed relatively constant temperatures at depth and a damped shallow temperature variation. The resultant fluxes were weakly upward or neutral with the largest upwelling flux of –0.17 m d^{-1} from 0.05 to 0 m (Figure 2.9). Using temperature data alone at this scale of measurement (i.e. 1.2 m depth below streambed), it was not possible to determine whether this upwelling flux was from groundwater or a long hyporheic flowpath (since both would be expected to have a relatively constant temperature signal).

Profile D3 was located in a slow moving glide just upstream from the top of the riffle where a neutral or slightly downwelling flux profile was expected. An almost constant downward mean flux of 0.39 m d^{-1} was estimated, excluding the very high downward flux of 42.3 m d^{-1} from 0 m to 0.05 m (Figure 2.9). It is possible that the apparent high flux from the surface to 0.05 m was due to a rapid current driven hyporheic exchange (a flux of 42.3 m d^{-1} appears plausible for medium–coarse grained sands with a mean hydraulic conductivity of 91 m d^{-1}). While observed downward hydraulic gradients across the site ranged from 0.002 to 0.027 (between surface water and 1.2 m below the riverbed), higher pressure gradients are plausible close to the riverbed surface. It is unclear why such a rapid shallow exchange was not observed elsewhere.

Profile C4 represents a convergent flow system with a temperature signal propagating rapidly downward from the surface to 0.15 m, but with apparent upward fluxes from greater depths (Figure 2.9). It is possible that this is an example of a shallow (0 – 0.15 m) current driven hyporheic exchange overlying an upwelling section of a larger scale

(deeper) flowpath. This variation in flux direction demonstrates the importance of detailed vertical measurements with depth, as the shallow data indicated downwelling while the deeper data indicated upwelling fluxes.

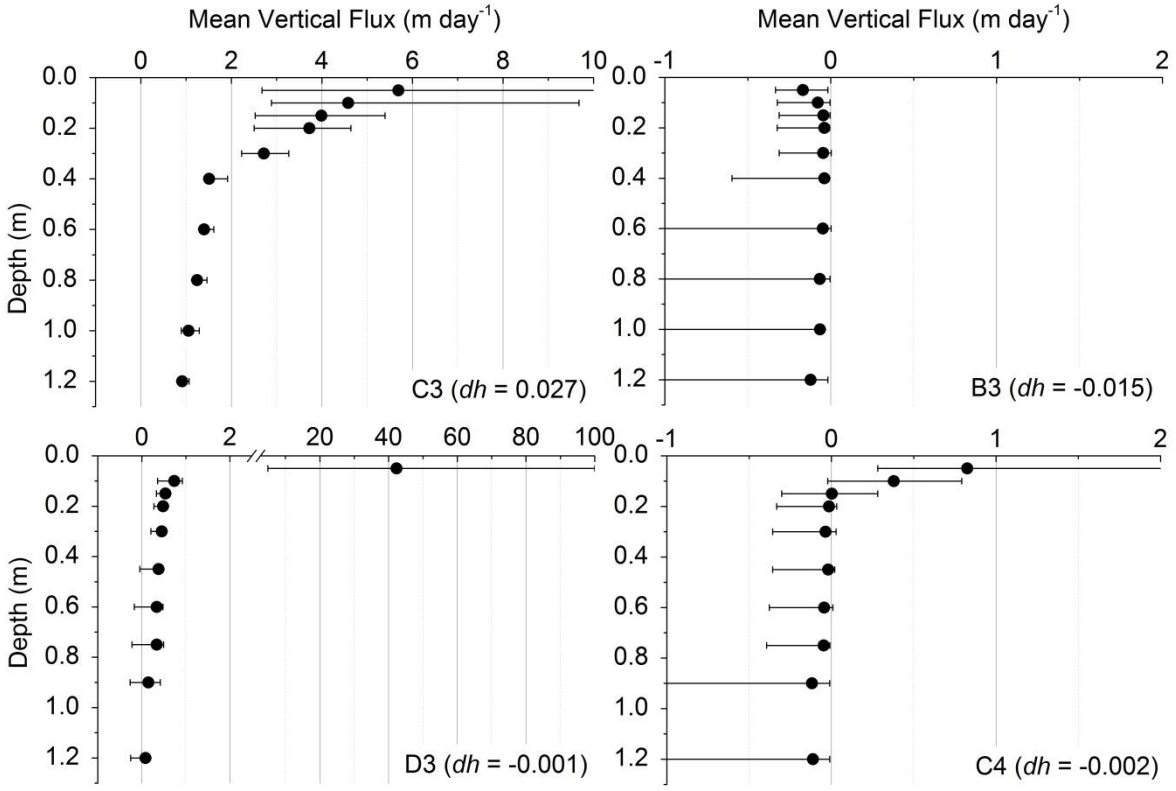

Figure 2.9. The mean vertical flux from the surface to each observation depth using the 1D numerical model to best fit the 24 hours of temperature data analysed. Error bars on the numerical model fluxes are the upper and lower q_z that lie within 0.091 °C (standard deviation of temperature calibration measurements) of the minimum RMSE from the Monte Carlo analysis for each depth of observation. Note that the positive sign indicates a downward flux while the negative sign indicates an upward flux and additionally that there are different x–axis scales between profiles to better show the variation of flux and error ranges. The hydraulic gradient (*dh*) was measured between the river and 1.2 m below the riverbed; a negative sign indicates an upward gradient and a positive sign indicates a downward gradient.

2.4.3. Error Analysis of Vertical Fluxes with Depth

Error bounds for vertical flux estimates have been derived by considering temperature measurement error and the uncertainty of k_e values. Although they do not include other possible sources of uncertainty (e.g. non-steady state flowfield or spatial variability of parameter values), they provide an indication of the accuracy of the estimated fluxes. The error associated with each optimised flux generally increased with increasing flux magnitude (Figure 2.10). Most downward fluxes had smaller errors than their flux values

(plotting below the 1:1 line) while upward fluxes generally had larger errors relative to their values (plotting above the 1:1 line). The data presented in Figure 2.10 separates the error bars extending from the optimised flux value towards zero (solid symbols) from those away from zero (hollow symbols). This is important for a number of observation depths where one of the error bars crossed zero and hence the direction of the flux is uncertain (all solid symbols plotting to the left of the 1:1 line). Generally this occurred for approximately half of the fluxes smaller in magnitude than 0.3 m d^{-1} (both upward and downward). This is particularly apparent for the slowly downwelling profile D3, where the vertical flux error crossed zero for each of the five depths that were deeper than 0.3 m below the riverbed (Figure 2.9). A potential explanation for these error bars crossing zero is the incorporation of a wide range of k_e values during the Monte Carlo analysis where the higher k_e values would have enhanced the conductive component of heat transport (i.e. the upper bound of k_e values was 0.062 m^2 day^{-1} compared to the mean value of 0.041 m^2 day^{-1}). This can be seen in the scatter of the relationship between RMSE and q_z for D3 to 0.45 m, where the error bound crosses zero (Figure 2.6). In contrast the relationship between RMSE and q_z for C3 to 0.3 m is more clearly defined. This shows that the magnitude of the conduction term becomes less important for evaluating high fluxes than for evaluating low fluxes.

Errors that extend from the optimised flux value away from zero (hollow symbols), were greater than the magnitude of their respective flux values when the fluxes were less than approximately 0.3 m d^{-1}. For example, each of the upward flux estimates from the lower depths of profiles B3 and C4 had large errors away from zero (Figure 2.9) meaning that the magnitude of the upward flux could not be well constrained. This was a result of the insensitivity of the temperature signal to changes in flux because of the small differences in temperature with depth. Similarly, for some of the larger downwelling fluxes, an increase in the magnitude of flux had little effect on the RMSE because the difference in the temperature signal between the surface and the observation depth was

very small. When all data is considered together, relative errors range from 5% to >1000%, although large relative errors are mostly associated with small estimated flux values. The lowest errors are found for fluxes between 0.3 and approximately 6 m d^{-1}. Outside of this range, errors are always >50% of the flux value.

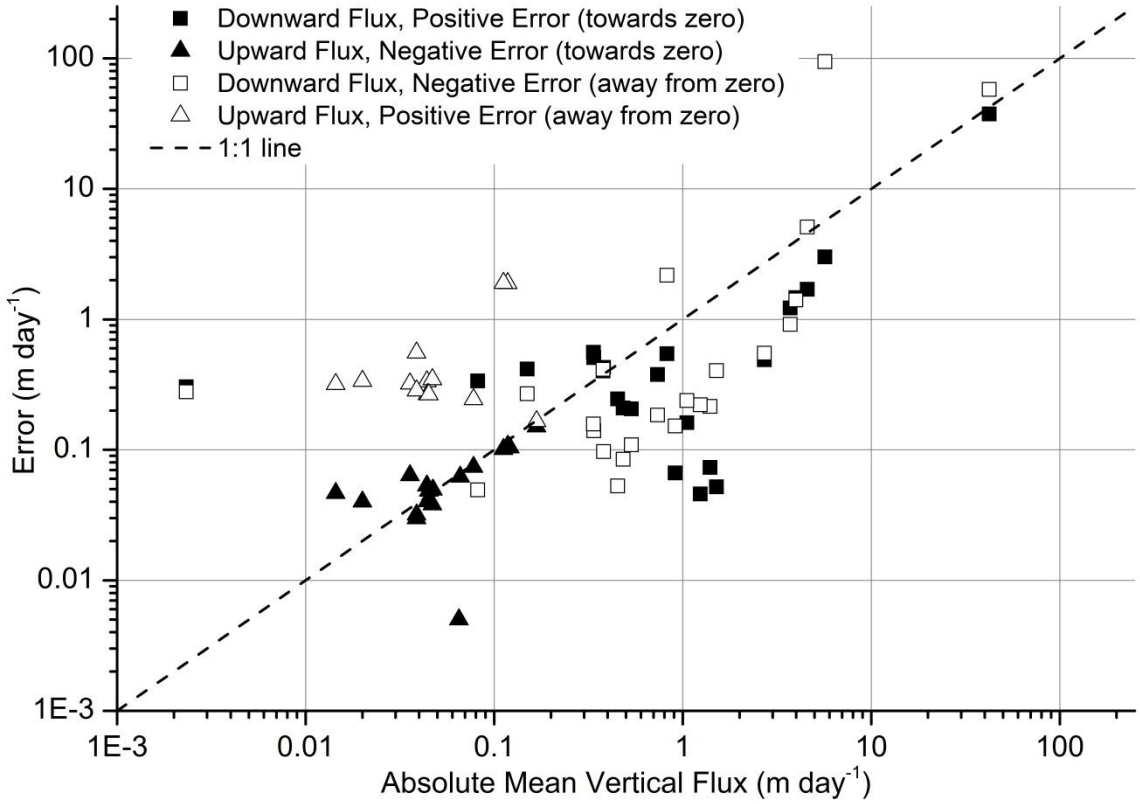

Figure 2.10. Absolute values of mean vertical flux plotted against positive and negative error bars for profiles C3, B3, C4 and D3 (data also presented in Figure 2.9). Solid symbols represent fluxes with their error towards and crossing zero while hollow symbols represent fluxes with their error increasing away from zero. Errors are generally less than mean vertical flux values between 0.3 and approximately 6 m d^{-1}.

2.5. Discussion

2.5.1. Variations in Vertical Flux with Depth

Variation in the vertical component of flux with depth along a pool–riffle sequence has been demonstrated in this study using a simple numerical model. Several recent studies have also identified variations in vertical flux using temperature profiles with a high vertical resolution (e.g. Swanson and Cardenas, 2010; Vogt *et al.*, 2010a, Gordon *et al.*, 2012, Briggs *et al.*, 2012). These authors have presented similar interpretations for data

describing the transition of vertical to horizontal flow with depth in downwelling sections. Briggs *et al.* (2012) also presented four flux profiles showing a reversal in vertical flux direction (i.e. downward at the surface and upward at lower depths which is similar to the shallow section of one of our profiles). Hence, this and other recent studies indicate that the interpretation of streambed vertical temperature profiles should not assume a constant flux with depth. Increased vertical resolution of temperature observations allows the dynamics of the shallow hyporheic zone to be better understood, which in turn could be used to better constrain groundwater–surface water exchanges and biogeochemical processes in riverbeds.

The above studies analyse successive subsurface pairs of temperature data with depth and hence assume vertical flow between these depths. In this paper, we treat each depth observation independently and thus allow the temperature observations to represent the mean vertical flux of the flowpath between the surface and that depth (which does not require purely vertical flow). This assumes that the flowpath reaching each observation depth originates from the surface water in the vicinity of the observation point rather than directly above. This is considered a more robust interpretation because it does not assume that flow is purely vertical.

2.5.2. Model Assumptions and Errors in Flux Estimates

Potential sources of error in vertical flux estimates derived from temperature profiles include the uncertainty of measurements (e.g. sensor spacing and accuracy), uncertainty in parameter values (e.g. γ and k_e) and uncertainty in the conceptual model (e.g. purely 1D vertical flow, sinusoidal temperature input, steady state flowfield, homogenous and isotropic sediments). Shanafield *et al*. (2011) showed that when relatively high uncertainty in the value of k_e, sensor spacing and of sensor accuracy are combined, there was >50% error for all upward fluxes and downward fluxes less than approximately 1.2 m d^{-1}. The simplification of a river temperature signal to a sinusoidal function was shown by Lautz

(2010) to result in flux errors of >25 %. Lautz (2010) also showed that disagreement between the phase shift and amplitude ratio methods using the Stallman (1965) solution meant that the analytical solutions could not resolve downward fluxes smaller than approximately 0.35 m d^{-1}.

The numerical model developed in this study shares some of these sources of uncertainty. However, our model approach has the versatility of using raw temperature data as its upper and lower temperature boundary conditions. Hence, there is no need to filter or average data to force the boundary condition assumptions of the analytical solutions. Additionally, the model does not rely on hydraulic conductivity or head gradient information to drive flow in the system and therefore does not introduce this potential source of uncertainty. By treating each observation depth independently, we do not assume purely 1D flow, as would be the case if sequential pairs of data down a profile were analysed.

In our study, the uncertainty of the value used for k_e and the temperature measurement error are accounted for by the upper and lower error bars of q_z derived from the Monte Carlo analysis. An asymmetric relationship was found between q_z and RMSE, where RMSE was generally less sensitive to flux as its magnitude increased away from zero than towards zero. In general, downward fluxes between 0.3 and approximately 6 m d^{-1} were well resolved (errors significantly less than estimated fluxes). Larger downward fluxes were not well resolved, but this is due to the small sensor spacing (high downward fluxes only occurred within the upper 10 cm of the profiles). Smaller fluxes (both upward and downward) were not well-resolved, and in most cases the direction of the flux could not be determined (error greater than flux value). The approximate lower limit of resolution of 0.3 m d^{-1} is similar to that reported by Lautz (2010). High upward fluxes were not recorded at our field site.

2.5.3. Effective Spatial Footprint of Temperature Observations

Conceptually along a 2D pool–riffle sequence, the vertical component of the flow decreases with depth along the flowpath, until reversing so that the vertical component of flow is upward at the tail of the riffle (Figure 2.1). In a similar 2D system (Figure 2.3) we found that the 1D analysis overpredicts vertical flux compared to the mean vertical flux profile at the same location in the 2D flowfield. This is because temperature observations made at a point were actually representative of the integrated temperature signal along the flowpath traveling through that point. In the downwelling zone, more rapid downwelling fluxes at upgradient locations caused faster propagation of the surface water temperature signal to the observation depths, resulting in higher flux estimates using a 1D approach than those observed in the 2D model at the same location (Figure 2.3B). In the upwelling zone, we suggest that higher upward fluxes adjacent to the profile location affected the temperature profile via horizontal conduction and hence vertical flux estimates were different for the 1D and 2D models (Figure 2.3C). This potential influence of horizontal conduction on fluxes is consistent with the findings of Ferguson and Bense (2011), who used a simple 2D model with two hydraulic conductivity zones to demonstrate that temperature observations can be greatly influenced by adjacent flow zones.

In a 2D system, the difference between the vertical flux derived from 1D analysis of temperature data and the actual vertical flux at the measurement location depends on the location of the profile, as shown for different flow systems by Cuthbert and Mackay (2013) and Roshan *et al.* (2012). Both of these studies found that the largest discrepancy between 1D and 2D fluxes occurred where the non–uniformity in the flowfield was greatest (i.e. where there is horizontal variation in vertical flux). This finding was also validated by our study. Our simulations suggest that differences between fluxes derived from 1D analysis and those derived from 2D (or 3D) approaches should not be considered as “errors”. Rather, the vertical flux derived from analysis of a temperature observation in a

downwelling section of a pool–riffle sequence represents of the mean vertical flux along the flowpath travelling through that observation point. This flowpath would have originated some distance upgradient and we can think of this as an effective "spatial footprint", defined by the horizontal distance the water has travelled from the point of infiltration. The size of this spatial footprint would depend on the horizontal component of flow, although this cannot be easily determined from vertical temperature profiles. It is plausible for a spatial footprint to be on the order of tens of meters in the field, depending on the geometry of the flow system (see Figures 2.2A and 2.3A) and hydraulic properties of the aquifer material.

The concept of a spatial footprint associated with each mean vertical flux derived from subsurface temperature measurements may warrant further exploration. The application of 2D numerical models could be coupled with closely spaced temperature observations in vertical profiles (i.e. a 2D transect along inferred horizontal flowpath) to better resolve this spatial footprint for a particular field setting. It may then be possible to develop a methodology that uses single vertical profiles to better estimate the spatial footprints of each depth observation. This would particularly relevant for studies hyporheic exchange where characterising the horizontal component of flow is often important. Applied tracer tests combined with detailed subsurface observations would also provide a means for describing these flowpaths.

2.6. Conclusion

A simple 1D numerical approach using riverbed temperature observations has shown that the vertical component of hyporheic flux is not constant with depth. This approach is able to characterise the vertical flux variation using multiple temperature observations with depth in downwelling, upwelling, convergent and neutral sections of the hyporheic zone. Each temperature observation with depth was treated independently and allowed for a robust interpretation of the variation in vertical fluxes with depth to be made. Vertical

fluxes ranged from 5.7 m d^{-1} (downward) to –0.2 m d^{-1} (upward) and detailed profiling demonstrated the importance of considering how flux varies with depth so that we can better describe the vertical variability of hyporheic exchange fluxes. Vertical fluxes between 0.3 and approximately 6 m d^{-1} were well constrained whereas fluxes outside of this range had large errors. The temperature signal at any particular depth should be thought of as representative of the mean vertical flux from the surface along a flowpath to that point. Thus, the vertical fluxes derived from temperature data using a 1D analysis have spatial footprints, which are equal to the upgradient length of each flowpath. This is an important consideration when evaluating the differences between vertical fluxes derived from 1D and 2D approaches.

2.7. Acknowledgments

Funding for this research was provided by the National Centre for Groundwater Research and Training, an Australian Government initiative, supported by the Australian Research Council, the National Water Commission and the CSIRO Water for a Healthy Country Flagship. We also wish to thank the anonymous reviewers who helped to improve the clarity of the manuscript.

3. MANUSCRIPT II: HYPORHEIC ZONE EXCHANGE FLUXES AND RESIDENCE TIMES INFERRED FROM RIVERBED TEMPERATURE AND RADON DATA

Submitted to Journal of Hydrology: 4th of February, 2014:

Re-submitted to Journal of Hydrology: 26th of May, 2014:

Cranswick RH, Cook PG, Lamontagne S. Submitted (2014). Hyporheic zone exchange fluxes and residence times inferred from riverbed temperature and radon data. *Journal of Hydrology*. HYDROL16517R1.

Authors:

Roger H. Cranswick, Peter G. Cook and Sebastien Lamontagne

Abstract:

Vertical profiles of temperature, radon and electrical conductivity are used to characterise downwelling, neutral and upwelling hyporheic zones along a pool–riffle sequence in the Haughton River in north-eastern Australia. Water residence times and vertical fluxes are derived from temperature and radon data and then directly compared for downwelling profiles. Temperature and radon-derived fluxes in downwelling zones ranged from 0.02 to 24 m day^{-1} with a mean of 1.69 m day^{-1} while residence times across the study site ranged from tens of minutes to greater than 15 days. The radon approach has the lowest uncertainty for residence times between 0.1 and 15 days while the uncertainty of the temperature approach (using a diel river signal) is lowest for residence times that are less than a few days. For 83 % of depths in downwelling profiles, radon-derived residence times were greater (some up to two orders of magnitude greater) than temperature-derived residence times. When the error bounds of the residence time estimates were accounted for, 57 % of radon-derived residence times were significantly greater than temperature-derived residence times in downwelling profiles. We suggest that this discrepancy indicates that the influence of small scale heterogeneity on temperature and radon methods must be far more important than previously considered. Our data is consistent with sediments of a mostly lower hydraulic conductivity with some high hydraulic conductivity zones. We suggest that the temperature approach is more representative of flow through these higher hydraulic conductivity zones, while the radon approach may be more representative of flow through the bulk of the sediments.

3.1. Introduction

Hyporheic exchange is the movement of water from a river into the underlying or adjacent sediments and then back into the river. The hyporheic zone, where this exchange occurs, is now widely recognised as a biogeochemical hotspot in river ecosystems (Boulton *et al.*, 1998). Hyporheic zones exist across a broad range of spatial and temporal scales depending on the riverbed substrate, geomorphology and larger scale river-aquifer exchanges (Harvey and Wagner, 2000). The biological, chemical and hydraulic characterisation and dynamics of hyporheic zones have been the focus of numerous studies since the mid-1950s (Boulton *et al.*, 2010). However, methods for quantifying exchange fluxes and associated water residence times in the hyporheic zone across a range of spatial scales require further development.

Two environmental tracers that have been applied to quantify the exchange between rivers and the subsurface are temperature and radon (^{222}Rn). The natural temperature variation of rivers allows the water fluxes into or out of the hyporheic zone and (or) groundwater system to be calculated (e.g. Conant Jr., 2004; Lautz and Fanelli, 2008; Bhaskar *et al.*, 2012). This is done by comparing the temperature signal in the river with the temperature signal in the subsurface at one or more depths. Where downward vertical flux is large, diel temperature signals propagate rapidly into the subsurface while if fluxes are small or upwards the diel temperature signal in the subsurface is attenuated. Radon is produced by riverbed sediments so that as river water travels into the subsurface the radon activity of that water increases with time. This allows the residence time and flux of water travelling into the subsurface to be calculated (e.g. Hoehn and von Gunten 1989; Hoehn and Cirpka 2006; Lamontagne and Cook, 2007). These naturally occurring tracers are often used independently to quantify groundwater–surface water exchanges but only a few examples can be found where they have been directly compared (e.g. Hoehn and Cirpka, 2006; Vogt *et al.*, 2010). Other tracers, including electrical conductivity (EC) in some

cases, can also be used to differentiate between sources of water (e.g. regional groundwater and river water) if the end members have distinct signatures (e.g. McCallum *et al.*, 2010).

In this study we use temperature, radon and electrical conductivity data collected in detailed vertical profiles, to describe the spatial variability of hyporheic exchange along a pool–riffle sequence (Figure 3.1). Observed trends in these parameters are used to characterise the downwelling, neutral and upwelling locations along the study reach. Hyporheic exchange processes are observed on both small (tens of centimetres) and larger scales (meters to tens of meters). For downwelling profiles, the vertical flux and residence times of water are quantified using both temperature and radon profile data. The uncertainty of these residence time values are quantified, compared and discussed along with the practical limitations of each approach. The field site selected for this study is a shallow, primarily gaining river in north-eastern Australia (Haughton River), which flows within a wide sandy alluvial channel.

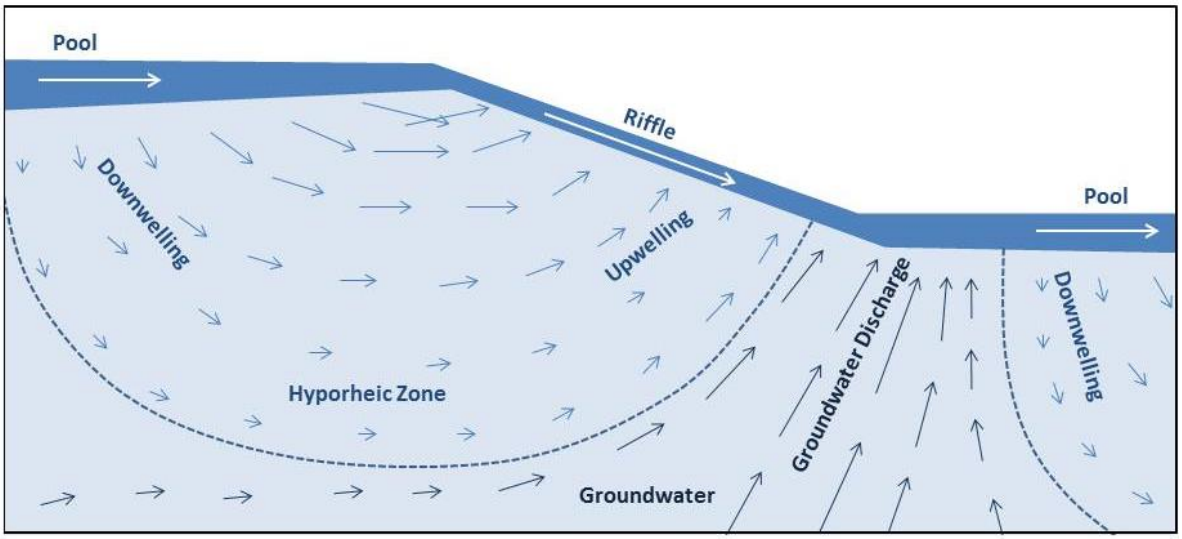

Figure 3.1. A conceptual model of the exchange processes occurring over a pool–riffle sequence longitudinal cross section for a gaining river, including the partitioning between the hyporheic zone and groundwater system. Zones of downwelling in the pool sections and zones of upwelling in the lower portion of the riffle section can be seen. Additionally, groundwater discharge may occur concurrently with upwelling hyporheic exchange. Note that this figure does not display the current driven hyporheic exchange (Thibodeaux and Boyle, 1987) that may also occur.

3.2. Theory

3.2.1. Temperature

Heat has been used as an environmental tracer for investigating groundwater–surface water interaction for over 50 years and by numerous researchers (see reviews by Anderson; 2005; Constantz, 2008; Rau *et al.*, 2014). This is possible because of diel temperature variations in surface water bodies and the damped or constant temperature signals in the hyporheic zone and shallow groundwater. These temperature differences can be used to estimate the vertical water flux between surface and subsurface water bodies. One dimensional (1D) heat transport in a homogenous porous media (i.e. with constant heat parameters) can be described by the conduction-advection equation:

$$\frac{\partial T}{\partial t} = k_e \frac{\partial^2 T}{\partial z^2} - \frac{q_H}{\gamma}\frac{\partial T}{\partial z} \tag{3.1}$$

where T is temperature (°C), k_e is the effective thermal diffusivity of the saturated sediments (m^2 day^{-1}), γ is the ratio of the volumetric heat capacity of the saturated sediments to the volumetric heat capacity of water, q_H is the water flux (m day^{-1}), t is time (days) and z is depth (m). Although they share the same units, the q_H term is a flux and should not be confused with the pore water velocity or thermal front velocity used in some heat tracer studies (Gordon *et al.*, 2012). The positive direction for z and q_H is downward into the subsurface. Eq. 3.1 assumes that heat is transported through a representative volume where thermal equilibrium exists instantaneously between the fluid and solid phases and that θ, k_e and γ are constant both spatially and temporally. The heat parameter terms (k_e and γ) are commonly estimated from the literature (e.g. Carslaw and Jaeger, 1959 or Lunardini, 1981) but can also be measured in sediment samples. In this study we have approximated k_e and γ using experimentally derived relationships for coarse grained sediments developed by Lunardini (1981) as presented in Figure 2 of Lapham (1987).

It is common to approximate the diel temperature variation of the river with a sinusoidal function and hence solve Eq. 3.1 analytically to calculate the vertical water flux (e.g. Suzuki, 1960; Stallman, 1965). In this paper, we have used a 1D numerical solution to avoid making this assumption and instead use raw temperature data collected from the river and subsurface (see Section 3.3 and Cranswick *et al.*, 2014).

The residence time of water in the hyporheic zone can be derived from temperature data if there is a downward flux. In this study temperature-derived residence time is calculated using:

$$t_r = \frac{z\Theta}{q_H} \tag{3.2}$$

where t_r is residence time (days) and other variables are as defined previously.

3.2.2. Radon

Radon (^{222}Rn) is a noble gas with a half-life of 3.82 days. It is produced by the decay of radium (^{226}Ra) (which is part of the uranium (^{238}U) decay series) that is found both in the aquifer material itself and as dissolved radium adsorbed onto sediment surfaces in low salinity environments (Cecil and Green, 2000). There have been many studies that have used measurements of radon to calculate river infiltration rates into alluvial aquifers (e.g. Bertin and Bourg, 1994; Hoehn and von Gunten, 1989; Snow and Spalding, 1997). These studies assume that infiltrating water starts with a known radon activity, which increases with time due to production in the aquifer until secular equilibrium is reached. The equilibrium activity is dependent on the production rate of the aquifer material and can also be measured from sediment samples. It takes approximately 30 days for full secular equilibrium to be reached and the time since water entered the aquifer can theoretically be calculated within this range. While the absolute error is small at very early times, the relative error can be large due to the uncertainty of the infiltrating water radon activity. Conversely, the absolute error can be large for late times due to the uncertainty of the

production rate in sediments. The radon activity at a particular time can be calculated using (after Cecil and Green, 2000):

$$A_t = A_e\left(1 - e^{-\lambda t_r}\right) + A_0 e^{-\lambda t_r} \quad (3.3)$$

where A_t, A_e and A_o are the radon activities (Bq L^{-1}) at time t, at equilibrium and at time 0 respectively, λ is the decay coefficient (0.181 day^{-1}) and t_r (days) is the residence time in the subsurface. Eq. 3.3 can be rearranged to solve for residence time:

$$t_r = ln\left(\frac{A_e - A_0}{A_e - A_t}\right)\frac{1}{\lambda} \quad (3.4)$$

This approach can be applied to the hyporheic zone to determine the residence time of water within riverbed sediments when the equilibrium activity, river activity and subsurface sample activity are estimated or measured. The residence time calculated here, represents the time taken for water to travel from the river to the location from which the sample was collected. Residence times derived from samples collected in upwelling zones can be considered a conservative underestimate of the total residence time of that flowpath in the subsurface. A practical upper limit for radon-derived residence times of 15 days has been generally adopted after the work of Hoehn and von Gunten (1989). This is because the radon activity is within 5% of equilibrium after this time, which is close to the analytical uncertainty of the radon measurements. If $A_t > A_o$, then the residence time of that sample is assumed to be > 15 days. When samples are collected from discrete screen intervals using drivepoint piezometers, vertical profiles of residence time can be constructed. The vertical component of the water flux (q_{Rn}) can be estimated from radon activity using:

$$q_{Rn} = \frac{z\Theta}{t_r} \quad (3.5)$$

Chapter 3.

It should be noted that the approach based on Eq. 3.3 does not consider diffusion and dispersion. If this is important (e.g. for very small advective fluxes), then fluxes can be estimated by solving the 1D advection-dispersion equation with decay and production:

$$\frac{\partial A}{\partial t} = D_e \frac{\partial^2 A}{\partial z^2} - \frac{q_{Rn}}{\theta}\frac{\partial A}{\partial z} - \lambda A + \beta \quad (3.6)$$

where A is the radon activity (Bq L^{-1}), D_e is the effective dispersion coefficient (m^2 day^{-1}), β is the production rate (Bq L^{-1} day^{-1}) and other terms are defined as previously. The effective dispersion coefficient can be defined as $D_e = D_0\tau + \alpha\frac{|q_{Rn}|}{\theta}$ where D_0 is the molecular diffusion coefficient (m^2 day^{-1}), τ is tortuosity and α is dispersivity (m).

A comparison was made between residence times derived from the radon disequilibrium method (Eq. 3.3) and a numerical solution of Eq. 3.6. It was found that for q_{Rn} > 0.1 m day^{-1} there was no significant difference in residence time (see Appendix 3.A). However for fluxes below this value, the radon disequilibrium method overestimated the residence times compared to the 1D transport equation. Hence dispersion should be considered when using the radon disequilibrium method to determine residence times if fluxes are below 0.1 m day^{-1}. The downwelling profiles analysed later in this chapter generally have fluxes greater than 0.1 m day^{-1}, and thus we use Eq. 3.4 to estimate their radon-derived residence times and Eq. 3.5 to estimate radon-derived fluxes.

3.3. Field and Analysis Methods

3.3.1. Field Location

The Haughton River is located approximately 100 km south of Townsville in the tropical northeast of Australia (Figure 3.2) and receives approximately 1200 mm of precipitation per year (BoM, 2012). The river is highly seasonal, having a mean dry season (May to October) flow of 2 m^3 s^{-1} and a mean wet season (November to April) flow of 25 m^3 s^{-1} with floods up to 2 600 m^3 s^{-1} (Figure 3.3) (DERM, 2012). In the dry season, the upper Haughton River flows as a narrow meandering or braided river (<30 m width, <0.5

m depth) with some pool–riffle sequences that are contained within a wide sandy alluvial channel. Adjacent to the alluvial channel are other Late Tertiary to Quaternary alluvial sediments containing interbedded sands, clays, silty sands and silty clays. Underlying these sediments is igneous bedrock, which is the dominant geological unit in the hills to the north and within the upper catchment to the northwest.

The river is thought to be primarily gaining due to its largely perennial nature and the high precipitation within the catchment. Losing reaches are expected to occur locally during the sugar cane irrigation season, when groundwater is heavily pumped from the alluvial aquifer. In addition to natural dry season flows, it is common for flow to be augmented by diversions from the nearby Burdekin River to supply downstream irrigation.

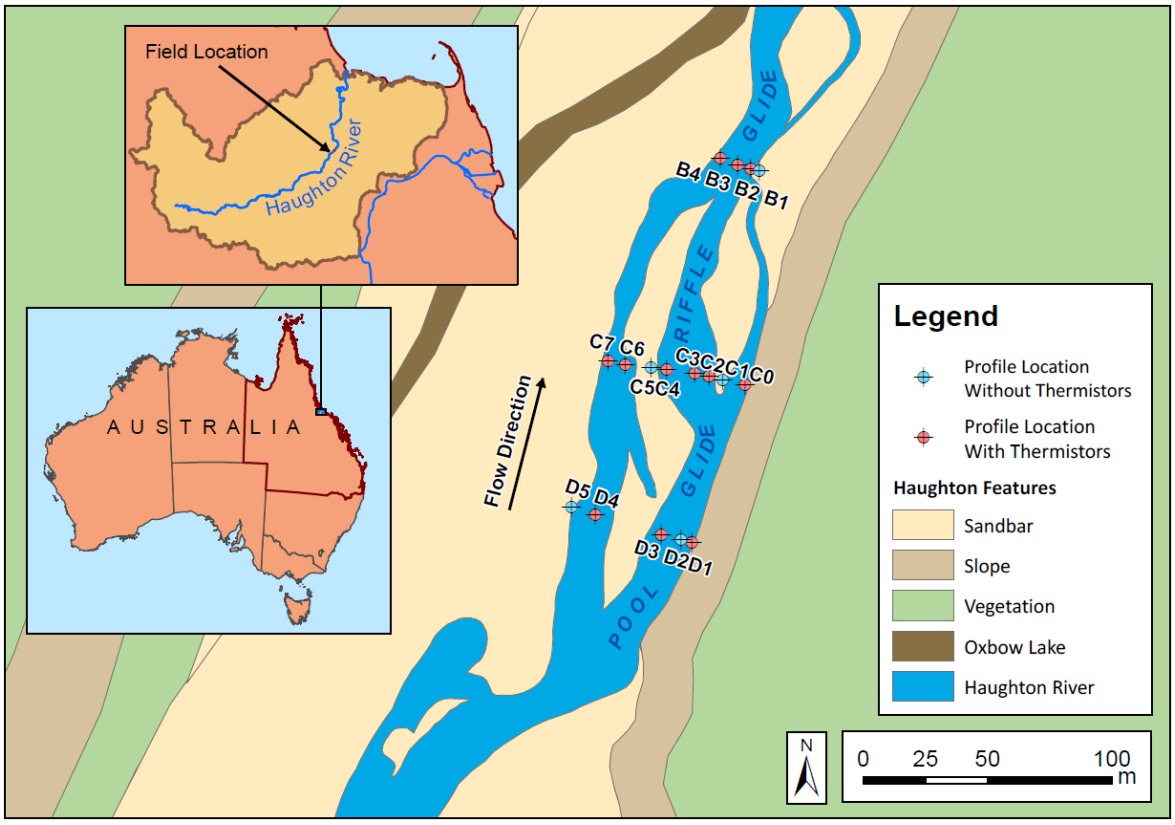

Figure 3.2. Overview of the study reach showing profile locations and generalised descriptions of the nature of flow in the river. Other land features are also shown including the extent of the sandy channel and adjacent slopes and tropical scrub vegetation. Profile locations with and without thermistors installed are shown as red and blue symbols respectively. Vertical radon sampling was conducted at all profile locations.

3.3.2. Data Collection

A four-day field campaign was conducted along a 300 m reach of the upper Haughton River in late September 2011. The selected site contained an upper pool followed by a split riffle that converged as the river gradient flattened. Three cross sections were established perpendicular to the flow direction: across the upper pool, at the head of the riffle below the pool, and at the tail of the same riffle (Figure 3.2).

Thermochron iButton© thermistors (Maxim Integrated, San Jose CA) were installed at depths of 0, 0.05, 0.1, 0.15, 0.2, 0.3, 0.4 (or 0.45), 0.6, 0.8 (or 0.75), 1.0 (or 0.9) and 1.2 m below the streambed at 12 locations along the cross sections (B2, B3, B4, C0, C2, C3, C4, C6, C7, D1, D3 and D4), and recorded streambed temperatures for 2 days at 5 minute intervals. These were installed by driving a 0.025 m steel pipe with a disposable tip into the sediments to the desired depth, placing a 0.015 m diameter plastic rod (with thermistors inset) into the pipe and then gently removing the steel pipe while keeping downward pressure on the plastic rod. The thermistors have a reported accuracy of 0.2 °C and a resolution of 0.0625 °C. The temperature data from the 132 thermistors used in the field were then compared with three NIST certified thermistors in a calibration bath. The mean residual between the 132 thermistors and the average of the three NIST certified thermistors was 0.039 °C with a standard deviation of 0.091 °C (n = 23 100).

At each of the above 12 locations (and an additional 5 locations where thermistors were not installed), samples were collected for radon at depths of 0, 0.05, 0.10, 0.15, 0.2, 0.3, 0.4, 0.6, 0.8, 1.0 and 1.2 m below the riverbed. Mini-piezometers (after Duff *et al.*, 1998) with a diameter of 0.003 m and a screen length of 0.01 m were used for sampling depths of 0.05, 0.10 and 0.15 m while the remaining depths were sampled using 0.025 m diameter drivepoint piezometers with screen lengths of 0.05 m. Samples were extracted from the subsurface using a 30 mL syringe with small diameter tubing and a three-way valve from

mini-piezometers before being injected directly below the liquid scintillation mineral oil in pre-prepared PET vials (after Leaney and Herczeg, 2006). Similarly, a hand-held manual Masterflex® peristaltic pump was used to extract samples through the drivepoint piezometers before injecting into the PET vials. The lines were minimally flushed such that the samples were no longer turbid and/or field EC and temperature were stable if available for deeper samples. Field temperature and electrical conductivity were measured at depths greater than 0.15 m using a WTW Cond 3310 conductivity meter. Field parameters were not collected for shallower depths so that the flow system was not overly disturbed by pumping. Vertical hydraulic head gradients were measured between the surface water and the deepest drivepoint sampling depth using an air–water manometer (after Winter *et al.*, 1998). The site was surveyed to evaluate the gradient of the riverbed. Twenty five slug tests were conducted within the alluvial sediments adjacent to the river at an approximate depth of 0.5 m below the watertable. These hydraulic tests give both an indicative value and the potential variability of the hydraulic conductivity (K) of alluvial sediments. They represent the horizontal hydraulic conductivity of the alluvial sediments while the vertical hydraulic conductivity was not assessed. Three sediment cores from the riverbed were collected using a 44 mm Undisturbed Wet Soil Sampler (Dormer Engineering, Murwillumbah South New South Wales), to later measure porosity, bulk density and the radon equilibrium activity of pore water in the laboratory.

Snapshot surveys of river temperature, EC and radon activity were conducted to support the development of a conceptual model for the study site and observe any spatial variability in these parameters on the reach scale. The river radon survey was conducted on 28/09/2011 (n = 25) while the river EC survey was conducted during the afternoon of 29/09/2011 (n = 71). Water temperatures were recorded during the EC survey both in the river and approximately 0.1 m into the sediments using a WTW Cond 3310.

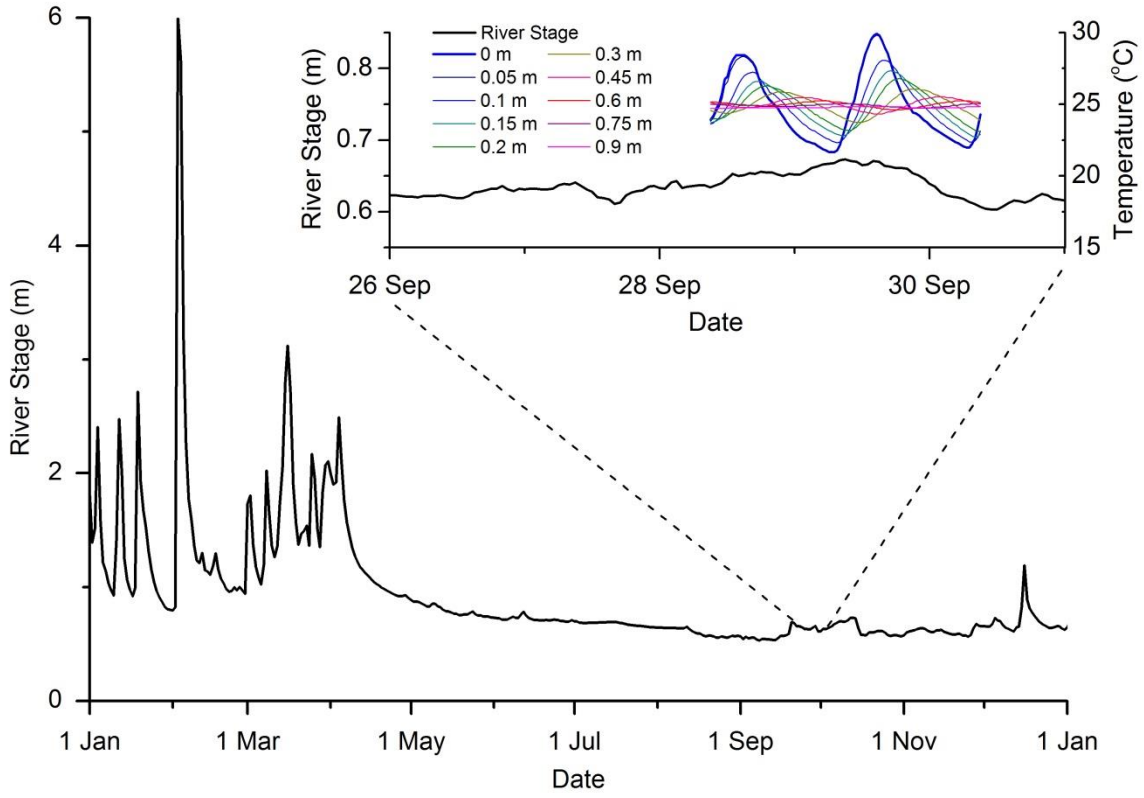

Figure 3.3. Hydrograph from river gauge (119003A) approximately 300 m downstream of the study reach, showing historical river stage with typical seasonal variation between the wet season (November to April) and the dry season (May to October). Inset hydrograph shows the river stage variation at the time of the field campaign and an example of the temperature time-series at a range of depths below the river (Profile D3).

A simple method was used to estimate the equilibrium activity of radon in the pore water of riverbed sediments. Samples were packed into 150 mL glass jars and filled with deionised water making sure no air remained in the jar and that free water above the sediments was minimised. These were left to equilibrate for two months before triplicate pore water samples were collected from each jar using mini-piezometers.

All radon samples were analysed using liquid scintillation counting at the Commonwealth Science and Industrial Research Organization (CSIRO) Land and Water Waite Campus Environmental Isotope Laboratory. Subsurface samples (14 mL) were collected using the direct method while an enhanced concentration (PET) method (1.25 L samples) was used for surface water samples as described in Leaney and Herczeg (2006).

3.3.3. Numerical Modelling Approaches

A 1D numerical approach was used to estimate the mean vertical flux between the river and each temperature observation depth for selected profiles (after Cranswick *et al.*, 2014). The temperature signal at each observation depth was simulated independently so that the resulting flux represented the mean vertical flux along the flowpath from the surface to that observation depth (Cranswick *et al.*, 2014). The use of a 1D model does not inherently assume only vertical flow, but does assume that the river temperature signal is relatively constant spatially (i.e. in the vicinity of the downwelling zone). The numerical approach is a finite differencing approximation to Eq. 3.1. All parameters except temperature are assumed to be constant with depth for each simulation. The spatial and temporal discretization values were chosen so that the numerical scheme was stable and numerical dispersion minimised (see Cranswick *et al.*, 2014). For most simulations the model spatial discretisation was 0.01 m and the temporal discretisation was 0.0001 days but both were made smaller for q_H > 1 m day^{-1}. The upper temperature boundary for all model runs was the measured river temperature. The lower temperature boundary was modelled as a constant temperature and placed at a sufficient depth (5 m) so that it did not adversely influence the simulations. The value of this temperature was either the mean temperature of surface water for downwelling profiles or deepest observation data for upwelling profiles.

Similarly, a numerical approximation to Eq. 3.6 was developed for the 1D transport of radon with production and decay. All parameters except radon activity are assumed to be constant with depth. The spatial and temporal discretisation was chosen in a similar fashion to those of the temperature simulations. The upper boundary condition was the river radon activity while the lower boundary condition was the equilibrium activity and placed at a sufficient depth (5 m) so that it did not influence the simulations. Porosity was set at a value of 0.35, while the production rate (β) was calculated by multiplying the measured

equilibrium activity (A_e) by the decay coefficient (λ). This numerical solution was used only for the comparison discussed in Section 3.2.2 and in Appendix 3.A. Eq. 3.4 and Eq. 3.5 were used to determine radon-derived residence times and fluxes respectively, for the remainder of the study.

3.3.4. Vertical Flux Estimation and Uncertainty Analysis

Each temperature observation depth from the downwelling profiles was treated independently to estimate the mean vertical flux along the flowpath from the river to that depth. The parameter estimation software PEST was used (Doherty, 2010) to iteratively vary q_H to best fit the temperature observation data. It did this by minimising the sum of the squared differences between temperature observation data and simulated temperature. This flux was considered representative of the mean vertical flux from the surface to that depth, and could be converted into a mean residence time for each depth using Eq. 3.2.

To quantify the uncertainty of the flux values determined by parameter optimization, a Monte Carlo analysis was applied using 2000 simulations of temperature transport and a range of q_H and k_e values. The random numbers for k_e were generated from a uniform distribution between ± 50% of the estimated k_e value (see Cranswick *et al.*, 2014). Random values for q_H with a uniform distribution were generated within an initial range from 15 m day^{-1} (downwards) to –5 m day^{-1} (upwards). As described in Cranswick *et al.* (2014), the upper and lower error bounds were considered separately because the RMSE increased at different rates as q_H increased or decreased away from the best fit value (i.e. the RMSE vs q_H relationship was not symmetrical). Some scatter was observed in this relationship because the q_H values were paired with randomly generated k_e values. The uncertainty of k_e was thus incorporated into the relationship between RMSE and q_H. For consistency, an observation error of 0.091° C (standard deviation of field thermistors compared with NIST certified thermistors during calibration, see Data Collection) was added to the minimum RMSE and all values of q_H that fell within this range were

considered plausible values. In order to accurately resolve the error bounds, the range of random q_H was subsequently narrowed to better define the relationship between RMSE and q_H, and the Monte Carlo analysis was run a second time for each observation depth of each profile (i.e. a further 2000 simulations using random q_H and k_e to simulate the temperature signal at each observation depth).

The uncertainty of radon-derived residence times was also estimated using a Monte Carlo analysis. Normally distributed random values of A_o and A_e were generated based on the mean and standard deviation of surface water radon and measured equilibrium activities from sediment cores collected at the site. The 5th and 95th percentiles of the 2000 Monte Carlo simulations using the A_e and A_o pairs were considered the upper and lower bounds on the radon-derived residence times. Analytical errors for radon samples were small relative to the uncertainty in initial and equilibrium activity values and so were not considered. These estimates of residence time and their error bounds were also converted to vertical fluxes using Eq. 3.5.

3.4. Results

3.4.1. Site Characterisation

Across the study site, the riverbed sediments consisted of medium to coarse grained sands with some small cobble armoring present on the riverbed surface across the faster flowing sections. Sediments collected from the core samples had a mean porosity of 0.34 and standard deviation of 0.01 (n = 3) resulting in a mean dry bulk density of 1.28 g cm^{-3}. Hydraulic tests resulted in a mean hydraulic conductivity of 91 m day^{-1} with a standard deviation of 44 m day^{-1} (n = 25). At gauging station 119003a (located approximately 300 m downstream from the study site) the river level had been relatively constant with flows less than 2 m^3 s^{-1} for the previous 4 months (Figure 3.3). During the study period there was a gradual increase in river stage before a relatively rapid decrease (stage level from 0.64 m to 0.67 m then down to 0.60 m above the reference elevation). This rapid fall in river stage

was most likely due to a decrease or shutting off of upstream river augmentation sourced from the nearby Burdekin River. The radon and temperature data used for analysis in this study was collected before this fall in river stage. The mean river discharge was 1.09 $m^3 s^{-1}$ for the time period before the decrease in stage occurred. Across the study site, the depth of water varied from 0.5 m in the slower pools to less than 0.1 m across riffle sections.

3.4.2. Spatial Variability of River EC, Radon and Temperature

The EC survey showed significant spatial variation across the study reach but no net downstream increase or decrease. The EC was consistently higher along the right bank (mean of 459 µS cm^{-1} and standard deviation of 15 µS cm^{-1}) compared with the mid-river and left bank locations (which had a combined mean of 451 µS cm^{-1} and standard deviation of 3 µS cm^{-1}).

Temperatures in the river and at approximately 0.1 m into the sediments were also recorded during the EC snapshot survey (conducted in the afternoon, when river temperature was near its maximum). Temperature differences between the river and subsurface were less than 1 °C in the upper two thirds of the study reach (surrounding D and C profiles). However, in the lower section (surrounding the B profiles) the subsurface was consistently between 1 and 4 °C cooler than the river. These patterns suggest the presence of downwelling fluxes along the upper reach and upwelling along the lower reach.

The river had a mean radon activity of 0.47 Bq L^{-1} (standard deviation of 0.15 Bq L^{-1}) based on 25 samples collected between 2 PM and 5 PM on 28/09/2013. However the radon activity in the river was not constant across the study reach. The upper pool had values of approximately 0.4 Bq L^{-1} which declined across the riffle section to 0.25 Bq L^{-1} before increasing to 0.6 Bq L^{-1} at the tail of the riffle. An increase in the gas transfer velocity as the river becomes shallow and wide across the riffle (i.e. <0.05 m depth and near 30 m wide) is a possible cause for the fall in river radon over that reach. Because the river radon

activity increases towards the tail of the riffle, an upwelling hyporheic flowpath (Figure 3.1) or groundwater discharge may be occurring along this section. This is supported by the upward vertical hydraulic gradients observed at B2 and B3 of 0.010 and 0.015 respectively. Regional groundwater from the alluvial aquifer was found to have a mean radon activity of 13.7 Bq L^{-1} and standard deviation of 6.3 Bq L^{-1} (n = 38, Cook *et al.*, 2004). Meanwhile, equilibrium activities from sediment samples collected from the study reach had a mean of 10.9 Bq L^{-1} (standard deviation of 1.1 Bq L^{-1}, n = 9) indicating that old hyporheic water may reach similar radon activities to regional groundwater.

3.4.3. Vertical Variation in Subsurface Temperature, Radon and EC

The subsurface sampling conducted along the three transects perpendicular to the pool–riffle sequence revealed a wide range in EC, radon and temperature patterns (Figure 3.4). Vertical hydraulic gradients between the river and deepest sampling depth ranged from 0.027 (downwards) to –0.021 (upwards). The measurements taken in the middle of the river were representative of the conceptual pool–riffle sequence presented in Figure 3.1 (downwelling at the top of the riffle, upwelling at the tail of the riffle and approximately neutral in the pool). The profiles where large downward gradients were observed (C3, C2) showed relatively constant EC with depth, slowly increasing radon and a diel temperature variation that was transferred beyond the deepest measurements. Profiles that were hydraulically neutral or had small upward or downward gradients (D3, D1, C0, C4, D4 and B4) generally had increasing EC and radon values with depth and a diel temperature variation that attenuated with depth. Locations with higher upward gradients (B2, B3) showed relatively constant temperatures with elevated EC and radon values at lower depths. A diel temperature variation was not observed below 0.2 m for these profiles. Trends in each of these parameters relate well to the measured hydraulic gradients, ranging from strongly downwelling to strongly upwelling (top left to bottom right of Figure 3.4).

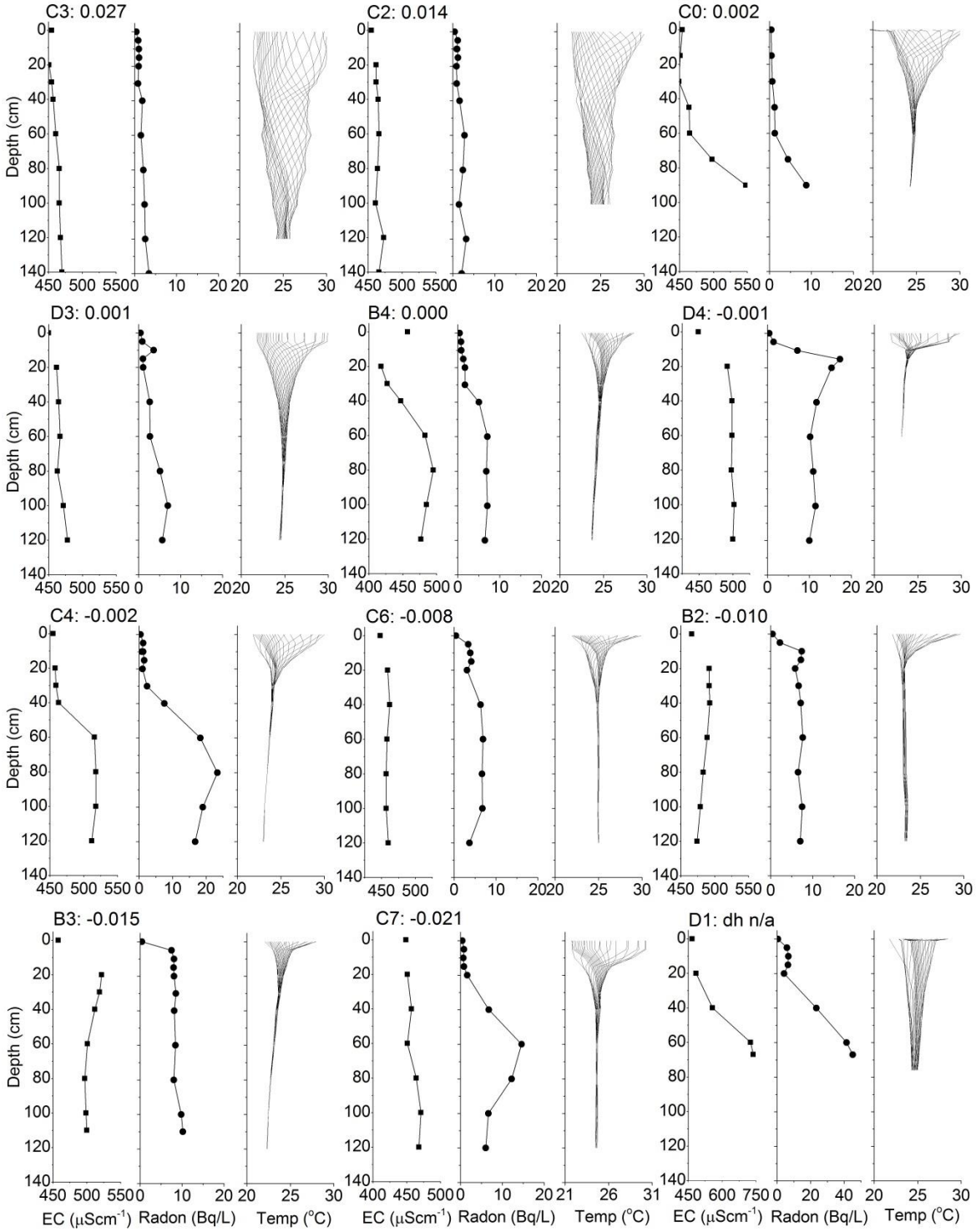

Figure 3.4. Vertical profiles of EC, radon and 24 hour temperature envelopes at 12 locations. Profiles are ordered from greatest downward hydraulic gradient (top left) to greatest upward hydraulic gradient (bottom right) measured between the surface water and deepest sampling depth. The value next to each profile label is the hydraulic gradient (*dh*) between the river and deepest drivepoint piezometer depth (positive values indicate a downward gradient while negative is an upward gradient).

Radon activities are elevated in the mid-depths for profiles C4, C7 and D4 and are in some cases higher than the highest regional alluvial groundwater activities reported by

Cook *et al.* (2004). We suggest that this is due to heterogeneity in the radon production rates within the sediments. This could be caused by heterogeneity in sediment mineralogy and/or by the preferential adsorption of radium onto metal oxides at a redox boundary as hypothesised by Lamontagne *et al.* (2010). Hence these observed high radon activities are not indicative of groundwater discharge but instead, may be either due to heterogeneity of sediment mineralogy or biogeochemical processes occurring within the hyporheic zone. This is additionally supported by the relatively low EC found at these locations (similar to river EC) suggesting no contribution from regional groundwater.

Profiles D4, C4 and C7 appear to have downward fluxes at shallow depths due to the large diel temperature signal, low EC (with the exception of D4) and low radon activity. However at greater depths they appear to have upward fluxes as indicated by constant temperatures, high EC (except C7) and high radon activity. The transition between these two apparently opposing flux directions, occurs at depths between approximately 0.05 – 0.15, 0.2 – 0.6 and 0.2 – 0.4 m for profiles D4, C4 and C7 respectively. The presence of these transition zones suggests a shallow zone of hyporheic exchange embedded within a larger scale flowfield (i.e. shallow downwelling and deeper upwelling).

High radon activities were observed at depth in profile D1 along with the highest EC values observed at the site. These elevated radon and EC values may represent groundwater from the shallow aquifer adjacent to the alluvial river channel. In contrast, the upwelling profiles at B2 and B3 did not have elevated EC or radon activities. Hence, the upwelling water at B2 and B3 is likely to be of hyporheic origin rather than from a groundwater source.

General agreement between spatial trends in river EC (low EC on left bank, higher EC on right bank) and potential subsurface flowpaths were observed at the B4, C0 and D1 profiles. Low subsurface EC values were found at 0.2, 0.3 and 0.4 m of the B4 profile and

appear to agree with lower river EC along the left bank in the lower section of the study reach. Meanwhile elevated EC was found at depth for the D1 and C0 profiles along the right bank which appears to agree with higher river EC along that bank.

3.4.4. Hyporheic Residence Time Estimates

Temperature-derived residence times could be calculated for profiles that contained continuously downward fluxes (i.e. diel temperature variations to all depths) and are discussed in the following sections. However many of the temperature profiles presented in Figure 3.4 have relatively constant temperature signals at depth. Because the diel signal of the river will attenuate to a constant value after a few days in the subsurface (using the heat parameters applied in this study), these constant temperature signals could indicate either a very slow downward flux or an upwelling flux. Hence, it is not possible to determine a temperature-derived residence time beyond an approximate limit of a few days for slow downwelling fluxes. Likewise, temperature-derived residence times cannot be calculated from upward fluxes because the origin of that water is uncertain.

The radon-derived residence times from the neutral and upwelling profiles had 80th and 20th percentile values of 10.1 and 0.8 days respectively, with a median of 4.8 days (n = 104). This residence time data (along with EC data from B profiles that is similar to river EC data) supports the conceptual model shown in Figure 3.1, where after downwelling near the C profiles, it is likely that the hyporheic flow direction changes to horizontal and then upward near the B profiles. Thus the median travel time through the sediments beneath the pool–riffle sequence was thought to be approximately equal to the median residence time found at profiles B1, B2, B3 and B4 which was 5.5 days (the 80th and 20th percentiles for the B profiles were 7.1 and 2.0 days respectively, n = 35). The radon-derived residence time values from the upwelling and neutral profiles could not be compared directly to temperature-derived values because they were older than the limits of the temperature based approach. Hence the following results give a more detailed analysis

of the downwelling profiles where a direct comparison between residence times estimated from both temperature and radon data can be made.

For the temperature profiles that appeared to have significant downward movement of water (C2, C3, C0 and D3), the mean vertical flux and associated uncertainty was calculated from the surface to each observation depth. The optimal vertical flux value and error bars were then converted into residence times using Eq. 3.2 and are displayed in Figure 3.5. Profiles for C0 and D3 show residence time slowly increasing to 2.3 and 7.7 days respectively at the deepest temperature observation point. The relative residence time error also increases with depth and is greater for smaller fluxes. The C2 and C3 profiles show residence times of 0.5 days at the deepest temperature observation points. The residence time error for these profiles was small because the flux error is small when fluxes are large.

Residence times were estimated directly using radon data for the same four profiles (C2, C3, C0 and D3) using Eq. 3.4 and measured mean values of A_o and A_e. Note that the subsurface radon data for profiles C2, C3, C0 and D3 were collected on the same day as the surface water radon samples and so the A_o term is considered representative of the starting river radon activity. Radon-derived residence times for all four profiles generally increase with depth (Figure 3.5). Residence times at the base of profiles C0 and D3 were approximately 9 and 4 days respectively. At profiles C2 and C3 the residence times were approximately 1 and 2 days respectively at the deepest sampling points. A number of depths (e.g. 0.1 m in the D3 profile) showed a higher radon activity than the next deepest sample and hence resulted in a longer residence time value. These discrepancies may indicate the presence of preferential pathways allowing particular flow paths to reach greater depths more rapidly or conversely, a zone of lower hydraulic conductivity material where the sample was collected. Error bars were greatest (relative to the residence time value) at shallow depths due to the uncertainty of initial river radon activity values.

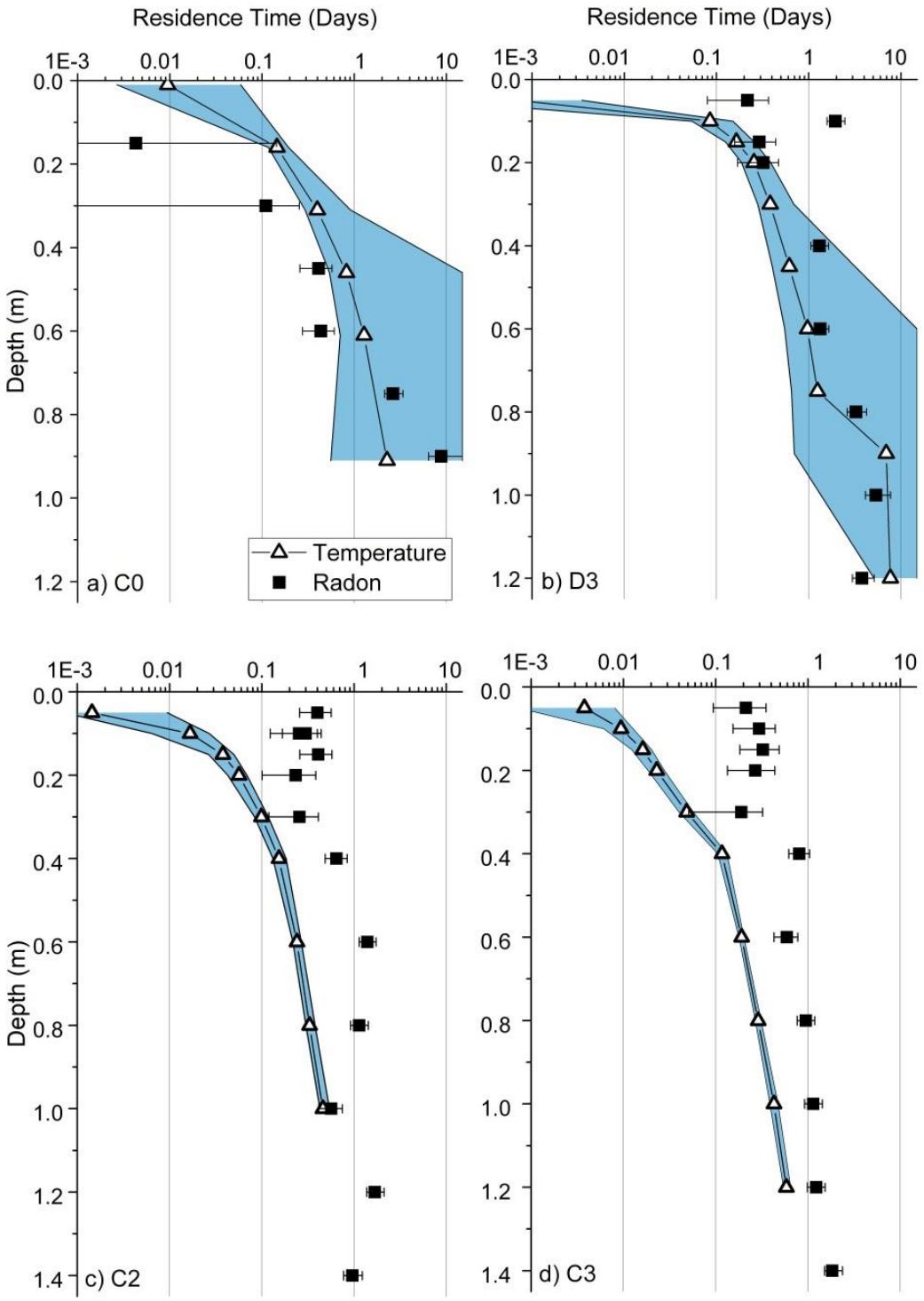

Figure 3.5. Residence time profiles for both radon and temperature-derived estimates for selected downwelling locations. Triangles represent the best fit temperature-derived residence time values with blue shading showing the upper and lower uncertainty bounds (based on vertical flux uncertainty analysis). If the lower vertical flux uncertainty crossed zero (i.e. upwelling) the residence time was truncated to a value of 15 days for display purposes. Radon-derived residence times are indicated by the square symbols with upper and lower error bounds representing the 5th and 95th percentiles based on the Monte Carlo analysis (where A_o and A_e were randomly varied within a normal distribution based on the mean and standard deviation of measured values). These residence times were also truncated at 15 days because this is the practical limit of the radon disequilibrium method (Hoehn and von Gunten, 1989).

The radon-derived and temperature-derived residence time profiles agree well in profile D3 where the range of residence times overlap within error bounds at all but the shallowest two depths. At profile C0 the radon-derived residence times were younger than temperature-derived residence times for depths less than 0.6 m but were older below 0.6 m. Likewise, the radon approach resulted in older residence times at shallow depths for D3 and at all depths for profiles C2 and C3. If the river radon activity at the time of infiltration was underestimated, the radon residence times would be systematically overestimated. The shallowest samples in particular would be most impacted because of the time taken for radon activity to increase significantly above the starting activity (approximately 0.1 days). The river radon activity required to match temperature-derived residence times at shallow depths would be approximately 10 % less than the observed values at each respective depth sampled (i.e. a range of 0.8 – 1.0 Bq L^{-1}). This elevated starting activity was considered unlikely based on measured river activities at or near these locations (river radon activity near the C and D profiles had a mean of 0.36 Bq L^{-1} and standard deviation of 0.05 Bq L^{-1}, n = 10). Hence, for C2 and C3 profiles in particular the radon approach appears to result in significantly older residence times compared to the temperature approach. Based on our model of flow through homogenous sediments, the temperature and radon residence times cannot be reconciled, with the differences being greater than the uncertainty.

3.5. Discussion

3.5.1. Depth of Hyporheic Exchange

The vertical depth of hyporheic exchange in this study can be considered on both small and larger spatial scales. The larger scale downwelling at the top of the riffle and upwelling at the tail of the riffle was clear from the mid-river profiles and support the conceptual model of the site (Figure 3.1). Downwelling profiles (e.g. C2 and C3) had common characteristics of downward vertical hydraulic gradients, constant and low EC, low radon activity and diel temperature signals transferred to all depths. In contrast, the

upwelling profiles (e.g. B2 and B3) showed upward vertical hydraulic gradients, constant or slightly elevated EC, high radon activity and no diel temperature variation at depth. The depth of circulation for this larger scale exchange (downwelling) was not delineated due to the relatively shallow measurements taken (i.e. hyporheic exchange is assumed to extend deeper than 1.2 m). The longitudinal extent could not be estimated without more intensive sampling but was assumed to be similar to the length of the riffle (approximately 80 m).

A smaller scale hyporheic exchange was seen for most upwelling and near neutral profiles. This shallow exchange was inferred for profiles where there was a sharp transition zone from low radon activity immediately below the riverbed to high radon activity at greater depth (and similarly from low EC to higher EC – note that river EC had gradually decreased from approximately 500 to 425 uS cm^{-1} over the 10 days prior to the study period). The change in radon and EC occurred at a similar depth to where a diel temperature variation becomes considerably attenuated. For the near neutral profiles B4, C0, C4, D4 this depth is approximately 0.4, 0.7, 0.4 and 0.1 m respectively below the river-sediment interface. For upwelling profiles the depth of small scale hyporheic exchange is much shallower (for B2 and B3 this depth is approximately < 0.1 and 0.05 m respectively). The deeper circulation of hyporheic exchange for neutral profiles compared to upwelling profiles described above was consistent with the modelling results of Cardenas and Wilson (2007) and experimental results of Fox *et al.* (2014) for bedform induced hyporheic exchange. The presence of co-occurring shallow hyporheic exchange and deeper exchange has also recently been resolved using heat as a tracer by Bhaskar *et al.* (2012).

The data from the river edge profiles C7 and D1 may indicate mixing with water from a long parafluvial flowpath (low EC, high radon activity and relatively attenuated temperature signal at depth) and groundwater flowpath (high EC, high radon activity and constant temperature at depth) respectively. However, vertical profiles from outside the river channel would need to be collected to confirm these potential flowpaths. Nevertheless

the river edge profiles suggest broader scale interaction, with longer hyporheic flowpaths and (or) regional groundwater.

The multi-scale hyporheic exchange observed along our pool–riffle sequence demonstrates the potential complexity of mixing zones near rivers. If it was not for the observed low EC data at the tail of the riffle, these upwelling profiles could have been interpreted as groundwater discharge (because they had constant temperature and high radon activities). Similarly, care should be taken when interpreting data from pool (e.g. D profiles) and top of riffle (e.g. C profiles) locations because downwelling temperature signals and hydraulic gradients do not necessarily suggest river loss. Some proportion of the flow (if not all) may return to the river further downstream (e.g. B profiles). Thus it is important to develop conceptual models for studies of groundwater–surface water interaction using multiple tracer approaches rather than a single tracer (see Cranswick and Cook, submitted).

3.5.2. Disparity between Heat and Solute Derived Results

There have been a limited number of studies directly comparing the use of heat and solutes as tracers to determine streambed fluxes or hyporheic residence times. These have included: sand column experiments (e.g. Taniguchi and Sharma, 1990); field based studies (e.g. Constantz *et al.*, 2003); modelling studies (e.g. Irvine *et al.*, 2013) and sand box experiments (e.g. Rau *et al.*, 2012a, 2012b). The synthesis of these studies suggests that a disparity between heat and solute derived fluxes (and hence residence times) is related to the magnitude of the flux, the degree of aquifer heterogeneity and the location of observations relative to higher and lower hydraulic conductivity sediments.

Radon is a conservative solute because it is not involved with any exchange processes apart from production and decay which are accounted for. Thus we can compare our results using radon and heat approaches with the above studies. Results from our study do not indicate a systematic relationship between heat-derived fluxes and radon-derived fluxes

(Figure 3.6). This is in contrast to linear relationships found by Rau *et al*. (2012a, 2012b) using relatively homogenous sediments and those of Irvine *et al*. (2013) using modelled synthetic heterogeneous sediments. Our heat-derived fluxes were found to be greater than radon-derived fluxes for the majority of depths compared (29 out of 35), particularly the strongly downwelling locations. Some heat-derived fluxes were up to two orders of magnitude greater than radon-derived fluxes which are far greater than the consistent 20% difference found by Rau *et al*. (2012a, 2012b).

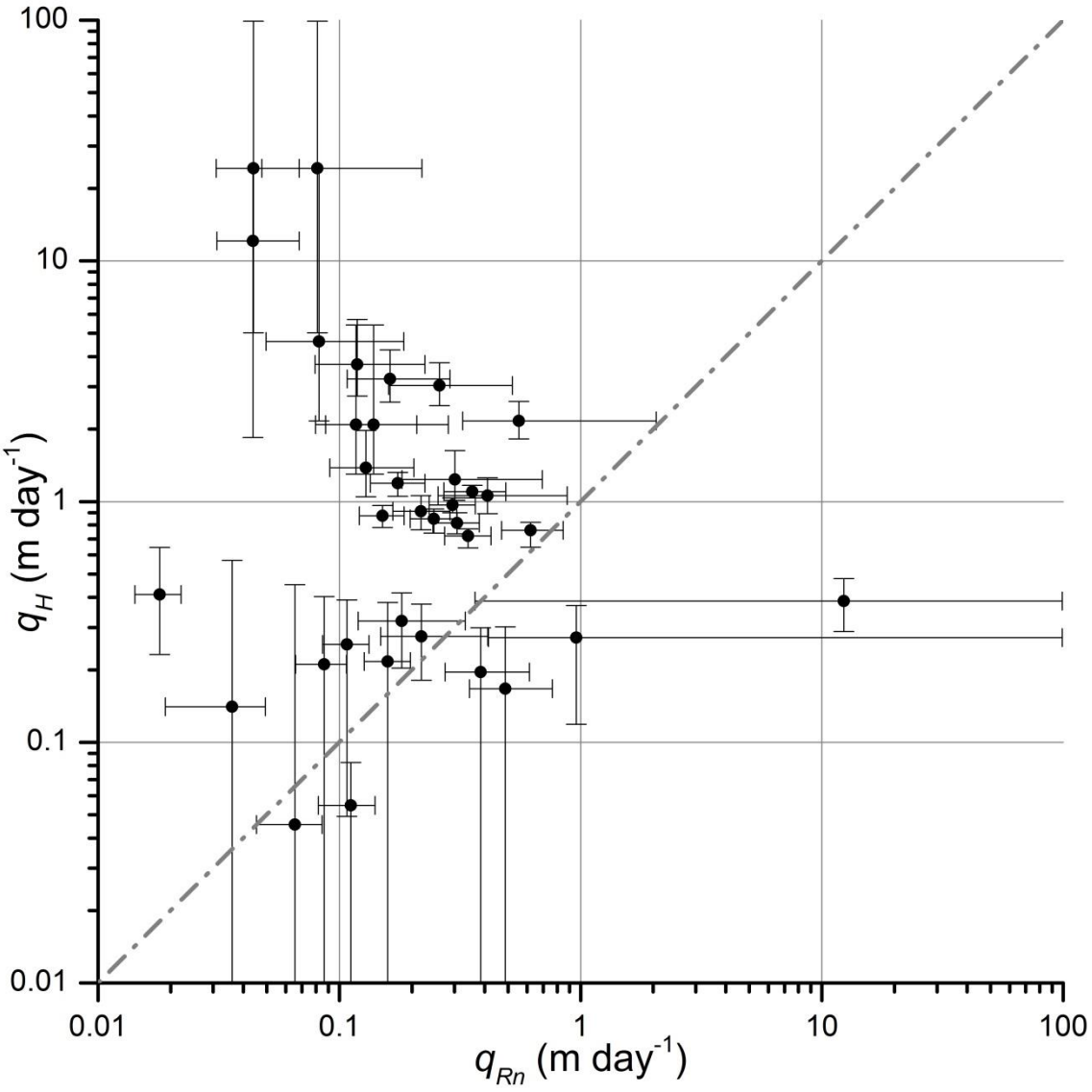

Figure 3.6. Relationship between radon and temperature-derived fluxes from downwelling profiles (C2, C3, D3 and C0). Error bars represent the 5th and 95th percentile radon-derived residence times (converted to fluxes) while temperature-derived flux errors represent the range for which q_H is within 0.091 ºC of the minimum RMSE.

Conversely, 6 of the 35 heat-derived fluxes were smaller than the radon-derived fluxes. This is supported by the work of Irvine *et al*. (2013), who found that heat derived fluxes were smaller than solute derived fluxes for measurements taken in high hydraulic conductivity zones (while heat-derived fluxes were greater than solute-derived fluxes in low *K* zones). In a natural system, the degree of heterogeneity and the measurement location relative to the heterogeneity is likely to vary between sites and between sampling depths, and therefore a wide scatter in the relationship between temperature-derived and radon-derived fluxes might be expected. These results suggest that in field settings, it is likely that large differences will be found between the values of vertical flux derived from temperature and radon data.

Our data shows heat-derived residence times that are up to two orders of magnitude smaller than radon-derived residence times at shallow depths (Figure 3.7). This may be due to the higher fluxes observed at shallow depths and (or) heterogeneity. Ferguson and Bense (2011) present a modelling study, where the presence of two contrasting hydraulic conductivity zones resulted in heat-derived fluxes near the boundary between the two *K* zones that were not representative of the advective water flux. In a modelling study with more complex heterogeneity, Schornberg *et al.* (2010) showed that the error in flux estimates increased as the difference in hydraulic conductivity between *K* zones increased. The idea that the temperature signal in low *K* zone could be influenced by flow in an adjacent higher *K* zone due to horizontal conduction was also discussed by Conant Jr (2004) and Schmidt *et al.* (2007) and was referred to as the "halo-effect". The "halo effect" may be a plausible explanation for the heat transport being orders of magnitude faster than radon transport at shallow depths in our study. It should be noted that the above studies examined features that were continuous on the tens of centimetre to meter scales. It is difficult to rationalise this scale of heterogeneity in the top 0.2 m of a sandy riverbed.

Nevertheless, this process should also occur on smaller scales, where preferential flowpaths through the sand have a large *K* contrast with the surrounding sediments.

In a case such as this, where there are relatively few high *K* zones within sediments of lower *K*, samples are more likely to be collected from within the lower *K* zone. Thus heat-derived fluxes would be influenced by flow through the high *K* zones and result in higher fluxes than the radon-derived fluxes. Hence, we suggest that where heat-derived fluxes are greater than solute-derived fluxes, the aquifer is likely to be composed of a significant proportion of low *K* material with a minor high *K* component. Temperature based approaches therefore, may be more influenced by flow through high *K* zones while radon and other solute based approaches may be more representative of flow through the more common or relatively low *K* zones. While the inclusion of some fraction of immobile water in the samples collected for radon analysis could result in artificially small fluxes, the presence of immobile water in the subsurface would also affect heat transport in a similar way. We therefore do not believe that this can explain the observed discrepancy between the two methods. Future research of these processes on the pore scale is required to better understand the effect of heterogeneity on radon and temperature methods.

3.5.3. Practical Limits and Residence Time Distributions

As suggested by Hoehn and von Gunten (1989) the upper practical limit of using radon as an age dating tool is approximately 15 days. This is because the radon activity is within 5% of secular equilibrium after this time which is close to the analytical uncertainty of the radon measurements. Conversely, there is also high relative uncertainty for residence times less than approximately 0.1 days because of the uncertainty of the initial radon activity before infiltration (unless time-series river radon data was available). These two sources of uncertainty have been taken into account in this study with a Monte Carlo analysis using the measured mean and standard deviation values for A_o and A_e.

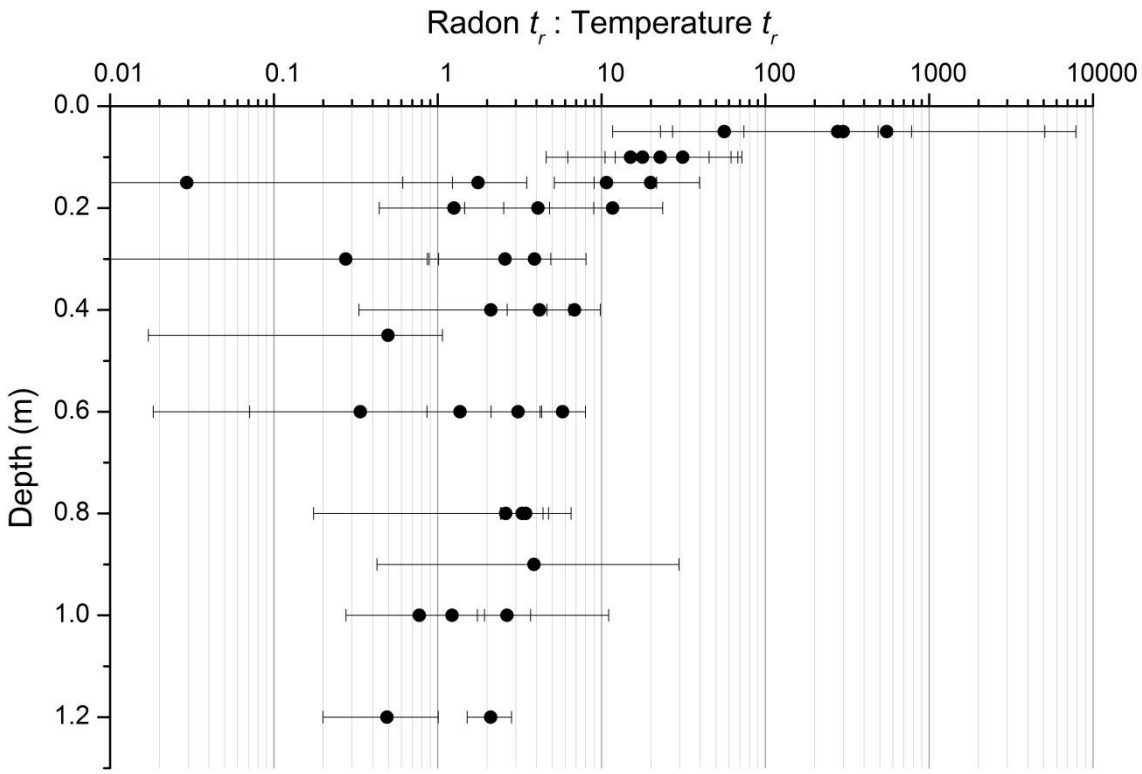

Figure 3.7. The ratio of radon-derived residence time to temperature-derived residence time plotted with sampling or measurement depth as appropriate. The upper and lower error bars represent the ratio of oldest radon-derived residence time to youngest temperature-derived residence time and youngest radon-derived residence time to oldest temperature-derived residence time respectively.

In our study, temperature-derived residence times could not be resolved for ages greater than a few days because of the attenuation of the diel temperature variation. Other sources of uncertainty related to the temperature-derived residence times are discussed in Cranswick *et al*. (2014) and by other authors (e.g. Anderson, 2005; Constantz, 2008; Rau *et al.*, 2014). A very short residence time (e.g. < 0.01 days) will also have a large uncertainty because the diel temperature variation measured between temperature sensors over a small time step, may not be distinguishable from measurement error (i.e. diel temperature signal changes too slowly). A comparison of the relationship between uncertainty and residence time for both the radon disequilibrium and temperature approaches is shown schematically in Figure 3.8. The radon disequilibrium method is best applied for residence times between 0.1 and 15 days while the temperature-derived

residence times are most confidently estimated if they are greater than 0.01 days and less a few days. The region of overlap therefore, occurs between approximately 0.1 and 2-3 days.

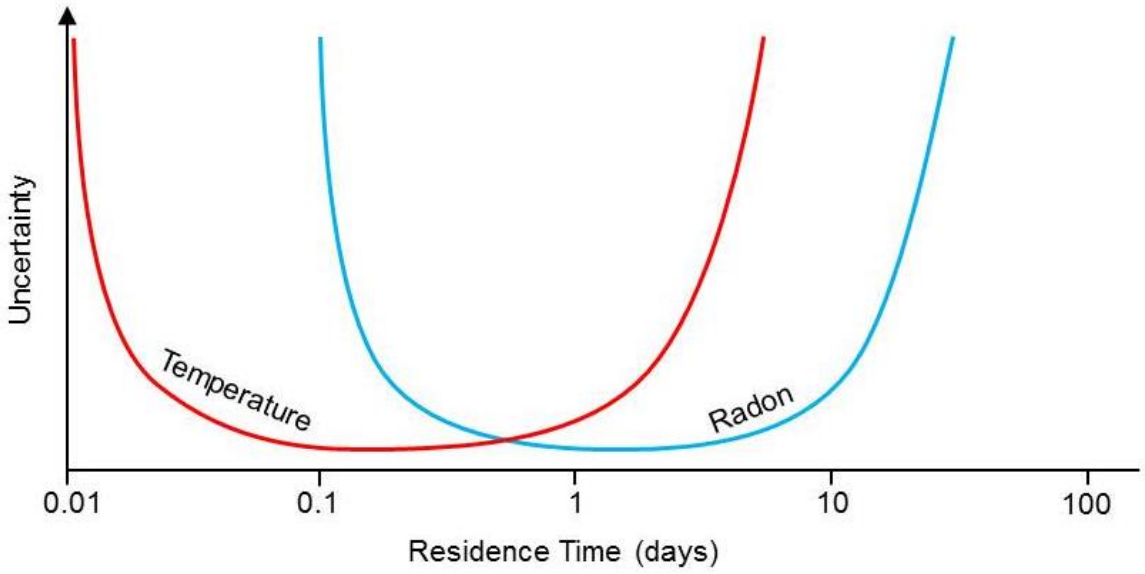

Figure 3.8. A conceptual comparison of the relationship between uncertainty and residence time estimates derived from radon and temperature data. The blue line indicates the uncertainty of radon-derived residence time and is low between 0.1 and 15 days. The red line indicates the uncertainty of temperature-derived residence time which increases as the diel signal attenuates and at very small residence times.

The traditional conceptualization of the hyporheic zone as a 1D transient storage zone (Bencala and Walters, 1984) includes a first-order exchange with an exponential distribution of residence times (Runkel, 1998). This conceptualisation is used to interpret results of the most common method for quantifying hyporheic exchange, the applied tracer test (Stream Solute Workshop, 1990). Harvey *et al.* (1996) showed that an exponential residence time distribution was appropriate for short-time hyporheic exchange but not for longer hyporheic flowpaths whose residence times were longer than the duration of typical applied tracer test (i.e. hours to <1 day). Haggarty *et al.* (2002) found that a power law distribution resulted in a better fit for applied tracer test data because the hyporheic exchange occurred over a range of spatial and therefore temporal scales. Cardenas (2008) showed that the simulated exchange between surface water and groundwater follows a power law on multiple scales (i.e. exchange through bedforms, meander bars and a

catchment) over 9 orders of magnitude in time and are fractal in nature, as has been suggested by other authors (Haggarty *et al.*, 2002; Kirchner *et al.*, 2000).

We have shown that relatively short-time environmental tracers (temperature and radon) are useful for quantifying a large part of the residence time distribution relevant for this scale of exchange (single pool–riffle sequence). The hyporheic residence times estimated in this study ranged from tens of minutes to greater than 15 days. Hyporheic flowpaths with both shorter and longer residence times were not captured due to the practical limits of each method and the placement and relatively shallow depth of vertical profiles. To identify longer residence times (i.e. weeks to months to years) for larger scale interaction, other environmental tracers could be used (e.g. Morgenstern *et al.*, 2010 and Solomon *et al.*, 2010). Alternatively, a long-term applied tracer test could be used to characterise the residence times of longer hyporheic flow paths (e.g. Bencala *et al.*, 1984), but this would be more labour intensive than the use of natural tracers. If shorter residence times were of interest (i.e. seconds to tens of minutes), traditional applied tracer tests with subsurface sampling would be able to resolve this part of the residence time distribution.

3.6. Conclusion

Hyporheic exchange along a pool–riffle sequence has been characterised broadly into downwelling and upwelling sections for a study reach of the Haughton River using vertical temperature, radon and electrical conductivity profiles. Hyporheic processes were observed on both small (centimetres to tens of centimetres in upwelling and neutral profiles) and large scales (metres to tens of meters along the pool–riffle sequence) using a combination of these environmental tracers. The residence times determined using radon and temperature approaches showed that this exchange occurs over a range of timescales, from tens of minutes to greater than 15 days. Using a diel temperature signal, we were able to derive residence times of up to a few days while radon-derived residence times could be estimated from approximately 0.1 to 15 days.

Chapter 3.

The residence times derived from temperature and radon data showed considerable disparity at all depths and flux ranges. Temperature-derived residence times were up to 2 orders of magnitude smaller than radon-derived residence times for some shallow locations. These field based results suggest that small scale heterogeneity may play a far more important role than has been previously considered in groundwater–surface water interaction studies. We suggest that temperature based approaches are more representative of fluxes through higher hydraulic conductivity zones while solute based approaches may be more representative of flow through lower hydraulic conductivity zones in heterogeneous sediments. Further exploration into the influence of small scale or even pore scale heterogeneity is needed to better understand the effect of heterogeneity on radon and temperature methods.

3.7. Acknowledgments

Funding for this research was provided by the National Centre for Groundwater Research and Training, an Australian Government initiative, supported by the Australian Research Council, the National Water Commission and the CSIRO Water for a Healthy Country Flagship. We would also like to thank the reviewers for their constructive comments which helped to improve the clarity of this manuscript.

3.8. Appendix 3.A

The comparison of the 1D transport of radon using a numerical solution to Eq. 3.6 and Eq. 3.3 (which neglects diffusion and dispersion) is shown in Figure 3.A.1 for a range of fluxes. The radon transport was modelled to different depths for each flux so that residence times between 0 and 20 days could be compared for each approach. The calculated residence times begin to deviate significantly from a 1:1 line when fluxes are less than 0.1 m day^{-1}. The radon disequilibrium method overestimates residence time compared to the 1D transport equation for slow fluxes. This is believed to be due to diffusion becoming a more dominant process as advection decreases.

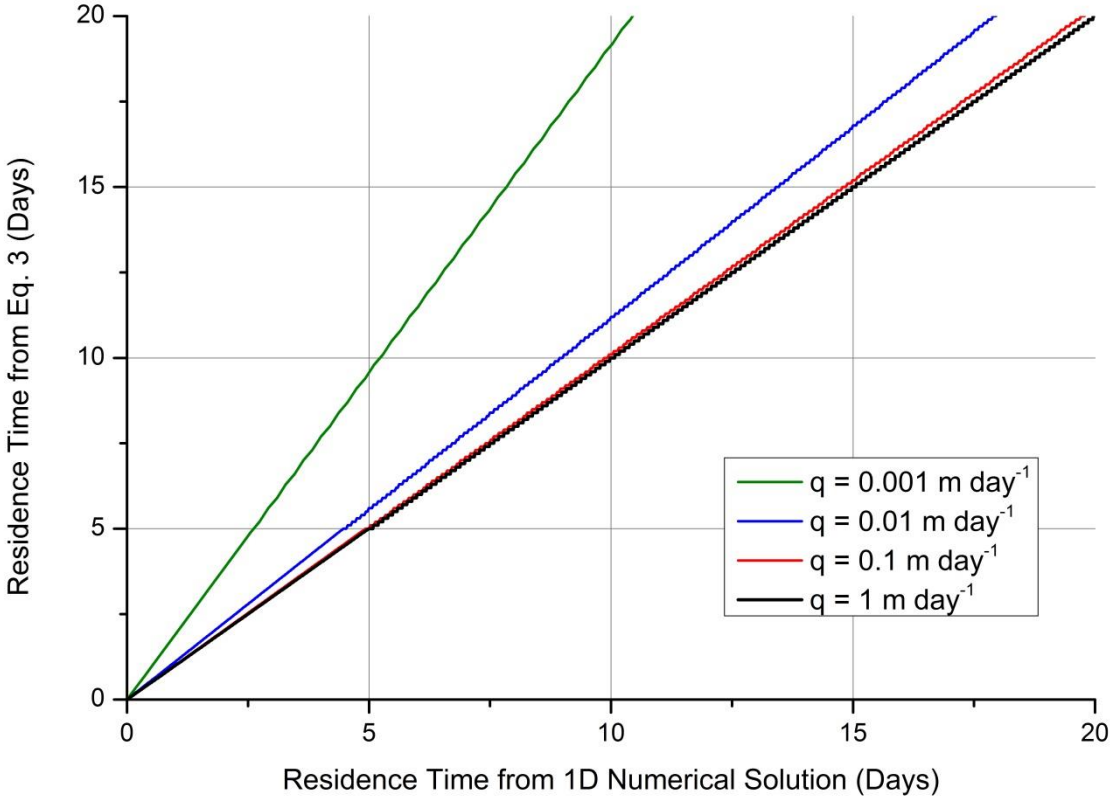

Figure 3.A.1. The calculated residence time at equivalent depths for 1D numerical solution of Eq. 3.6 and radon disequilibrium (Eq. 3.3). A range of fluxes are applied and are shown to deviate for fluxes less than 0.1 m day^{-1}. For slow fluxes the radon disequilibrium methods overestimates residence time.

4. MANUSCRIPT III: SCALES AND MAGNITUDE OF HYPORHEIC, RIVER–AQUIFER AND BANK STORAGE EXCHANGE FLUXES

Submitted to Hydrological Processes: 29th of April, 2014

Cranswick RH, Cook PG. Submitted (2014). Scales and magnitude of hyporheic, river–aquifer and bank storage exchange fluxes. *Hydrological Processes*. HYP-14-0333.

Authors:

Roger H. Cranswick and Peter G. Cook

Abstract:

Many studies have investigated the exchange processes that occur between rivers and groundwater and have successfully quantified the water fluxes involved. Specifically, these exchange processes include hyporheic exchange, river–aquifer exchange (groundwater discharge and river loss) and bank storage exchange. Remarkably, there are very few examples of field studies where more than one exchange process is quantified and as a consequence, the relationships between them are not well understood. To compare the relative magnitudes of common exchange processes, we have collected data from 53 studies that have quantified one or more of these exchange flux types. Although not necessarily from the same river, hydrogeological setting or relative position in the landscape, hyporheic exchange fluxes are almost an order of magnitude greater than river–aquifer exchange fluxes which are in turn, approximately three times greater than bank storage exchange fluxes for the same river discharge. Because exchange fluxes are measured in the vicinity of rivers, there is potential for hyporheic exchange fluxes to be misinterpreted as river–aquifer exchange fluxes, with possible implications for water resource management decisions. We discuss the importance of developing conceptual models that include multiple exchange processes, considering the scale of measurements and the use of multiple methods including environmental tracer approaches to clearly differentiate between exchange fluxes.

4.1. Introduction

The interaction between rivers and subsurface water in either the hyporheic zone or the groundwater has been the focus of numerous studies and review papers (e.g. Brunke and Gonser, 1997; Dahm *et al.*, 1998; Malard *et al.*, 2002; Woessner, 2000; Sophocleous, 2002). This is because a better understanding of these exchange fluxes is critical for water resource management and river health (Winter *et al.*, 1998; Brunke and Gonser, 1997). The importance of considering surface water and groundwater as a single resource is emphasised by both Winter *et al.* (1998) and Sophocleous (2002) and this is demonstrated through the conceptual models of groundwater–surface water interaction that they present. These include simple cross-sections showing conceptual groundwater flowpaths for gaining, losing and disconnected rivers, hyporheic exchange processes where water leaves and then returns to the river through underlying or adjacent sediments and bank storage exchange driven by a short lived rise and fall of river stage. Woessner (2000) emphasises the need to consider the complexity of the interaction of rivers and alluvial groundwater systems to improve upon traditional hydrogeological approaches applied at larger scales.

The ecological significance of river–aquifer exchanges is described in Brunke and Gonser (1997) and Boulton *et al.* (1998) while the nutrient dynamics at the interface between surface water and groundwater is reviewed by Dahm *et al.* (1998) and Malard et al. (2002). Jones and Mulholland (2000) give an overview of the hydrological framework for the nutrient cycling and biogeochemistry of near stream environments and methods to quantify hyporheic exchange, while Kalbus et al. (2006) reviews the methods for quantifying groundwater–surface water interactions more broadly. A recent review of the hyporheic zone by Boulton *et al.* (2010) discusses the challenges of linking measurements of hyporheic exchange with ecological management across multiple scales. Bencala *et al.* (2011) suggest that by conducting basic hydrological measurements of river and groundwater responses as well as their solute concentrations, the established small scale

conceptualisation of hyporheic exchange processes can be extended to the catchment scale. The importance of conceptual up-scaling is supported by the recent discussion of the fractal nature of residence time distributions for groundwater–surface water interactions (e.g. Cardenas, 2008; Haggerty *et al.*, 2002; Kirchner *et al.*, 2000).

Historically however, most groundwater–surface water interaction studies focus on a single exchange process rather than identifying and quantifying multiple processes across a range of spatial and temporal scales. The focus of a study is usually driven by its particular objectives and limited by the time and resources available. Thus our understanding of the relative magnitudes of exchange driven by these different processes is based on only a small number of field studies. Ruehl *et al.* (2006); Jones *et al.* (2008); and Bourke *et al.* (submitted) show that hyporheic exchange can be many times greater than other exchange fluxes. Where hyporheic exchange fluxes are large in relation to river–aquifer exchange fluxes, it can be difficult to accurately measure the smaller fluxes of groundwater discharge or river loss. This challenge is related to the scale at which methods are applied, the difficulty in differentiating between exchange processes, the conceptual uncertainty about how different exchange processes interact and general limitations of the scope of individual investigations.

In this study we review and compare the relative magnitudes of hyporheic, river–aquifer and bank storage exchange fluxes from a wide range of literature sources. A brief overview of the field methods used to estimate these fluxes and the representative spatial and temporal scale of each approach is also presented. We also discuss some of the challenges of differentiating between the different types of exchange flux and the importance of doing so.

4.2. Types of River–Aquifer Exchange

River–aquifer exchange occurs as groundwater discharge when regional or local hydraulic gradients are towards the river (Figure 4.1A) and occurs as river loss when hydraulic gradients are away from the river (Figure 4.1B). Superimposed on this larger scale interaction are hyporheic exchange and bank storage processes. Hyporheic exchange occurs where water leaves the river through underlying or adjacent sediments and then returns to the river, and can be categorised into three main exchange types. Current driven hyporheic exchange occurs in the shallow riverbed sediments and is induced by the river flowing over sandy bedforms or other small riverbed features (Thibodeaux and Boyle, 1987; Figure 4.1C). Larger scale hyporheic exchange can be driven by changes in riverbed slope along pool–riffle sequences (Vaux, 1968; Figure 4.1D). A third type of hyporheic exchange referred to in this study is parafluvial exchange. Parafluvial exchange occurs in the sediments adjacent to rivers and can be driven by hydraulic gradients across river meander bends (Boano *et al.*, 2006; Figure 4.1E). Bank storage exchange takes place when there is a rise and subsequent fall in river stage (Figure 4.1F). During a rising stage, river water infiltrates through the river banks and may displace the pre-existing hyporheic water. As the river stage falls, some or all of this recently infiltrated water then returns to the river. Characterising these hydrological exchanges can be challenging because of the high temporal and spatial variability of near river hydrogeological settings (Bencala *et al.*, 2011). Rivers can both gain and lose water to adjacent aquifers over the same reach or at different times of year while the hydraulic properties of riverbeds can be highly spatially variable (e.g. Calver, 2001). The spatial variability of riverbed hydraulic conductivity can cause high spatial variability of exchange fluxes even in dominantly gaining rivers (e.g. Conant, 2004).

Study reaches of field investigations are often selected based on the scale of interest. For example, hyporheic exchange studies generally have study reaches on the order of tens

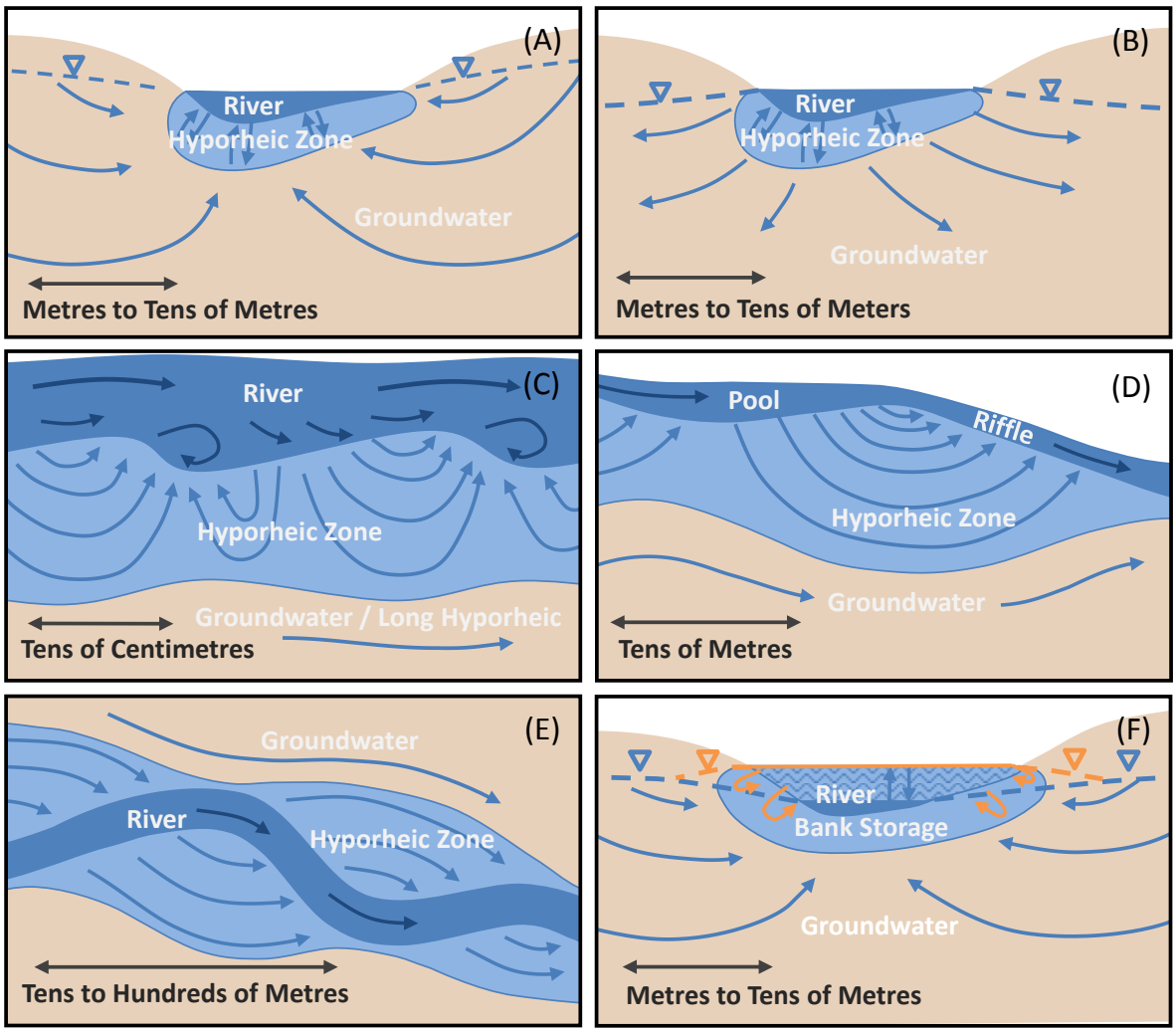

Figure 4.1. Conceptual models of common hyporheic exchange, river–aquifer exchange and bank storage exchange processes. (A) River–aquifer exchange showing groundwater discharge as the hydraulic gradient is towards the river. (B) River–aquifer exchange showing river loss as the hydraulic gradient is away from the river. (C) Current driven hyporheic exchange (after Thibodeaux and Boyle, 1987). (D) Hyporheic exchange driven by hydraulic head gradients along a pool–riffle sequence (after Vaux, 1968). (E) Parafluvial hyporheic exchange driven by hydraulic head gradients across meander bends (after Boano *et al.*, 2006). (F) Bank storage exchange induced by a rise and subsequent fall of the river level. The hyporheic water existing in the river before the stage rise would be displaced by bank storage exchange and is not shown in (F). Note that (E) shows a plan-view whereas other diagrams show cross-sections.

to hundreds of meters (e.g. Bencala *et al.*, 1983) while river–aquifer exchange studies may be on the order of kilometres to tens of kilometres (e.g. Ellins *et al.*, 1990 and Cook *et al.*, 2003). Bank storage exchange studies generally compare the hydraulic responses in near-river observation wells with river stage and the distance between them is on the order of meters to tens of meters (e.g. Welch *et al.*, 2014). The temporal scale of hyporheic exchange residence times can range from seconds to weeks, while the residence times of

groundwater can be much longer depending on the location of the recharge zone and the aquifer properties. Bank storage exchange residence times are dependent on the duration of the river stage change and aquifer properties, and can be induced by diel fluctuations, individual flood events or seasonal river stage variation. There are a wide range of field methods used to quantify these exchange fluxes which are briefly summarised in the following section.

4.3. Methods to Quantify Exchange Fluxes

The most well established method for quantifying hyporheic exchange fluxes on the reach scale is the *Applied Tracer Test* (Stream Solute Workshop, 1990; Table 4.1). Generally, a conservative tracer is applied to the stream at a known rate and the breakthrough curve of tracer concentration is measured at a series of observation locations downstream. The shape of the breakthrough curve is used to determine the hyporheic exchange rate (e.g. Bencala *et al.*, 1983). These tests quantify the exchange occurring over the temporal scale of the observations (i.e. hours to days) while flowpaths that have residence times longer than this are not captured (Harvey *et al.*, 1996). Thus the depth of exchange captured using applied tracer tests is commonly on the order of centimetres to tens of centimetres over a longitudinal scale of tens to hundreds of metres (Table 4.1). To characterise deeper hyporheic exchange on a scale of metres, vertical profiles of environmental tracers can be obtained at multiple locations across larger scale features such as pool–riffle sequences or meander bends (Table 4.1; *Vertical Temperature Profiling* and *Vertical Chemistry Profiling*). Recently, a combination of tracers such as temperature and major ions (e.g. Fanelli and Lautz, 2008) or temperature and radon (e.g. Cranswick *et al.*, submitted) have been applied to better describe a wider range of temporal scales. Advancements in measurement techniques using fibre optic cables (Selker *et al.*, 2006) for a range of scale applications are also becoming more common (e.g. Briggs *et al.*, 2012).

These methods are summarised in Table 4.1, giving an indication of the spatial and temporal scales at which each method can be applied.

Table 4.1. Common methods for quantifying hyporheic, river–aquifer and bank storage exchange fluxes. The indicative spatial and temporal scale relevant to each method is also shown. Note that the split in the spatial scale representation for the *Applied Tracer Test* is due to the vertical (left) and longitudinal (right) aspects of this approach.

Exchange Flux			Methods
Hyporheic	River-Aquifer	Bank Storage	
●	●		Applied Tracer Test (ATT)
●	●		Vertical Temperature Profiling (VTP)
●	●		Vertical Chemistry Profiling (VCP)
●	●		Seepage Meters (SM)
●	●	●	Longitudinal Flow Gauging (LFG)
●	●	●	Longitudinal Chemistry Sampling (LCS)
●	●	●	Hydraulic Head Measurements (HHM)
●	●	●	Observation Well Chemisty (OWC)

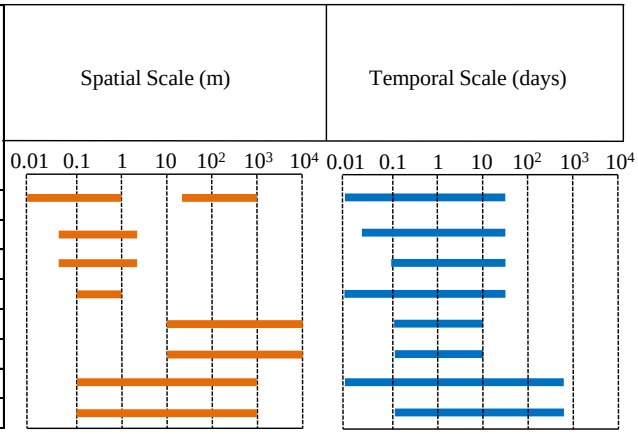

River–aquifer exchange fluxes for both gaining and losing rivers can be measured on a wide range of scales, from point measurements to measurements integrated over tens of kilometres as summarised by Kalbus *et al.* (2006) (see also Table 4.1). The exchange occurring over the hundreds of metres to the kilometre scale can be approximated by comparing groundwater level contour maps with river elevation and making assumptions about aquifer properties and geometry (Table 4.1; *Hydraulic Head Measurements*). Flux can then be calculated using Darcy's Law and a flownet analysis (Freeze and Cherry, 1979). *Longitudinal Flow Gauging* and *Longitudinal Chemistry Sampling* involve the gauging of river discharge and sampling of chemical species (e.g. environmental tracers) respectively, at a number of locations along a river to define sub-reaches. A water or chemical mass balance approach can then be used to determine the integrated river–aquifer exchange between upstream and downstream locations. Hence groundwater discharge on the kilometre to tens of kilometre scale, can be estimated even in remote catchments, without describing the spatial heterogeneity of aquifer and riverbed properties (e.g. Batlle-Aguilar *et al.*, 2014). Depending on which chemical species are sampled, these approaches

can also give information about the age and/or sources of groundwater discharge (e.g. Solomon *et al.*, 2010 or Smerdon *et al.*, 2012). The uncertainty of groundwater discharge can be reduced by the use of additional tracers (McCallum *et al.*, 2012) while our ability to estimate small fluxes is improved when the tracer concentration in groundwater is very distinct from that of the river (Cook, 2013). Point measurements using *Seepage Meters* (Table 4.1; e.g. Cey *et al.*, 1998) or vertical profiles of environmental tracers (Table 4.1; *Vertical Chemistry Profiling*; e.g. Ibrahim *et al.*, 2010) can be indicative of the exchange at that location. However, up-scaling this type of data can be problematic because it may not be representative of the larger scale exchange due to the heterogeneity of near river sediments. Calver (2001) summarised riverbed hydraulic conductivity (*K*) data from 41 studies to clearly demonstrate how this property can vary by many orders of magnitude over small spatial scales. Thus the likelihood of small scale measurements misrepresenting an overall exchange flux in such environments is high. The use of multiple methods and methods that integrate over larger scales (i.e. longitudinal sampling of environmental tracers) can be important for overcoming this potential limitation.

Bank storage exchange fluxes are often inferred based on the hydraulic responses in near-river observation wells and the application of Darcy's Law (Table 4.1; *Hydraulic Head Measurements*; e.g. Barlow *et al.*, 2000; Schilling *et al.*, 2004). The extent of bank storage infiltration into the bank and associated fluxes can also be determined by measuring changes in solute concentrations in near-river bores (Table 4.1; *Observation Well Chemistry*; e.g. Squillace, 1996; Schilling *et al.*, 2006; Arntzen *et al.*, 2006; and Welch *et al.*, 2013).

Many of the methods shown in Table 4.1 are commonly applied for quantifying both hyporheic and river–aquifer exchange fluxes while some can be used for all three exchange types (e.g. *Hydraulic Head Measurements* and *Observation Well Chemistry*). It is interesting to note that the methods listed here generally apply to spatial scales that range

over one to three orders of magnitude while the same methods have temporal scale ranges from two to five orders of magnitude (e.g. *Seepage Meters*). The temporal scale of the exchange represented by each approach is usually determined by the duration of the study (e.g. hours to tens of days for *Applied Tracer Tests*) or data collection period (e.g. days to weeks for *Vertical Temperature Profiling*). The temporal scale of some methods (e.g. *Observation Well Chemistry*) can be increased by using environmental tracers that inform us about longer residence times. It is clear from Table 4.1 that there is the potential to cover a broad range of spatial and temporal scales by using multiple methods and this approach is becoming increasingly adopted.

4.4. Data Collection for this Review

Data was gathered from 53 papers that quantified groundwater–surface water interaction in the form of hyporheic, river–aquifer or bank storage exchange flux. Instantaneous or mean river discharge values were also collected so that the exchange fluxes could be compared. Information on the rivers studied, methods used and the number of discrete flux values determined for each study are collated in Table 4.2. Where river discharge values during the study period were not mentioned in the text, mean annual flow was used (if reported). This was the case for some bank storage exchange studies where stage height at the time of analysis was reported rather than river discharge. If no river discharge values could be found for a particular study, the exchange flux data from that study was not added to our dataset. Where data was not presented in table format or in the text, flux and/or river discharge values have been estimated from graphs. The errors associated with these estimates are considered small relative to the trends seen across the range of study sites. Because there are very few studies that have differentiated between parafluvial exchange and other types of hyporheic exchange, we have added these flux values together where separate values are given (i.e. Ruehl *et al.*, 2006 and Bourke *et al.*, submitted only). *Applied Tracer Tests* are sometimes used to estimate the lateral inflow

Table 4.2. Data sources for the exchange flux comparison showing river names, type of study, methods used (acronyms defined in Table 4.1), number of values and study references. The hyporheic exchange (HE), river–aquifer exchange (RAE) and bank storage exchange (BSE) studies included here are not considered to be an exhaustive collection. However we consider that these studies represent the general trends and relative magnitudes of the exchange fluxes across a broad range of hydrogeological settings and climates.

River Name(s): Country	Type of Study	Methods	No. Values	Source	Ref. No.
Haller, Barslund, Karup: Denmark	RAE	LFG	9	Langhoff et al., 2006	1
Flint: USA	RAE	LFG	1	Opsahl et al., 2007	2
Lambourn, Pang: UK	RAE	LFG, LCS	2	Mullinger et al., 2007	3
Daly: Australia	RAE	LFG, LCS	5	Cook et al., 2003	4
Cockburn: Australia	RAE	LFG, LCS	1	Cook et al., 2006	5
Various: Australia	RAE	LFG, LCS, HHM	27	Cook et al., 2010	6
Souhegan (Upper/Lower): USA	RAE	LFG	32	Harte and Kiah, 2009	7
Pinal Ck: USA	HE	ATT	10	Harvey and Fuller, 1998	8
Pinal Ck: USA	HE	ATT	5	Harvey et al., 2003	9
West Fork, Walker Branch: USA	HE	ATT	20	Hart et al., 1999	10
St Kevin Gulch: USA	HE	ATT	2	Harvey et al., 1996	11
Aspen Ck, Gallina Ck, Rio Calveras: USA	HE	ATT	6	Morrice et al., 1997	12
Uvas Ck: USA	HE	ATT	3	Bencala, 1983	13
Swamp Oak Ck: Australia	HE	ATT	1	Lamontagne and Cook, 2007	14
St Kevin Gulch: USA	HE	ATT	1	Harvey and Bencala, 1993	15
Elder Ck: USA	HE	ATT	5	O'Connor et al., 2010	16
Various: USA	HE	ATT	37	Hall et al., 2002	17
Various in Jackson Hole: USA	RAE	LFG, HHM	4	Cey et al., 1998	18
Upper/Lower Red Canyon Ck, Cherry Ck: USA	HE	ATT	3	Lautz and Siegel, 2007	19
Various: USA	HE	ATT	39	Nordin and Sabol, 1974*	20
Colorado: USA	HE	ATT	2	Graf, 1995*	21
Various: Moldova	HE	ATT	3	Czernuszenko etal., 1998*	22
Green, Duwamish: USA	HE	ATT	2	Fischer etal., 1968b*	23
Various: USA	HE	ATT	12	Godfrey and Frederick, 1970*	24
Various, Brooks Range: USA	HE	ATT	30	Edwardson et al., 2003	25
Various, Willamette Basin: USA	HE	ATT	41	Laenen and Bencala, 2001	26
Six Tributaries to Columbia River: USA	RAE	LFG	230	Konrad, 2006	27
Stringer Ck: USA	RAE	LFG	55	Payn et al., 2009	28
Willamette: USA	HE	ATT	20	Fernald et al., 2001	29
Various Cascade and Appalachian Cks: USA	HE	ATT	22	D'Angelo et al., 1993	30
Pajaro: USA	HE, RAE	ATT, LFG	24	Ruehl et al., 2006	31
Lambourn: UK	RAE	LFG	12	Grapes et al., 2005	32
Tuolumne: USA	BSE	HHM	2	Loheide and Lunddquist, 2009	33
Cedar: USA	BSE	HHM, OWC	2	Squillace 1996	34
Colorado: USA	BSE	HHM	1	Sawyer et al., 2009	35
South Platte: USA	BSE	LFG	8	Sjodin et al 2001	36
Columbia: USA	BSE	HHM	2	Fritz and Arntzen, 2007	37
Cedar: USA	BSE	HHM	1	Barlow et al 2000	38
Fitzroy: Australia	BSE	Modelled HHM	6	Doble et al., 2011	39
Carmel: USA	BSE	LFG	12	Kondolf et al., 1987	40
Sycamore Ck: USA	HE	ATT	6	Marti et al., 1997	41
Cherokee, Cloud, Dry Cks: USA	HE	ATT	12	Haggard et al., 2001	42
Snake Den Branch: USA	HE	ATT	2	Thomas et al., 2003	43
Umtilla: USA	HE, RAE	LFG, OWC	16	Jones et al., 2008	44
Marillana Ck: Australia	HE, RAE	ATT, LFG, VTP, LCS	3	Bourke et al., submitted	45
West Bear Ck: USA	RAE	HHM, SM	2	Kennedy et al., 2010	46
West Bear Ck: USA	RAE	SM	8	Kennedy et al., 2009a	47
West Bear Ck: USA	RAE	HHM	21	Kennedy et al., 2009b	48
Bear Valley Ck: USA	HE	VTP	35	Gariglio et al., 2013	49
Pine: Canada	RAE	HHM, VTP	34	Conant, 2004	50
Various Ephemeral Cks: USA	RAE	VTP	3	Constantz et al., 2002	51
Aa: Belgium	RAE	VTP	24	Anibas et al., 2011	52
WS1, WS3: USA	HE	ATT	9	Wondzell, 2006	53

flux when the tracer concentration in the river is diluted by the addition of an external water source. However, we have omitted this flux value from hyporheic exchange studies where it was reported because the origin of this flux could equally be considered a long hyporheic flowpath, a returning bank storage flux or groundwater discharge. Both gaining and losing fluxes were included from studies of river–aquifer exchange (with losing fluxes being 31% of the total river–aquifer exchange flux data). Bank storage exchange fluxes include the values of mean flux over the study period, mean annual flux and maximum flux depending on what was reported in each study. We acknowledge that the data presented here are not an exhaustive collection and that there are other studies that could be added. However, this dataset is clearly sufficient to illustrate the trends of, and differences between each of the three types of exchange flux. In some cases it is possible for exchange fluxes to be attributed to a different type of exchange flux than the one reported, but we have adopted the author's interpretation.

4.5. Results

4.5.1. Studies with Multiple Exchange Fluxes

There are very few studies that have quantified two or more types of exchange flux within the same river system. For example, in a medium sized losing river in California (USA), Ruehl *et al.* (2006) found that hyporheic exchange fluxes were approximately 10 times greater than river loss and parafluvial inflows, which occurred concurrently. A combination of detailed river flow gauging and applied tracer tests were used to distinguish between exchange fluxes. In a smaller losing stream in northwestern Australia, Bourke *et al.* (submitted) found the current driven hyporheic exchange flux to be approximately 14 times greater than the parafluvial exchange flux, which was in turn 6 times greater than the groundwater recharge rate via river loss. This study used longitudinal chemistry sampling, river flow gauging, vertical radon profiling in the hyporheic zone and an applied tracer test to determine the exchange fluxes. In a study on a gaining medium sized river in Oregon

(USA), hyporheic exchange fluxes were on average 8 times greater than groundwater discharge in winter and 50 times greater in summer (Jones *et al.*, 2008). This study used water chemistry from observation wells and river samples to determine the exchange fluxes. These three studies suggest that hyporheic exchange fluxes are consistently much larger than river–aquifer exchange fluxes.

4.5.2. The Relative Magnitude of Exchange Fluxes

The hyporheic, river–aquifer and bank storage exchange fluxes determined from 53 studies were compared with river discharge (Figure 4.2; Note that each study has a unique symbol that is linked with references in Table 4.2). A trend of increasing exchange flux with increasing river discharge is generally seen for those studies that have multiple data points, although this is not always the case. These exceptions may be a result of the conditions found in each particular hydrogeological setting, or the methodology applied. For example, Fernald *et al.* (2001) (Ref. No. 29) conducted applied tracer tests over multiple reaches of the Willamette River during periods of similar river flow. Hence, the different hyporheic exchange fluxes were found to be related to channel complexity rather than river discharge (Fernald *et al.*, 2001). Some studies or individual flux values within a study appear to be outliers compared to the general trends. For example, Fritz and Arntzen (2007) (Ref. No. 37) calculate relatively small maximum and mean bank storage exchange fluxes compared to the general trend of the data. This is most likely due to the relatively small and regulated changes in river stage (rather than larger flood events) that drive the exchange at this particular study site at the time of investigation.

The data from each type of exchange flux was grouped and fit with a simple power law regression in the form of $Q_E = aQ^b$ using least squares, where Q_E is the exchange flux ($m^3\ s^{-1}\ km^{-1}$), Q is river discharge ($m^3\ s^{-1}$) and both a and b are fitting parameters (Figure 3). The exponent b, is the slope of the relationship between Q and Q_E on a log-log plot. A consistent trend of increasing exchange flux with increasing river discharge is evident for

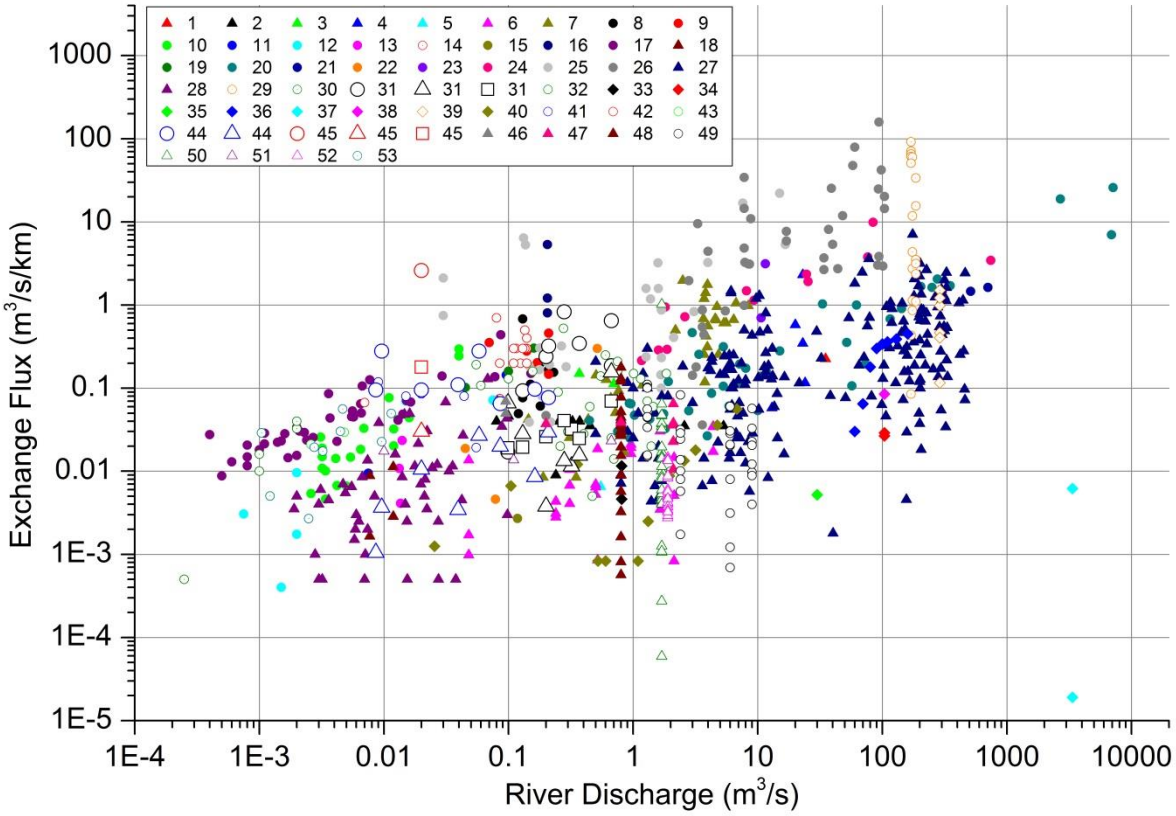

Figure 4.2. Indexed exchange flux and river discharge data from 53 different studies of groundwater–surface water interaction. Hyporheic exchange (circles), river–aquifer exchange (triangles) and bank storage exchange (diamonds) fluxes are plotted against river discharge. The larger hollow symbols are from studies where multiple exchange processes were quantified, with some including parafluvial hyporheic exchange (large hollow squares) as distinct from other types of exchange. River discharge values for hyporheic exchange, river–aquifer exchange and bank storage exchange were those recorded at the time of tracer test, at the downstream end of the study reach and at the maximum river discharge (or if unavailable the mean annual discharge) respectively.

each type of exchange flux. For approximately every two and a half orders of magnitude increase in river discharge, each of the exchange fluxes increase by approximately one order of magnitude (i.e. exponents of between 0.40 and 0.45). Since there is less data for the bank storage fluxes, this relationship is sensitive to the low flux values determined by Fritz and Arntzen (2007). If this data was to be excluded the exponent would change from 0.40 to 0.71 and hence the slope would be greater than for the other two exchange flux types.

Despite the exchange fluxes shown in Figure 4.3 not being from the same study location or measured at the same time, there are clear differences in the relative magnitude

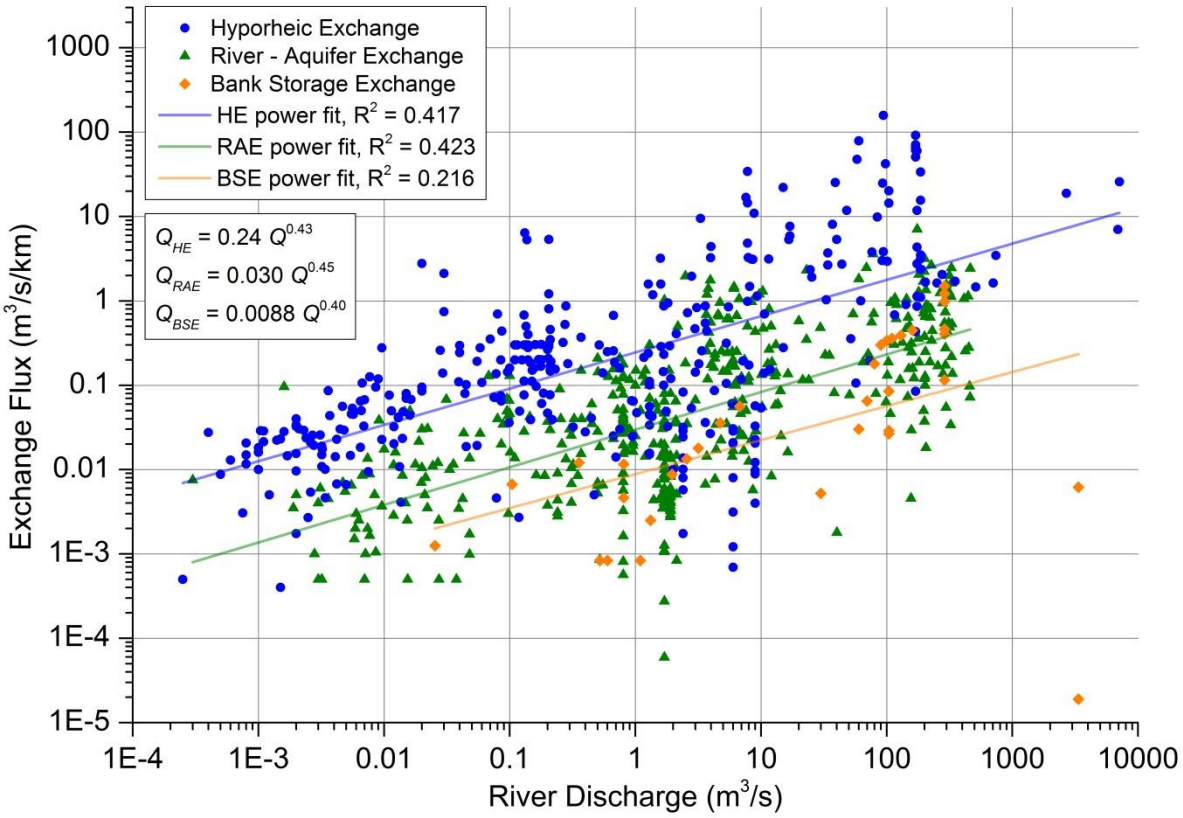

Figure 4.3. Hyporheic exchange fluxes (blue circles), river–aquifer exchange fluxes (green triangles) and bank storage exchange fluxes (orange diamonds) from a range of literature sources plotted against river discharge. For the two studies that reported parafluvial exchange and hyporheic exchange fluxes separately (Bourke *et al.*, submitted and Jones *et al.*, 2008) these values were added together in the above figure but are plotted separately in Figure 2. River discharge values for hyporheic exchange (HE), river–aquifer exchange (RAE) and bank storage exchange (BSE) were those recorded at the time of tracer test, at the downstream end of the study reach and at the maximum river discharge (or if unavailable the mean annual discharge) respectively. Each exchange group was fit with a power law regression using least squares with no data exclusions.

of each exchange flux group. Hyporheic exchange fluxes are approximately a factor of eight times greater than river–aquifer exchange fluxes which are in turn, approximately three times greater than bank storage exchange fluxes for the same river discharge. The relationship between the relative magnitudes of each of these fluxes may not hold for an individual study site because of its position in the landscape, specific geomorphology and larger scale hydrogeological conditions. However, as a general rule we suggest that hyporheic exchange fluxes are likely to be greater than those of other types of groundwater–surface water interaction. This finding is supported by the results of Ruehl *et*

al. (2006), Jones *et al.* (2008) and Bourke *et al.* (submitted) where both hyporheic and river–aquifer exchange fluxes were quantified at the same time and field location.

Although each flux increases with increasing river discharge, the ratio of exchange flux to river discharge becomes smaller in larger rivers. According to the power law regressions presented in Figure 4.3, the slope of this relationship on a log-log plot would be *b-1* (if we divide Q_E by Q). The resulting negative slope indicates a decrease in the relative proportion of each exchange flux with increasing river discharge. Conceptually, this may be controlled by a number of factors that change along the transition from headwater streams to large lowland rivers such as the grainsize distribution of riverbed sediments or riverbed slope (see also Harvey and Wagner, 2000). If we consider the same river at the same location but with an increased river discharge, the causes of the decrease in the ratio of the exchange flux to river discharge is less clear.

Conversely, the ratio of river discharge to hyporheic exchange flux (Q:Q_{HE}, in units of km), is equivalent to the distance required for river flow to be cycled through the hyporheic zone (i.e. the turnover length). At river discharges of 0.01, 0.1, 1 and 10 $m^3 s^{-1}$ this length is approximately 0.3, 1, 4 and 15 km respectively (Figure 4.4). Thus the relative magnitude of hyporheic exchange flux is much higher in small streams than in the larger rivers. This concept has also been discussed by Wondzell (2011) using data from four studies, and is clearly supported by the larger data collection presented here. Although some of the data deviates from the best fit regression by almost three orders of magnitude, the general trend of increasing turnover length with increasing river discharge holds true. The variance of turnover length values from the best fit regression appears to be smaller for smaller rivers and larger as river discharge increases. Here we assume that the condition of the river is the same (e.g. low flow) while the data actually includes small rivers at high flow and large rivers at low flow. This may have an influence on the apparent relationship between river discharge and turnover length variance.

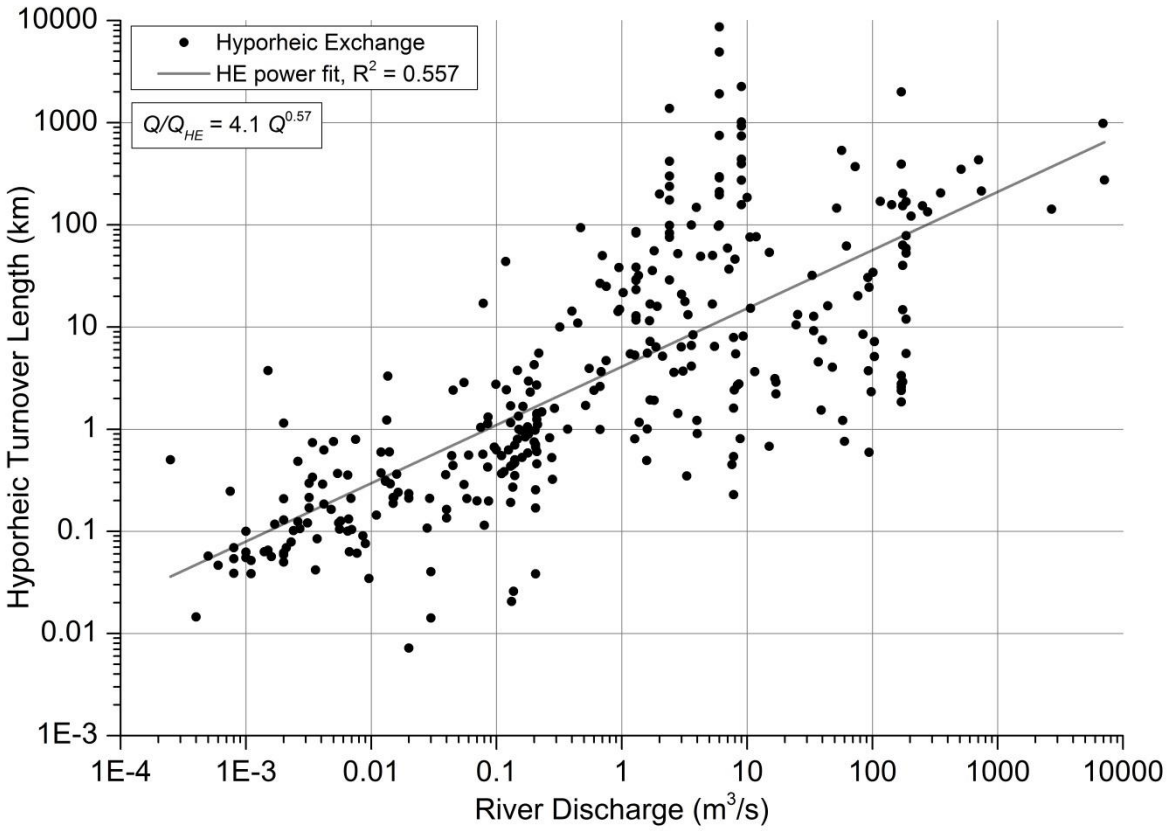

Figure 4.4. The relationship between the hyporheic turnover length (Q/Q_{HE}, units of km) and river discharge (Q). Data was fit with a power law regression using least squares with no data exclusions.

4.6. Discussion

4.6.1. Differences in Exchange Flux Magnitude

Hyporheic, river–aquifer and bank storage exchange fluxes all appear to increase in magnitude with increasing river discharge (Figure 4.3). However, the contributing or dominant factors driving these relationships have not been examined in detail within the present study. These factors are more comprehensively treated elsewhere (e.g. Harvey and Wagner, 2000; Woessner, 2000; Sophocleus, 2002) and are briefly discussed below where relevant. For hyporheic exchange fluxes, the exchange has been shown to be dependent on hydraulic properties of alluvial sediments, river hydraulics and geomorphology (e.g. D'Angelo *et al.*, 1993; Cardenas *et al.*, 2004; and Stonedahl *et al.*, 2010 respectively). Thus, larger rivers that may have greater surface areas through which hyporheic exchange could occur, might be expected to have greater exchange fluxes. A comparison of rivers in the Willamette Basin by Laenen and Bencala (2001) supports this, showing increased

hyporheic exchange in increasingly large rivers. In contrast, Harvey and Wagner (2000) discuss how many applied tracer tests conducted at higher river flows have shown that while hyporheic exchange increases at higher river flows, it plays a smaller relative role than at lower river flows (e.g. Lagrand-Marq and Laudelout, 1985 and D'Angelo *et al.*, 1993). This is supported by our study that shows an increase in Q_{HE} but a decrease in Q_{HE}:Q as river discharge increases. Harvey and Wagner (2000) also caution that the applied tracer approach is biased toward the faster exchange fluxes and does not represent the longer hyporheic flowpaths. Thus, hyporheic fluxes may be even greater than those determined in applied tracer test studies. In the case of groundwater, it may simply be that larger rivers have larger catchments and therefore greater areas for potential groundwater recharge and subsequent discharge to rivers. For river loss, rivers with higher flow rates are generally deeper and wider than rivers with smaller flow rates, and thus have the potential for higher loss rates. In the case of bank storage, larger rivers may have greater variation in stage than smaller rivers which could contribute to greater bank storage exchange fluxes. The duration of the stage change is also likely to be longer in large rivers which would result in larger volumes of bank storage but not necessarily larger fluxes.

It is common for different types of exchange processes to act in opposing directions (e.g. a gaining river would have a hydraulic gradient towards a river that would oppose downwelling hyporheic flowpaths). A modelling study by Cardenas and Wilson (2006) showed that bedform induced hyporheic exchange became damped with increasing groundwater discharge. Further modelling studies by Cardenas and Wilson (2007) and Cardenas (2009) showed that for both a triangular bedform feature and a meandering river respectively, applying stronger gaining and losing conditions resulted in a decrease to both the area and magnitude of hyporheic exchange fluxes compared to neutral conditions (note that groundwater fluxes were varied without any changes to river discharge). Superficially, this contradicts the trends of Figure 4.3 which suggest an increase for each type of

exchange flux with increasing river discharge, and hence a positive relationship between river–aquifer exchange and hyporheic exchange fluxes. It should be noted however, that our results do not imply that both hyporheic exchange and river–aquifer exchange will increase as river discharge increases in a particular river, because the datasets are not from the same field sites (with noted exceptions). Thus these relationships cannot be directly compared to the modelling studies which do not include any changes to river discharge. When compared to the few field studies that have measured multiple exchange fluxes, the relative magnitude differences in Figure 4.3 appear to hold. As more investigations endeavour to differentiate between hyporheic, river–aquifer and bank storage exchange fluxes, the relationships between these processes at different spatial and temporal scales in a range of hydrogeological settings should become clearer.

4.6.2. Differentiating Between Exchange Fluxes

As discussed by Bencala *et al.* (2011) and other authors, hyporheic exchange is critical for the cycling of nutrients and maintaining healthy river systems. In terms of water resource management however, the large fluxes associated with hyporheic exchange will, by definition, have no net effect on river discharge. However, the presence of large hyporheic exchange fluxes can make it more difficult to quantify the relatively small fluxes of groundwater discharge and river loss. To avoid unintentionally measuring hyporheic exchange, we should consider the scale of measurement carefully and the limitations of the chosen methods. Seepage meters, for example, cannot differentiate between river–aquifer exchange and hyporheic exchange without additional knowledge of the hydrogeological system. Even the measurement of downward hydraulic gradients, propagation of temperature or other tracers into a riverbed, could be equally interpreted as river loss or a downwelling hyporheic flowpath. Likewise, some characteristics of groundwater discharge can appear similar to a returning parafluvial flowpath or upwelling hyporheic flowpath (i.e. reduced conditions, constant temperature, hydraulic gradient towards the river etc.).

Shallow measurements in the riverbed (i.e. on the order of tens of centimetres) are very likely to be at least partly representative of hyporheic exchange. Measurements of river–aquifer exchange need to be collected from outside (or below) the influence of hyporheic exchange processes and/or using methods that allow these two exchange processes to be differentiated.

To delineate the extent of the hyporheic zone, the subsurface sampling of environmental tracers can be used if there are differences in the chemistry or age of each respective water source. For example, measuring the radon activity of water in the near river sediments can be used to determine the age of very young (up to 15 days old) infiltrating water. This could be coupled with measurements of subsurface water chemistry to determine the spatial extent of young hyporheic circulation (e.g. Cranswick *et al.*, submitted). To then estimate the true river loss or groundwater discharge, additional tracers that are useful at longer timescales could be measured beyond the spatial extent of the hyporheic zone. Such delineation would constitute a very robust conceptual model of the hydrogeological system.

Alternatively, because hyporheic exchange has a zero net flux over a large spatial scale, we can use methods that allow us to integrate the groundwater discharge or river loss that occurs over large river reaches. *Longitudinal Flow Gauging* can be used to infer groundwater discharge or river loss depending on the differences in river flow between upstream and downstream locations. Similarly, *Longitudinal Chemistry Sampling* can be effective in estimating groundwater discharge using a mass balance approach, provided the groundwater chemistry is different to the river chemistry. Groundwater may have distinctive isotopic or chemical signatures compared to those of the river for tracers such as chloride, other major ions, electrical conductivity, water isotopes or isotopes of strontium for example. The ability of these tracers to resolve groundwater discharge depends on how distinctive the concentrations in groundwater and the river are from each other (Cook,

2013). Conversely, estimating river loss is more difficult using environmental tracers because there is no change to the river chemistry through such loss. *Longitudinal Flow Gauging* may be the best approach for this on large spatial scales.

The delineation of the extent of bank storage exchange can be difficult or impractical. This is particularly the case where long term bank storage is considered in large alluvial aquifers because the classification of each exchange process can become unclear (i.e. at what residence time is bank storage considered to be groundwater?). Long term bank storage can clearly be important for water resources by providing recharge to alluvial aquifers and prolonging periods of higher river discharge (e.g. Kondolf *et al.*, 1987). Bank storage can be distinguished from groundwater if measurements of solutes with distinct groundwater or river signatures are made (Welch *et al.*, 2013). If environmental tracers are used to delineate the zone of bank storage exchange, then hydraulic gradients from beyond this zone should represent larger scale river–aquifer exchanges. Of course, the transient nature of infiltrating bank storage and subsequent return to the river can make it difficult to estimate the total volumes and fluxes of the exchange. *Differential Flow Gauging* will show returning bank storage as an increase in river discharge (which could be incorrectly interpreted as groundwater discharge).

If the potentially large hyporheic exchange fluxes are not included in the conceptual model of a study, there is a danger that the magnitude of groundwater discharge and river loss estimates could be overestimated. Thus, to more confidently estimate river–aquifer exchange fluxes, measurements should be made beyond the influence of hyporheic exchange and/or bank storage exchange processes. The use of multiple methods and environmental tracers can help differentiate between exchange flux types and add robustness to the conceptual model developed. In studies where only one type of exchange flux is considered there will remain a large degree of uncertainty as to the influence of both larger and smaller scale exchange fluxes.

4.6.3. Unclear Ecological Dependence

Both hyporheic exchange and groundwater discharge are considered important components of healthy river ecosystems (Brunke and Gonser, 1997; Boulton *et al.*, 1998; Malard *et al.*, 2002). However, the role of each exchange process is difficult to separate because quantifying distinct fluxes remains a challenge. Hyporheic exchange is known to moderate river temperatures, facilitate the cycling of nutrients and support a diversity of habitats where the exchange occurs (Malard *et al.*, 2002). Meanwhile, groundwater discharge can moderate river temperature, maintain refuge pools in times of low river flow and add nutrients to the river environment. To our knowledge there have been no studies comparing the dependence of an ecological community on an upwelling hyporheic flowpath versus the dependence on a groundwater discharge zone. Thus the impact of changes to the nature of groundwater–surface water interaction (e.g. as a result of groundwater pumping), could be very different depending on differences in the roles that groundwater discharge and hyporheic exchange play in the way a river ecosystem functions. For example, what will the ecological response be if the river–aquifer exchange changes from primarily gaining to primarily losing while hyporheic exchange continues to occur? As recently discussed by other authors, the future of groundwater–surface water interaction studies is towards a more robust understanding of the relationships between different exchange processes. Coupled with this, is the need to both link and predict the ecological response to any changes in the hydrological system.

4.7. Conclusion

We compared a wide range of exchange flux and river discharge values from studies quantifying hyporheic, river–aquifer and bank storage exchange processes. Hyporheic exchange fluxes were found to be almost an order of magnitude greater than river–aquifer exchange fluxes which were in turn, approximately three times greater than bank storage exchange fluxes. This demonstrates the difficulty of accurately estimating river–aquifer

exchange fluxes when smaller scale hyporheic processes are influencing measurements. These hyporheic exchange fluxes could be much larger than the river–aquifer exchange fluxes one intends to measure. Care should be taken to develop integrated conceptual models and use methods that enable a distinction to be made between each type of groundwater–surface water exchange flux. We suggest that the use of environmental tracers in addition to traditional methods can be a powerful tool to achieve this.

4.8. Acknowledgments

Funding for this research was provided by the National Centre for Groundwater Research and Training, an Australian Government initiative, supported by the Australian Research Council, the National Water Commission and the CSIRO Water for a Healthy Country Flagship. We also wish to thank Andrew Boulton for his enthusiastic support for earlier versions of this manuscript.

5. CONCLUSIONS

5.1. Summary of Findings and Implications

This research began with an understanding of the limitations of the traditional method (applied tracer tests) for quantifying hyporheic exchange. It was known that these tests cannot adequately characterise the spatial variability of hyporheic exchange between sampling locations or quantify the flowpaths that occur on temporal scales that are greater than the duration of the observation period. Thus, the use of naturally occurring environmental tracers as tools to fill these gaps in our understanding was explored using temperature and radon. The residence times and fluxes derived from temperature and radon data collected in detailed vertical profiles had not been directly compared in the literature. It was also apparent that there was a lack of understanding about the relative scales and magnitudes of groundwater–surface water exchange processes. These include hyporheic exchange, river–aquifer exchange (groundwater discharge and river infiltration) and bank storage exchange. There are only a limited number of studies that clearly quantify more than one type of exchange flux and so a broad review of the literature was necessary in order to compare them.

The major findings and implications of this research are summarised below:

1) Detailed vertical profiles of temperature, radon and electrical conductivity data have allowed the spatial variability of vertical flux, residence time and depth of hyporheic circulation to be characterised beneath a pool–riffle sequence. This demonstrates the usefulness of combining multiple naturally occurring environmental tracers to improve the understanding hyporheic processes when spatial variability is important.
2) Subsurface temperature data was interpreted using a 1D numerical approach that treated each observation depth independently from those above or below it. This meant that the resulting vertical flux was representative of the mean vertical

component of flux along the flowpath between the river and that depth. Thus, the vertical fluxes derived from temperature data using a 1D analysis inherently have spatial footprints, which are equal to the upgradient length of each flowpath. This is an important consideration when evaluating the differences between vertical fluxes derived from 1D and 2D approaches. Conceptualising the 1D approach in this way is considered to be an improvement on the more common approach of comparing sequential pairs of data to estimate vertical flux because the assumption that flow is purely vertical is not required. This approach also allows temperature derived fluxes and residence times to be directly compared with other tracer methods (i.e. applied or naturally occurring tracers such as radon).

3) The radon approach has the lowest uncertainty for residence times between 0.1 and 15 days while the uncertainty of the temperature approach (using a diel river signal) is lowest for residence times that are less than a few days. By combining temperature and radon approaches, hyporheic flowpaths that have residence times ranging from tens of minutes up to 15 days can be easily characterised. This allows a wider range of hyporheic flowpaths to be quantified in a day or two of field work rather than by conducting an extended applied tracer test that may be logistically impractical or costly.

4) A disparity was found when directly comparing temperature-derived and radon-derived residence times. It is suggested that this is caused by the different influence of small scale heterogeneity on heat and solute transport processes. The temperature approach may be more influenced by flow through zones of higher hydraulic conductivity and result in higher fluxes and lower residence times than those derived from the radon approach. Because the radon approach is not as influenced by flow through higher hydraulic conductivity zones, it may be more representative of the flow

occurring where the sample is collected (i.e. rather than influenced by fluxes occurring through adjacent sediments).

5) In a review of 53 studies that quantified different types of groundwater–surface water exchange fluxes, hyporheic exchange fluxes were found to be approximately an order of magnitude greater than river–aquifer exchange fluxes, which were in turn approximately three times greater than bank storage exchange fluxes. This finding is important as it reveals the potential for measurements in or near rivers to be influenced by large hyporheic exchange fluxes. Hence, even (or especially) when hyporheic exchange is not the focus of an investigation, it is critical that hyporheic exchange processes are considered and distinguished from other processes. Otherwise there is potential for large fluxes to be measured in the near river environment and then misinterpreted as river–aquifer exchange (i.e. groundwater discharge or river infiltration). In order to more confidently measure river–aquifer exchange fluxes, measurements must therefore be taken outside of the influence of hyporheic exchange and by using methods that allow these processes to be clearly delineated and (or) quantified (e.g. environmental tracers in combination with hydraulic methods).

5.2. Future Investigations

The spatial variability of hyporheic exchange processes along the study reach of the Haughton River was successfully characterised using vertical profiles of radon, temperature and electrical conductivity. However, the ultimate comparison of this characterisation would be with a long term applied tracer test that was conducted over a similar (or longer) duration as the residence times derived from environmental tracer data. The practicalities of such a study would be challenging, particularly if the spatial variability of hyporheic flowpaths was to be captured on a scale representative of the entire reach (including any processes occurring outside of the river itself, e.g. parafluvial fluxes or river–aquifer exchange fluxes). It would be useful to compare and contrast the

information provided by such a tracer test, with that of the data collected from spatially representative vertical profiles of environmental tracers along the same study reach.

A major finding of Chapter 3 was that small scale heterogeneity influences heat and radon transport differently resulting in a disparity of the flux and residence time values in some cases. This could be further investigated both experimentally (similarly to Rau *et al.*, 2012a; 2012b but with more heterogeneous sediments) or by using detailed numerical models for downwelling flowfields (see Irvine *et al.*, submitted). This may then allow a greater understanding of field results that show a disparity between heat and solute-derived residence times or fluxes. Furthermore, additional comparisons of field data using both temperature and solute tracers are also required to add to our understanding of the influence of heterogeneity in a range of hydrogeological settings.

Chapter 4 demonstrated the importance of being able to quantify hyporheic exchange fluxes as distinct from river–aquifer exchange fluxes (i.e. so that groundwater discharge or river infiltration fluxes are not overestimated). It follows that there may be ecological functions and responses that are dependent on either or both of these processes. For example, Baxter and Hauer (2000) demonstrate that the spawning locations of bull trout were consistently found in downwelling sections (hyporheic exchange) along gaining reaches (groundwater discharge) of the streams studied. The relationship between hyporheic exchange and river–aquifer exchange fluxes in future climates or river management regimes could be thus explored, with key ecological responses such as this in mind. For example, what would the potential impacts be on individual species and the overall ecological function of a river reach if it were to change from predominantly gaining to losing while hyporheic exchange was maintained?

6. REFERENCES

Anderson MP. 2005. Heat as a ground water tracer. *Ground Water*, 43: 951-968. DOI: 10.1111/j.1745-6584.2005.00052.x.

Anibas C, Fleckenstein JH, Volze N, Buis K, Verhoeven R, Meire P, Batelaan O. 2009. Transient or steady-state? Using vertical temperature profiles to quantify groundwater-surface water exchange. *Hydrological Processes*, 23: 2165-2177. DOI: 10.1002/hyp.7289.

Arntzen EV, Geist DR, Dresel PE. 2006. Effects of fluctuating river flow on groundwater/surface water mixing in the hyporheic zone of a regulated, large cobble bed river. *River Research and Applications*, 22: 937-946. DOI: 10.1002/rra.947.

Barlow PM, DeSimone LA, Moench AF. 2000. Aquifer response to stream-stage and recharge variations. II. Convolution method and applications. *Journal of Hydrology*, 230: 211-229. DOI: 10.1016/s0022-1694(00)00176-1.

Batlle-Aguilar J, Harrington GA, Leblanc M, Welch C, Cook PG. 2014. Chemistry of groundwater discharge inferred from longitudinal river sampling. *Water Resources Research*, 50: 1550-1568.

Baxter CV, Hauer FR. 2000. Geomorphology, hyporheic exchange, and selection of spawning habitat by bull trout (*Salvelinus confluentus*). *Canadian Journal of Fisheries and Aquatic Sciences*, 57: 1470-1481.

Bencala KE. 1983. Simulation of solute transport in a mountain pool-and-riffle stream with a kinetic mass-transfer model for sorption. *Water Resources Research*, 19: 732-738. DOI: 10.1029/WR019i003p00732.

Bencala KE. 1993. A perspective on stream-catchment connections. *Journal of the North American Benthological Society*, 12: 44-47. DOI: 10.2307/1467684.

Bencala KE, Gooseff MN, Kimball BA. 2011. Rethinking hyporheic flow and transient storage to advance understanding of stream-catchment connections. *Water Resources Research*, 47. DOI: W00h0310.1029/2010wr010066.

Bencala KE, Kennedy VC, Zellweger GW, Jackman AP, Avanzino RJ. 1984. Interaction of solutes and streambed sediment .1. an experimental-analysis of cation and anion transport in a mountain stream. *Water Resources Research*, 20: 1797-1803. DOI: 10.1029/WR020i012p01797.

Bencala KE, Walters RA. 1983. Simulation of solute transport in a mountain pool-and-riffle stream - a transient storage model. *Water Resources Research*, 19: 718-724. DOI: 10.1029/WR019i003p00718.

Bertin C, Bourg ACM. 1994. Rn-222 and chloride as natural tracers of the infiltration of river water into an alluvial aquifer in which there is significant river groundwater mixing. *Environmental Science & Technology*, 28: 794-798. DOI: 10.1021/es00054a008.

Bhaskar AS, Harvey JW, Henry EJ. 2012. Resolving hyporheic and groundwater components of streambed water flux using heat as a tracer. *Water Resources Research*, 48. DOI: 10.1029/2011wr011784.

Boano F, Camporeale C, Revelli R, Ridolfi L. 2006. Sinuosity-driven hyporheic exchange in meandering rivers. *Geophysical Research Letters*, 33. DOI: 10.1029/2006gl027630.

Boulton AJ. 1993. Stream ecology and surface hyporheic hydrologic exchange - implications, techniques and limitations. *Australian Journal of Marine and Freshwater Research*, 44: 553-564.

Boulton AJ, Datry T, Kasahara T, Mutz M, Stanford JA. 2010. Ecology and management of the hyporheic zone: stream-groundwater interactions of running waters and their floodplains. *Journal of the North American Benthological Society*, 29: 26-40. DOI: 10.1899/08-017.1.

Boulton AJ, Findlay S, Marmonier P, Stanley EH, Valett HM. 1998. The functional significance of the hyporheic zone in streams and rivers. *Annual Review on Ecological Systems*, 29: 59-81. DOI: 10.1146/annurev.ecolsys.29.1.59.

Bourke SA, Cook PG, Shanafield M, Dogramaci S, Clark JF. Submitted (2014). Characterization of hyporheic exchange in a losing stream using radon-222. *Journal of Hydrology*.

Bredehoeft JD, Papadopulos IS. 1965. Rates of vertical groundwater movement estimated from earths thermal profile. *Water Resources Research*, 1: 325-328. DOI: 10.1029/WR001i002p00325.

Briggs MA, Lautz LK, McKenzie JM, Gordon RP, Hare DK. 2012. Using high-resolution distributed temperature sensing to quantify spatial and temporal variability in vertical hyporheic flux. *Water Resources Research*, 48. DOI: W02527, 10.1029/2011wr011227.

Brunke M, Gonser T. 1997. The ecological significance of exchange processes between rivers and groundwater. *Freshwater Biology*, 37: 1-33. DOI: 10.1046/j.1365-2427.1997.00143.x.

Bureau of Meteorology (BoM). 2012. Monthly Rainfall Climate Data (1934 – 2012). Majors Creek (Station 033151). Australian Government, Canberra.

Calver A. 2001. Riverbed permeabilities: Information from pooled data. *Ground Water*, 39: 546-553. DOI: 10.1111/j.1745-6584.2001.tb02343.x.

Cardenas MB. 2008. The effect of river bend morphology on flow and timescales of surface water-groundwater exchange across pointbars. *Journal of Hydrology*, 362: 134-141. DOI: 10.1016/j.jhydrol.2008.08.018.

Cardenas MB. 2008. Surface water-groundwater interface geomorphology leads to scaling of residence times. *Geophysical Research Letters*, 35. DOI: 10.1029/2008gl033753.

Cardenas MB. 2009. Stream-aquifer interactions and hyporheic exchange in gaining and losing sinuous streams. *Water Resources Research*, 45. DOI: W06429, 10.1029/2008wr007651.

Cardenas MB, Wilson JL. 2006. The influence of ambient groundwater discharge on exchange zones induced by current-bedform interactions. *Journal of Hydrology*, 331: 103-109. DOI: 10.1016/j.jhydrol.2006.05.012.

Cardenas MB, Wilson JL. 2007. Exchange across a sediment-water interface with ambient groundwater discharge. *Journal of Hydrology*, 346: 69-80. DOI: 10.1016/j.jhydrol.2007.08.019.

Cardenas MB, Wilson JL. 2007. Thermal regime of dune-covered sediments under gaining and losing water bodies. *Journal of Geophysical Research*, 112: G04013. DOI: 10.1029/2007jg000485.

Cardenas MB, Wilson JL, Zlotnik VA. 2004. Impact of heterogeneity, bed forms, and stream curvature on subchannel hyporheic exchange. *Water Resources Research*, 40. DOI: W08307, 10.1029/2004wr003008.

Carslaw HS, Jaeger JC. 1959. Conduction of Heat in Solids. Oxford University Press, London.

Cecil LD. Green JR. 2000. Radon-222. In *Environmental Tracers in Subsurface Hydrology*, Cook PG, Herczeg AL (eds). Kluwer Academic Publishers: Boston; 175-194.

Cey EE, Rudolph DL, Parkin GW, Aravena R. 1998. Quantifying groundwater discharge to a small perennial stream in southern Ontario, Canada. *Journal of Hydrology*, 210: 21-37. DOI: 10.1016/s0022-1694(98)00172-3.

Cheong TS, Younis BA, Seo IW. 2007. Estimation of key parameters in model for solute transport in rivers and streams. *Water Resources Management*, 21: 1165-1186. DOI: 10.1007/s11269-006-9074-7.

Conant B. 2004. Delineating and quantifying ground water discharge zones using streambed temperatures. *Ground Water*, 42: 243-257. DOI: 10.1111/j.1745-6584.2004.tb02671.x.

Constantz J. 2008. Heat as a tracer to determine streambed water exchanges. *Water Resources Research*, 44. DOI: 10.1029/2008wr006996.

Constantz J, Cox MH, Su GW. 2003. Comparison of heat and bromide as ground water tracers near streams. *Ground Water*, 41: 647-656. DOI: 10.1111/j.1745-6584.2003.tb02403.x.

Constantz J, Stewart AE, Niswonger R, Sarma L. 2002. Analysis of temperature profiles for investigating stream losses beneath ephemeral channels. *Water Resources Research*, 38. DOI: 131610.1029/2001wr001221.

Constantz J, Thomas CL, Zellweger G. 1994. Influence of diurnal-variations in stream temperature on streamflow loss and groundwater recharge. *Water Resources Research*, 30: 3253-3264. DOI: 10.1029/94wr01968.

Cook PG. 2013. Estimating groundwater discharge to rivers from river chemistry surveys. *Hydrological Processes*, 27: 3694-3707. DOI: 10.1002/hyp.9493.

Cook PG, Favreau G, Dighton JC, Tickell S. 2003. Determining natural groundwater influx to a tropical river using radon, chlorofluorocarbons and ionic environmental tracers. *Journal of Hydrology*, 277: 74-88. DOI: 10.1016/s0022-1694(03)00087-8.

Cook PG, Lamontagne S, Berhane D, Clark JF. 2006. Quantifying groundwater discharge to Cockburn River, southeastern Australia, using dissolved gas tracers Rn-222 and SF6. *Water Resources Research*, 42. DOI: W10411 10.1029/2006wr004921.

Cook PG, Stieglitz T, Clark J. 2004. Groundwater Discharge from the Burdekin Floodplain Aquifer, North Queensland. CSIRO Land and Water Technical Report No 26/04: 120.

Cook PG, Bohlke J-K. 2000. Determining timescales for groundwater flow and solute transport. In *Environmental Tracers in Subsurface Hydrology*, Cook PG, Herczeg AL (eds). Kluwer Academic Publishers: Boston; 1-30.

Cook PG, McCallum J, Hoban M, Evans R, McMahon G, Rumpf C. 2010. Methods for estimating groundwater discharge to streams - Summary of field trials. Stage 2 Summary report, Prepared by Sinclair Knight Merz and the Commonwealth Scientific and Industrial Research Organisation Land and Water for the National Water Commission, Australia.

Cranswick RH, Cook PG. Submitted (2014). Scales and magnitude of hyporheic, river-aquifer and bank storage exchange fluxes. *Hydrological Processes*, HYP-14-0333.

Cranswick RH, Cook PG, Lamontagne S. Submitted (2014). Hyporheic zone exchange fluxes and residence times inferred from riverbed temperature and radon data. *Journal of Hydrology*, HYDROL16517R1.

Cranswick, RH, Cook PG, Shanafield M, Lamontagne S. 2014. The vertical variability of hyporheic fluxes inferred from riverbed temperature data. *Water Resources Research*, 50. DOI:10.1002/2013WR014410.

Cuthbert MO, Mackay R. 2013. Impacts of nonuniform flow on estimates of vertical streambed flux. *Water Resources Research*, 49: 19-28. DOI: 10.1029/2011wr011587.

Dahm CN, Grimm NB, Marmonier P, Valett HM, Vervier P. 1998. Nutrient dynamics at the interface between surface waters and groundwaters. *Freshwater Biology*, 40: 427-451. DOI: 10.1046/j.1365-2427.1998.00367.x.

D'Angelo DJ, Webster JR, Gregory SV, Meyer JL. 1993. Transient storage in appalachian and cascade mountain streams as related to hydraulic characteristics. *Journal of the North American Benthological Society*, 12: 223-235. DOI: 10.2307/1467457.

Dehghan M. 2004. Weighted finite difference techniques for the one-dimensional advection-diffusion equation. *Applied Mathematics and Computation*, 147: 307-319. DOI: 10.1016/s0096-3003(02)00667-7.

Department of Environment and Resource Management (DERM). 2012. Streamflow Data: 119003A Haughton River at Powerline. Queensland Government, Australia.

Dickson BL. 1990. Radium in groundwater. In *The Environmental Behaviour of Radium*. International Atomic Energy Agency – Technical Report (310), Vienna.

Doble R, Brunner P, McCallum J, Cook PG. 2012. An Analysis of River Bank Slope and Unsaturated Flow Effects on Bank Storage. *Ground Water*, 50: 77-86. DOI: 10.1111/j.1745-6584.2011.00821.x.

Doherty JE. 2010. PEST Model Independent Parameter Estimation User Manual: 5th Edition. Watermark Numerical Computing. Australia.

Duff JH, Murphy F, Fuller CC, Triska FJ, Harvey JW, Jackman AP. 1998. A mini drivepoint sampler for measuring pore water solute concentrations in the hyporheic zone of sand-bottom streams. *Limnology and Oceanography*, 43: 1378-1383.

Edwardson KJ, Bowden WB, Dahm C, Morrice J. 2003. The hydraulic characteristics and geochemistry of hyporheic and parafluvial zones in Arctic tundra streams, north slope, Alaska. *Advances in Water Resources*, 26: 907-923. DOI: 10.1016/s0309-1708(03)00078-2.

Ellins KK, Romanmas A, Lee R. 1990. Using Rn-222 to examine groundwater surface discharge interaction in the Rio-Grande-De-Manati, Puerto-Rico. *Journal of Hydrology*, 115: 319-341. DOI: 10.1016/0022-1694(90)90212-g.

Fanelli RM, Lautz LK. 2008. Patterns of water, heat, and solute flux through streambeds around small dams. *Ground Water*, 46: 671-687. DOI: 10.1111/j.1745-6584.2008.00461.x.

Ferguson G, Bense V. 2011. Uncertainty in 1D Heat-Flow Analysis to Estimate Groundwater Discharge to a Stream. *Ground Water*, 49: 336-347. DOI: 10.1111/j.1745-6584.2010.00735.x.

Fernald AG, Wigington PJ, Landers DH. 2001. Transient storage and hyporheic flow along the Willamette River, Oregon: Field measurements and model estimates. *Water Resources Research*, 37: 1681-1694. DOI: 10.1029/2000wr900338.

Fox A, Boano F, Arnon, S. 2014. Impact of losing and gaining streamflow conditions on hyporheic exchange fluxes induced by dune-shaped bed forms. *Water Resources Research* 50. DOI:10.1002/2013WR014668.

Freeze RA, Cherry J A. 1979. *Groundwater.* Prentice-Hall: United States of America; 604.

Fritz BG, Arntzen EV. 2007. Effect of rapidly changing river stage on uranium flux through the hyporheic zone. *Ground Water*, 45: 753-760. DOI: 10.1111/j.1745-6584.2007.00365.x.

Gariglio FP, Tonina D, Luce CH. 2013. Spatiotemporal variability of hyporheic exchange through a pool-riffle-pool sequence. *Water Resources Research*, 49: 7185-7204. DOI: 10.1002/wrcr.20419.

Gooseff MN, Anderson JK, Wondzell SM, LaNier J, Haggerty R. 2006. A modeling study of hyporheic exchange pattern and the sequence, size, and spacing of stream bedforms in mountain stream networks, Oregon, USA (Retraction of vol 19, pg 2915, 2005). *Hydrological Processes*, 20: 2441-+. DOI: 10.1002/hyp.6350.

Gordon RP, Lautz LK, Briggs MA, McKenzie JM. 2012. Automated calculation of vertical pore-water flux from field temperature time series using the VFLUX method and computer program. *Journal of Hydrology*, 420–421: 142-158.

Grapes TR, Bradley C, Petts GE. 2005. Dynamics of river-aquifer interactions along a chalk stream: the River Lambourn, UK. *Hydrological Processes*, 19: 2035-2053. DOI: 10.1002/hyp.5665.

Haggard BE, Storm DE, Tejral RD, Popova YA, Keyworth VG, Stanley EH. 2001. Stream nutrient retention in three Northeastern Oklahoma agricultural catchments. *Transactions of the American Society of Agricultural Engineers*, 44: 597-605.

Haggerty R, Wondzell SM, Johnson MA. 2002. Power-law residence time distribution in the hyporheic zone of a 2nd-order mountain stream. *Geophysical Research Letters*, 29. DOI: 10.1029/2002gl014743.

Hall RO, Bernhardt ES, Likens GE. 2002. Relating nutrient uptake with transient storage in forested mountain streams. *Limnology and Oceanography*, 47: 255-265.

Hart DR, Mulholland PJ, Marzolf ER, DeAngelis DL, Hendricks SP. 1999. Relationships between hydraulic parameters in a small stream under varying flow and seasonal conditions. *Hydrological Processes*, 13: 1497-1510. DOI: 10.1002/(sici)1099-1085(199907)13:10<1497::aid-hyp825>3.0.co;2-1.

Harte PT, Kiah RG. 2009. Measured river leakages using conventional streamflow techniques: the case of Souhegan River, New Hampshire, USA. *Hydrogeology Journal*, 17: 409-424. DOI: 10.1007/s10040-008-0359-1.

Harvey JW, Bencala KE. 1993. The effect of streambed topography on surface-subsurface water exchange in mountain catchments. *Water Resources Research*, 29: 89-98. DOI: 10.1029/92wr01960.

Harvey JW, Conklin MH, Koelsch RS. 2003. Predicting changes in hydrologic retention in an evolving semi-arid alluvial stream. *Advances in Water Resources*, 26: 939-950. DOI: 10.1016/s0309-1708(03)00085-x.

Harvey JW, Fuller CC. 1998. Effect of enhanced manganese oxidation in the hyporheic zone on basin-scale geochemical mass balance. *Water Resources Research*, 34: 623-636. DOI: 10.1029/97wr03606.

Harvey JW, Wagner BJ, Bencala KE. 1996. Evaluating the reliability of the stream tracer approach to characterize stream-subsurface water exchange. *Water Resources Research*, 32: 2441-2451. DOI: 10.1029/96wr01268.

Harvey JW, Wagner, B. J. 2000. Quantifying Hydrologic Interactions between Streams and Their Subsurface Hyporheic Zones. In *Streams and Ground Water*s. Jones JB, Mulholland PJ (eds). Academic Press: San Diego; 3-44.

Hatch CE, Fisher AT, Revenaugh JS, Constantz J, Ruehl C. 2006. Quantifying surface water-groundwater interactions using time series analysis of streambed thermal records: Method development. *Water Resources Research*, 42. DOI: W10410, 10.1029/2005wr004787.

Hoehn E, Cirpka OA. 2006. Assessing residence times of hyporheic ground water in two alluvial flood plains of the Southern Alps using water temperature and tracers. *Hydrology and Earth Systems Sciences*, 10: 553-563.

Hoehn E, Vongunten HR. 1989. Radon in groundwater - a tool to assess the infiltration from surface waters to aquifers. *Water Resources Research*, 25: 1795-1803. DOI: 10.1029/WR025i008p01795.

Ibrahim TG, Thornton SF, Wainwright J. 2010. Interplay of geomorphic and hydrogeologic features at reach- and channel unit-scales on riverbed hydrology and hydrochemistry: a conceptual model in the Lower Coal Measures, South Yorkshire, UK. *Hydrogeology Journal*, 18: 1391-1411. DOI: 10.1007/s10040-010-0623-z.

Irvine DJ, Cranswick RH, Simmons CT, Shanafield S, Lautz L. Submitted (2014). The effect of streambed heterogeneity on temperature time series methods to quantify groundwater-surface water exchange. *Water Resources Research*, 2014WR015769.

Irvine DJ, Simmons CT, Werner AD, Graf T. 2013. Heat and Solute Tracers: How Do They Compare in Heterogeneous Aquifers? *Ground Water*, DOI: 0.1111/gwat.12146

Jones JB, Mulholland PJ. 2000. *Streams and Ground Water*s. Academic Press: San Diego; 425.

Jones KL, Poole GC, Woessner WW, Vitale MV, Boer BR, O'Daniel SJ, Thomas SA, Geffen BA. 2008. Geomorphology, hydrology, and aquatic vegetation drive seasonal hyporheic flow patterns across a gravel-dominated floodplain. *Hydrological Processes*, 22: 2105-2113. DOI: 10.1002/hyp.6810.

Kalbus E, Reinstorf F, Schirmer M. 2006. Measuring methods for groundwater - surface water interactions: a review. *Hydrology and Earth Systems Sciences*, 10: 873-887.

Keery J, Binley A, Crook N, Smith JWN. 2007. Temporal and spatial variability of groundwater-surface water fluxes: Development and application of an analytical method using temperature time series. *Journal of Hydrology*, 336: 1-16. DOI: 10.1016/j.jhydrol.2006.12.003.

Kennedy CD, Genereux DP, Corbett DR, Mitasova H. 2009b. Relationships among groundwater age, denitrification, and the coupled groundwater and nitrogen fluxes through a streambed. *Water Resources Research*, 45. DOI: 10.1029/2008wr007400.

Kennedy CD, Genereux DP, Corbett DR, Mitasova H. 2009a. Spatial and temporal dynamics of coupled groundwater and nitrogen fluxes through a streambed in an agricultural watershed. *Water Resources Research*, 45. DOI: 10.1029/2008wr007397.

Kennedy CD, Murdoch LC, Genereux DP, Corbett DR, Stone K, Pham P, Mitasova H. 2010. Comparison of Darcian flux calculations and seepage meter measurements in a sandy streambed in North Carolina, United States. *Water Resources Research*, 46. DOI: 10.1029/2009wr008342.

Kirchner JW, Feng XH, Neal C. 2000. Fractal stream chemistry and its implications for contaminant transport in catchments. *Nature*, 403: 524-527. DOI: 10.1038/35000537.

Kondolf GM, Maloney LM, Williams JG. 1987. Effects of Bank Storage and Well Pumping on Base-Flow, Carmel-River, Monterey-County, California. *Journal of Hydrology*, 91: 351-369. DOI: 10.1016/0022-1694(87)90211-3.

Konrad CP. 2006. Location and timing of river-aquifer exchanges in six tributaries to the Columbia River in the Pacific Northwest of the United States. *Journal of Hydrology*, 329: 444-470. DOI: 10.1016/j.jhydrol.2006.02.028.

Laenen A, Bencala KE. 2001. Transient storage assessments of dye-tracer injections in rivers of the Willamette Basin, Oregon. *Journal of the American Water Resources Association*, 37: 367-377. DOI: 10.1111/j.1752-1688.2001.tb00975.x.

Lamontagne S, Cook PG. 2007. Estimation of hyporheic water residence time in situ using Rn-222 disequilibrium. *Limnology and Oceanography*-Methods, 5: 407-416.

Lamontagne S, Cook, P.G., Taylor, A.R. 2010. Evaluation of the Rn-222 disequilibrium technique to estimate hyporheic exchange in a gaining river. *Water for a Healthy Country Flagship Report Series*: 25.

Langhoff JH, Rasmussen KR, Christensen S. 2006. Quantification and regionalization of groundwater-surface water interaction along an alluvial stream. *Journal of Hydrology*, 320: 342-358. DOI: 10.1016/j.jhydrol.2005.07.040.

Lapham WW. 1987. Use of temperature profiles beneath streams to determine rates of vertical ground-water flow and vertical hydraulic conductivity. *U.S. Geological Survey Water-Supply Paper 2337*. Unites States Government Printing Office: Denver; 35.

Lautz L, Fanelli R. 2008. Seasonal biogeochemical hotspots in the streambed around restoration structures. *Biogeochemistry,* 91: 85-104.DOI: 10.1007/s10533-008-9235-2.

Lautz LK. 2010. Impacts of nonideal field conditions on vertical water velocity estimates from streambed temperature time series. *Water Resources Research*, 46. DOI: 10.1029/2009wr007917.

Lautz LK, Siegel DI. 2007. The effect of transient storage on nitrate uptake lengths in streams: an inter-site comparison. *Hydrological Processes*, 21: 3533-3548. DOI: 10.1002/hyp.6569.

Leaney FW, Herczeg AL. 2006. A rapid field extraction method for determination of radon-222 in natural waters by liquid scintillation counting. *Limnology and Oceanography-Methods*, 4: 254-259.

Legrand-Marq C, Laudelout H. 1985. Longitudinal dispersion in a forest stream. *Journal of Hydrology*, 78:317-324.

Lewandowski J, Angermann L, Nuetzmann G, Fleckenstein JH. 2011. A heat pulse technique for the determination of small-scale flow directions and flow velocities in the streambed of sand-bed streams. *Hydrological Processes*, 25: 3244-3255. DOI: 10.1002/hyp.8062.

Loheide SP, II, Lundquist JD. 2009. Snowmelt-induced diel fluxes through the hyporheic zone. *Water Resources Research*, 45. DOI: 10.1029/2008wr007329.

Lunardini VJ. 1981. *Heat transfer in cold climates*. Van Nostrand Reinhold Company: New York; 731.

Malard F, Tockner K, Dole-Olivier MJ, Ward JV. 2002. A landscape perspective of surface-subsurface hydrological exchanges in river corridors. *Freshwater Biology*, 47: 621-640. DOI: 10.1046/j.1365-2427.2002.00906.x.

Marti E, Grimm NB, Fisher SG. 1997. Pre- and post-flood retention efficiency of nitrogen in a Sonoran Desert stream. *Journal of the North American Benthological Society*, 16: 805-819. DOI: 10.2307/1468173.

McCallum JL, Cook PG, Berhane D, Rumpf C, McMahon GA. 2012. Quantifying groundwater flows to streams using differential flow gaugings and water chemistry. *Journal of Hydrology*, 416: 118-132. DOI: 10.1016/j.jhydrol.2011.11.040.

McCallum JL, Cook PG, Brunner P, Berhane D. 2010. Solute dynamics during bank storage flows and implications for chemical base flow separation. *Water Resources Research*, 46. DOI: W07541, 10.1029/2009wr008539.

Morgenstern U, Stewart MK, Stenger R. 2010. Dating of streamwater using tritium in a post nuclear bomb pulse world: continuous variation of mean transit time with streamflow. *Hydrology and Earth Systems Sciences*, 14: 2289-2301. DOI: 10.5194/hess-14-2289-2010.

Morrice JA, Valett HM, Dahm CN, Campana ME. 1997. Alluvial characteristics, groundwater-surface water exchange and hydrological retention in headwater streams.

Hydrological Processes, 11: 253-267. DOI: 10.1002/(sici)1099-1085(19970315)11:3<253::aid-hyp439>3.0.co;2-j.

Mullinger NJ, Binley AM, Pates JM, Crook NP. 2007. Radon in Chalk streams: Spatial and temporal variation of groundwater sources in the Pang and Lambourn catchments, UK. *Journal of Hydrology*, 339: 172-182. DOI: 10.1016/j.jhydrol.2007.03.010.

Nield DA, Bejan A. 2006. *Convection in Porous Media*. Springer Science+Business Media, Inc. New York, 608.

Opsahl SP, Chapal SE, Hicks DW, Wheeler CK. 2007. Evaluation of ground-water and surface-water exchanges using streamflow difference analyses. *Journal of the American Water Resources Association*, 43: 1132-1141. DOI: 10.1111/j.1752-1688.2007.00093.x.

Orghidan T. 1959. Ein neuer Lebensraum des unterirdischen Wassers: der hyporheischhe Biotop. *Archiv Fur Hydrobiologie*: 392-414.

Payn RA, Gooseff MN, McGlynn BL, Bencala KE, Wondzell SM. 2009. Channel water balance and exchange with subsurface flow along a mountain headwater stream in Montana, United States. *Water Resources Research*, 45. DOI: 10.1029/2008wr007644.

Pollard RA. 1955. Measureing seepage through salmon spawning gravel. *Journal of the Fisheries Research Board of Canada*, 706-741.

Rau GC, Andersen MS, Acworth RI. 2012a. Experimental investigation of the thermal dispersivity term and its significance in the heat transport equation for flow in sediments. *Water Resources Research*, 48. DOI: W03511, 10.1029/2011wr011038.

Rau GC, Andersen MS, Acworth RI. 2012b. Experimental investigation of the thermal time-series method for surface water-groundwater interactions. *Water Resources Research*, 48. DOI: W03530, 10.1029/2011wr011560.

Rau GC, Andersen MS, McCallum AM, Roshan H, Acworth RI. 2014. Heat as a tracer to quantify water flow in near-surface sediments. *Earth-Science Reviews*, 129: 40-58. DOI: 10.1016/j.earscirev.2013.10.015.

Roshan H, Rau GC, Andersen MS, Acworth IR. 2012. Use of heat as tracer to quantify vertical streambed flow in a two-dimensional flow field. *Water Resources Research*, 48. DOI: 10.1029/2012wr011918.

Ruehl C, Fisher AT, Hatch C, Los Huertos M, Stemler G, Shennan C. 2006. Differential gauging and tracer tests resolve seepage fluxes in a strongly-losing stream. *Journal of Hydrology*, 330: 235-248. DOI: 10.1016/j.jhydrol.2006.03.025.

Runkel RL. 1998. One-dimensional transport with inflow and storage (OTIS): A solute transport model for streams and rivers. *U.S. Geological Survey Water-Resources Investigations Report 98-4018*. USGS: Denver; 73.

Sawyer AH, Cardenas MB, Bomar A, Mackey M. 2009. Impact of dam operations on hyporheic exchange in the riparian zone of a regulated river. *Hydrological Processes*, 23: 2129-2137. DOI: 10.1002/hyp.7324.

Schilling KE, Li Z, Zhang Y-K. 2006. Groundwater - surface water interaction in the riparian zone-of an incised channel, Walnut Creek, Iowa. *Journal of Hydrology*, 327: 140-150. DOI: 10.1016/j.jhydrol.2005.11.014.

Schilling KE, Zhang YK, Drobney P. 2004. Water table fluctuations near an incised stream, Walnut Creek, Iowa. *Journal of Hydrology*, 286: 236-248. DOI: 10.1016/j.jhydrol.2003.09.017.

Schmidt C, Bayer-Raich M, Schirmer M. 2006. Characterization of spatial heterogeneity of groundwater-stream water interactions using multiple depth streambed temperature measurements at the reach scale. *Hydrology and Earth Systems Sciences*, 10: 849-859.

Schmidt C, Conant B, Bayer-Raich M, Schirmer M. 2007. Evaluation and field-scale application of an analytical method to quantify groundwater discharge using mapped streambed temperatures. *Journal of Hydrology*, 347: 292-307. DOI: 10.1016/j.jhydrol.2007.08.022.

Schornberg C, Schmidt C, Kalbus E, Fleckenstein JH. 2010. Simulating the effects of geologic heterogeneity and transient boundary conditions on streambed temperatures - Implications for temperature-based water flux calculations. *Advances in Water Resources*, 33: 1309-1319. DOI: 10.1016/j.advwatres.2010.04.007.

Schwoerbel J. 1965. Bemerkungen uber die interstitielle hyporheische Fauna einiger Backe der sudlichen Vogesen. *Vie et Milieu*: 465-485.

Selker JS, Thevenaz L, Huwald H, Mallet A, Luxemburg W, de Giesen NV, Stejskal M, Zeman J, Westhoff M, Parlange MB. 2006. Distributed fiber-optic temperature sensing for hydrologic systems. *Water Resources Research*, 42. DOI: 10.1029/2006wr005326.

Shanafield M, Hatch C, Pohll G. 2011. Uncertainty in thermal time series analysis estimates of streambed water flux. *Water Resources Research*, 47. DOI: 10.1029/2010wr009574.

Simunek J, Sejna M, van Genuchten MT. 1999. The Hydrus-2D software package for simulating the two-dimensional movement of water, heat, and multiple solutes in variably saturated media, Vesion 2.0, IGWMC-TPS-??. *International Ground Water Modeling Center*. Colorado School of Mines: Golden; 251.

Sjodin A, Lewis WM, Saunders JF. 2001. Analysis of groundwater exchange for a large plains river in Colorado (USA). *Hydrological Processes*, 15: 609-620. DOI: 10.1002/hyp.173.

Smerdon BD, Gardner WP, Harrington GA, Tickell SJ. 2012. Identifying the contribution of regional groundwater to the baseflow of a tropical river (Daly River, Australia). *Journal of Hydrology*, 464: 107-115. DOI: 10.1016/j.jhydrol.2012.06.058.

Snow DD, Spalding RF. 1997. Short-term aquifer residence times estimated from Rn-222 disequilibrium in artificially-recharged ground water. *Journal of Environmental Radioactivity*, 37: 307-325. DOI: 10.1016/s0265-931x(97)00001-5.

Solomon DK, Genereux DP, Plummer LN, Busenberg E. 2010. Testing mixing models of old and young groundwater in a tropical lowland rain forest with environmental tracers. *Water Resources Research*, 46. DOI: 10.1029/2009wr008341.

Sophocleous M. 2002. Interactions between groundwater and surface water: the state of the science. *Hydrogeology Journal*, 10: 52-67. DOI: 10.1007/s10040-001-0170-8.

Squillace PJ. 1996. Observed and simulated movement of bank-storage water. *Ground Water*, 34: 121-134. DOI: 10.1111/j.1745-6584.1996.tb01872.x.

Stallman RW. 1965. Steady 1-dimensional fluid flow in a semi-infinite porous medium with sinusoidal surface temperature. *Journal of Geophysical Research*, 70: 2821-2827. DOI: 10.1029/JZ070i012p02821.

Stonedahl SH, Harvey JW, Worman A, Salehin M, Packman AI. 2010. A multiscale model for integrating hyporheic exchange from ripples to meanders. *Water Resources Research*, 46. DOI: W12539, 10.1029/2009wr008865.

Storey RG, Howard KWF, Williams DD. 2003. Factors controlling riffle-scale hyporheic exchange flows and their seasonal changes in a gaining stream: A three-dimensional groundwater flow model. *Water Resources Research*, 39. DOI: 103410.1029/2002wr001367.

Suzuki S. 1960. Percolation measurements based on heat flow through soil with special reference to paddy fields. *Journal of Geophysical Research*, 65: 2883-2885.

Swanson TE, Cardenas MB. 2010. Diel heat transport within the hyporheic zone of a pool-riffle-pool sequence of a losing stream and evaluation of models for fluid flux estimation using heat. *Limnology and Oceanography*, 55: 1741-1754. DOI: 10.4319/lo.2010.55.4.1741.

Taniguchi M, Sharma ML. 1990. Solute and heat-transport experiments for estimating recharge rate. *Journal of Hydrology*, 119: 57-69.DOI:10.1016/0022-1694(90)90034-u.

Thibodeaux LJ, Boyle JD. 1987. Bedform-generated convective-transport in bottom sediment. *Nature*, 325: 341-343. DOI: 10.1038/325341a0.

Thomas SA, Valett HM, Webster JR, Mulholland PJ. 2003. A regression approach to estimating reactive solute uptake in advective and transient storage zones of stream ecosystems. *Advances in Water Resources*, 26: 965-976. DOI: 10.1016/s0309-1708(03)00083-6.

Tonina D, Buffington JM. 2007. Hyporheic exchange in gravel bed rivers with pool-riffle morphology: Laboratory experiments and three-dimensional modeling. *Water Resources Research*, 43. DOI: W01421, 10.1029/2005wr004328.

Triska FJ, Kennedy VC, Avanzino RJ, Zellweger GW, Bencala KE. 1989. Retention and transport of nutrients in a 3rd-order stream in northwestern California - hyporheic processes. *Ecology*, 70: 1893-1905. DOI: 10.2307/1938120.

Vaux WG. 1968. Intragravel flow and interchange of water in a streambed. *United States Fish and Wildlife Service Fishery Bulletin*, 66: 479-489.

Vogel JC. 1967. Investigation of groundwater flow with radiocarbon. *Isotopes in Hydrology*: 355-369.

Vogt T, Hoehn E, Schneider P, Freund A, Schirmer M, Cirpka OA. 2010b. Fluctuations of electrical conductivity as a natural tracer for bank filtration in a losing stream. *Advances in Water Resources*, 33: 1296-1308. DOI: 10.1016/j.advwatres.2010.02.007.

Vogt T, Schneider P, Hahn-Woernle L, Cirpka OA. 2010a. Estimation of seepage rates in a losing stream by means of fiber-optic high-resolution vertical temperature profiling. *Journal of Hydrology*, 380: 154-164. DOI: 10.1016/j.jhydrol.2009.10.033.

Walker GR, Cook PG. 1991. The importance of considering diffusion when using C-14 to estimate groundwater recharge to an unconfined aquifer. *Journal of Hydrology*, 128: 41-48. DOI: 10.1016/0022-1694(91)90130-a.

Ward AS, Gooseff MN, Singha K. 2010. Imaging hyporheic zone solute transport using electrical resistivity. *Hydrological Processes*, 24: 948-953. DOI: 10.1002/hyp.7672.

Welch C, Cook PG, Harrington GA, Robinson NI. 2013. Propagation of solutes and pressure into aquifers following river stage rise. *Water Resources Research*, 49: 5246-5259. DOI: 10.1002/wrcr.20408.

Welch C, Harrington GA, Leblanc M, Batlle-Aguilar J, Cook PG. 2014. Relative rates of solute and pressure propagation into heterogeneous alluvial aquifers following river flow events. *Journal of Hydrology*, 511: 891-903.

Winter TC, Harvey JW, Franke OL, Alley WM. 1998. Ground water and surface water: A single resource, U.S. Geological Survey, Circular 1139, ISBN 0–607–89339–7, Denver, Colorado.

Winter TC, Labaugh JW, Rosenberry DO. 1988. The design and use of a hydraulic potentiomanometer for direct measurement of differences in hydraulic-head between groundwater and surface-water. *Limnology and Oceanography*, 33: 1209-1214.

Woessner WW. 2000. Stream and fluvial plain ground water interactions: Rescaling hydrogeologic thought. *Ground Water*, 38: 423-429. DOI: 10.1111/j.1745-6584.2000.tb00228.x.

Wondzell SM. 2006. Effect of morphology and discharge on hyporheic exchange flows in two small streams in the Cascade Mountains of Oregon, USA. *Hydrological Processes*, 20: 267-287. DOI: 10.1002/hyp.5902.

Wondzell SM. 2011. The role of the hyporheic zone across stream networks. *Hydrological Processes*, 25: 3525-3532. DOI: 10.1002/hyp.8119.

Worman A, Packman AI, Johansson H, Jonsson K. 2002. Effect of flow-induced exchange in hyporheic zones on longitudinal transport of solutes in streams and rivers. *Water Resources Research*, 38. DOI: 10.1029/2001wr000769.

7. APPENDIX A: RADON EMANATION EXPERIMENTS

7.1. Introduction

Radon (^{222}Rn) emanation rates from sediments can be determined using a number of methods including: the brass cell equilibrium method (after Cook *et al.*, 2006); and the glass jar equilibrium method described below. These methods were compared by variably using, coarse grained sand, dolomite gravel, glass beads, deionised water and two standard solutions of radium (^{226}Ra). The combination of these variables is outlined in Table 7.1 below. The equilibrium activities of radon calculated using the brass cell method should in theory, be the same as equivalent samples using the glass jar equilibrium method. Previous investigations have shown non-equivalence between methods and so this work intends to clarify the cause(s) of the apparent errors in either or both methods.

Table 7.1. Emanation experimental setup summary.

Vessel	Material	Approximate Mass (g)	Liquid*	Number of Samples
500 mL Glass Jar	Glass Beads	830	DI	3
500 mL Glass Jar	Glass Beads	830	Std 1	3
500 mL Glass Jar	Glass Beads	830	Std 2	3
500 mL Glass Jar	Sand	790	DI	3
500 mL Glass Jar	Gravel	750	DI	3
Brass Cell	Glass Beads	30	DI	3
Brass Cell	Glass Beads	30	Std 1	3
Brass Cell	Glass Beads	30	Std 2	3
Brass Cell	Sand	20	DI	3
Brass Cell	Sand	30	DI	3
Brass Cell	Sand	40	DI	3
Brass Cell	Gravel	20	DI	3
Brass Cell	Gravel	30	DI	3
Brass Cell	Gravel	40	DI	3
Brass Cell	None	0	DI	3
Brass Cell	None	0	Std 1	3
Brass Cell	None	0	Std 2	3
Total				51

*DI = deionised water, Std 1 = 1 Bq/L radium–226 standard solution, Std 2= 10 Bq/L radium–226 standard solution.

7.2. Methods

In addition to weighing the samples and components at each stage, the glass jar equilibrium method included the following steps:

1) According to Table 7.1, filling 500 mL glass jars to capacity with acid washed and oven dried 2 mm glass beads, washed 8/16 coarse grained sand and dolomite gravel;
2) The addition of deionised water to until the sediments were completely covered while agitating the jars for compaction and to release any trapped air bubbles;
3) Leaving two batches of samples for periods of 40 (9/12/11 – 18/1/12) and 58 (18/1/12 – 16/3/12) days to ensure secular equilibrium was reached between the emanation and decay processes;
4) Sampling the pore water using the direct method for dissolved radon sampling and analysis (after Leaney and Herczeg, 2006); and
5) Analysis using the LKB Wallace Quantulus Liquid Scintillation Counter at CSIRO Land and Water Waite Campus Environmental Isotopes Laboratory.

The brass cell equilibrium method is described in Cook *et al.* (2006) and the following variations were conducted according to Table 7.1:

1) The mass of sediments placed in the cells was varied at 20, 30 and 40 g for gravel and sand sediments;
2) A series of controls were included, using glass beads with deionised water, 1 Bq/L and 10 Bq/L radium standard solutions; and
3) A series of blanks were included, using deionised water, 1 Bq/L and 10 Bq/L radium standard solutions.

To convert emanation rates (Bq/kg) calculated in the brass cell method to equilibrium activities (Bq/L) the following equations were used:

$$\beta = \frac{\varepsilon(1-\theta)\rho_s\lambda}{\theta} \qquad (7.1)$$

$$A_e = \frac{\beta}{\lambda} \quad (7.2)$$

where β is the production rate (Bq L^{-1} d^{-1}), ε is the emanation rate (Bq kg^{-1}), ρ is the density of solids (kg cm^3), λ is the decay coefficient (d^{-1}) and θ is porosity.

7.3. Results

Summarised results of the emanation tests are shown in Table 7.2 while detailed results tables for each component of the experiments are also shown in Tables 3 to 7. At first glance, the counts per minute (CPM) raw data of triplicate groups and between the brass cells and glass jars appear to compare reasonably well (see Tables 7.4 and 7.7). However, once emanation rates are converted to equilibrium activities some marked differences and trends appear as outlined below:

- Emanation rates show a decreasing trend with increasing sediment mass (i.e. gravel and sand from 20 to 30 to 40 g) despite inherent corrections for sediment mass;
- Equilibrium activities for sand and gravel using the brass cells are a factor of 2 to 4 times the activities found in the glass jars;
- CPM for brass cells with no known introduced source of radon (i.e. glass beads and /or deionised water only) were shown to be higher than reported background (0.3 CPM);
- Equilibrium activities using glass beads compared well between methods (with the exception of glass beads in deionised water from the brass cells which were non zero);
- Blanks overestimate the deionised water and radium standards with respect to CPM, although calculations may need to be revised for equilibrium activities due to the constancy of the radium source;
- A number of samples appear to be erroneous or have higher variability than expected (see Table 7.6; Blank_0_Std2_2; Gr_20_1; Gr_20_2; and Gr_20_3). It is possible that there was a background source of radon in the brass cells to explain this variability; and

- It was deemed appropriate to apply a background correction of -1.37 CPM to brass cell results (in addition to the previously established background of 0.3 CPM). This value was the mean background count found for the glass beads in deionised water within the brass cells where a zero CPM was expected (Table 7.5).

Table 7.2. Summarised results of emanation experiments.

	Emanation Cells (mean values)					Jars (mean values)		
Sample	Mass (g) or Liquid	CPM	CPM corr	Emanation Rate (Bq/kg)	Equil. Activity (Bq/L)	CPM	Emanation Rate (Bq/kg)	Equil. Activity (Bq/L)
Gravel	20	2.95	1.58	1.18	3.76	4.44	0.68	2.16
	30	3.49	2.12	1.02	3.25			
	40	4.19	2.82	0.90	2.87			
Sand	20	1.68	0.31	0.23	0.85	1.66	0.21	0.76
	30	2.03	0.66	0.32	1.16			
	40	1.89	0.52	0.20	0.72			
Glass Beads	DI	1.37	0.00	0.00	-	0.33	0.02	-
	Std 1	2.98	1.61	0.71	-	1.58	0.73	-
	Std 2	21.39	20.02	9.06	-	14.60	8.31	-
Blanks*	DI	2.61	1.24	0.26	-	-	-	-
	Std 1	3.46	2.09	0.87	-	-	-	-
	Std 2	28.67	27.30	12.56	-	-	-	-

* Since there was no sediment mass in the blank brass cells, the mass of the liquid added was used.

Table 7.3. Summary of bulk sediment characteristics.

Material	Porosity (n=3)	Density (n=3)
Sand (Sa)	0.43	2.78
Gravel (Gr)	0.47	2.85
Glass Beads (GB)	0.38	2.69
Liquid within Glass Beads	0.62	1.00

Table 7.4. Results from brass cell emanation experiments with sand and gravel.

Sample ID	CPM	CPM corr	Emanation Rate (Bq/kg)	Equilibrium Activity (Bq/L)
Gr_20_1	1.854	0.484	0.44	1.40
Gr_20_2	3.955	2.585	2.07	6.60
Gr_20_3	3.044	1.674	1.03	3.29
Gr_30_1	3.079	1.709	0.99	3.17
Gr_30_2	3.606	2.236	1.09	3.46
Gr_30_3	3.793	2.423	0.98	3.12
Gr_40_2	3.798	2.428	0.85	2.71
Gr_40_3	4.573	3.203	0.95	3.02
Sa_20_1	1.823	0.453	0.39	1.42
Sa_20_2	1.464	0.094	0.07	0.26
Sa_20_3	1.757	0.387	0.24	0.88
Sa_30_1	1.737	0.367	0.19	0.71
Sa_30_2	2.289	0.919	0.46	1.67
Sa_30_3	2.061	0.691	0.30	1.10
Sa_40_1	1.535	0.165	0.07	0.26
Sa_40_2	1.919	0.549	0.20	0.74
Sa_40_3	2.228	0.858	0.32	1.16

Table 7.5. Results from brass cell emanation experiments with glass beads.

Sample ID	CPM	CPM corr	Emanation Rate (Bq/L)
GB_30_DI_1	1.671	0.301	0.08
GB_30_DI_2	1.145	-0.225	-0.06
GB_30_DI_3	1.297	-0.073	-0.02
GB_30_Std1_1	3.023	1.653	0.72
GB_30_Std1_2	2.644	1.274	0.63
GB_30_Std1_3	3.267	1.897	0.79
GB_30_Std2_1	20.101	18.731	8.38
GB_30_Std2_2	22.031	20.661	9.27
GB_30_Std2_3	22.03	20.66	9.54

Table 7.6. Results from brass cell emanation experiments with blanks*.

Sample ID	CPM	CPM corr	Emanation Rate (Bq/kg)
Blank_0_DI_1	4.639	3.269	0.68
Blank_0_DI_2	1.221	-0.149	-0.04
Blank_0_DI_3	1.955	0.585	0.14
Blank_0_Std1_1	3.262	1.892	0.80
Blank_0_Std1_2	4.219	2.849	1.07
Blank_0_Std1_3	2.902	1.532	0.73
Blank_0_Std2_1	25.09	23.72	9.66
Blank_0_Std2_2	32.357	30.987	17.23
Blank_0_Std2_3	28.564	27.194	10.79

* Since there was no sediment mass in the blank Brass cells, the mass of the liquid added was used.

Table 7.7. Results from glass jar emanation experiments.

Sample ID	CPM	Emanation Rate (Bq/kg)	Equilibrium Activity (Bq/L)
GB_DI_1	0.258	-0.02	-
GB_DI_2_1	0.365	0.03	-
GB_DI_2_2	0.279	-0.01	-
GB_DI_3	0.43	0.07	-
Gr_DI_1	4.892	0.73	2.33
Gr_DI_2	4.34	0.67	2.12
Gr_DI_3	4.102	0.63	2.03
Sa_DI_1	1.616	0.20	0.72
Sa_DI_2	1.712	0.21	0.78
Sa_DI_3	1.666	0.21	0.79
GB_Std1_1	1.813	0.81	-
GB_Std1_2	1.641	0.75	-
GB_Std1_3	1.276	0.57	-
GB_Std2_1	14.474	7.17	-
GB_Std2_2	15.887	8.14	-
GB_Std2_3	13.831	7.28	-
GB_Std1_1_2	1.712	0.81	-
GB_Std1_2_2	1.737	0.82	-
GB_Std1_3_2	1.322	0.62	-
GB_Std2_1_2	14.343	8.79	-
GB_Std2_2_2	14.692	9.21	-
GB_Std2_3_2	14.378	9.30	-

7.4. Conclusion

Based on the results shown above, it is recommended that the glass jar method be used in preference to the brass cell method because: 1) it has fewer sources or error; and 2) can provide triplicate subsamples from the same jar sample if required. The brass cell method may still be appropriate for use where sediment samples are of a very limited volume (e.g. drilling cuttings from a core library) as was initially intended.

Further investigation will be required if the brass cell method is to be used in future, to address the possibility that the brass cells are a source of radon. Each cell may have a unique background source which could potentially be influenced by the cleaning stage if they were more rigorously acid washed.

8. APPENDIX B: FIELD DATA

The file RCranswick_HaughtonRawFieldData.xlsx found in the CD insert, contains sheets with raw field data from the primary field campaign conducted along a 300 m reach of the Haughton River from 26/09/2011 – 30/09/2011. These show details of the vertical profiles, sediment cores, the bromide tracer test, river electrical conductivity, flow gauging, snapshot sampling, surveying, GPS locations and temperature data from each profile where thermistors were installed. Data collected during a reconnaissance trip to the study reach on 10/05/2011 are also included. Additionally, the data collected during a prior field campaign to the Cockburn River (NSW) from 11/04/2011 – 15/04/2011 are included in the CD insert within the file RCranswick_CockburnRawFieldData.xlsx. Although this data has not been presented within this thesis or published elsewhere, it is included here for future use.

The Monte Carlo analysis and PEST input files are not included in these appendices but can be made available upon request from the author. Similarly, the FORTRAN code for numerically solving the 1D heat transport, 1D radon transport and their variations for Monte Carlo and PEST simulations can also be made available upon request.